BOSTON UNIVERSITY

COLLEGE OF ENGINEERING

Dissertation

UNLOCKING MACROPHAGE ENGINEERING AND THERAPIES WITH SYNTHETIC POLARIZATION CIRCUITS

by

HANRONG (BELLE) YE

B.A., Vanderbilt University, 2017
M.S., Boston University, 2021

Submitted in partial fulfillment of the

requirements for the degree of

Doctor of Philosophy

2025

Approved by

First Reader

Ahmad S. Khalil, Ph.D.
Professor of Biomedical Engineering

Second Reader

Joyce Y. Wong, Ph.D.
Professor of Biomedical Engineering
Professor of Materials Science and Engineering

Third Reader

Wilson W. Wong, Ph.D.
Professor of Biomedical Engineering

Fourth Reader

Mikko Taipale, Ph.D.
Anne and Max Tanenbaum Chair in Biomedical Research
Canada Research Chair in Functional Proteomics and Proteostasis
Associate Professor of Molecular Genetics
University of Toronto

Fifth Reader

David H. Sherr, Ph.D.
Professor of Environmental Health
Boston University, School of Public Health
Professor of Pathology and Laboratory Medicine
Boston University, Aram V. Chobanian & Edward Avedisian School of Medicine

DEDICATION

I would like to dedicate this work to my grandfather, Wang Yong Hua, who had always shown unwavering faith in me and encouraged me to think and dream wildly. You are not here to witness the end of my PhD journey, but your legacy will forever live within me.

ACKNOWLEDGMENTS

First and foremost, I would like to acknowledge the trust, patience, and support from my advisors, Professor Ahmad (Mo) Khalil and Professor Joyce Wong. Thank you for letting me find my own path through my PhD journey and fulfill my ambition to build my own interdisciplinary project. Thank you, Mo, for guiding me through the world of synthetic biology and inspiring me to become a better scientist. Your enthusiasm for science, relentless pursuit for innovation and insatiable curiosity motivate me to think, imagine and dream bigger. Thank you, Joyce, for supporting me through the challenges of graduate school—especially at the beginning—and helping me navigate the toughest moments, rescuing me when I was stuck outside the country during the pandemic. I am deeply grateful to you both.

I would also like to acknowledge all our collaborators who helped shape this project and made all the ambitious experiments possible. Thank you, Professor Igor Kramnik, for introducing me to the world of macrophages. Thank you, Professor Mikko Taipale, and your brilliant student, He, for turning the BioID experiment from an idea to reality. I am deeply grateful to my committee members, Professor Wilson Wong, for your invaluable research advice (and occasionally life wisdom and humor), and Professor David Sherr, for generously joining my committee despite your impending retirement.

I want to acknowledge my lab mates, especially those who contributed to the development of synZiFTR 1.0 and 2.0—Dr. Huishan Li, Dr. Divya Israni, Dr. Kok Ann (Sam) Gan, Dr. Keith Gagnon, Thea Orstein and Liz Tchantouridze, and those who offered their scientific expertise and mentorship through my graduate career, Dr. Giulio

Chiesa and Dr. Michael Raymond. I want to thank Ben Fitzsimmons for being my most respected foodie friend in the world. Thank you, Dr. Hagar Moussa, for taking care of me when I'm at my lowest and being my best friend in lab and in life. I would also like to thank our finance administrator, Dave Michaels, for doing an amazing job keeping things running smoothly in lab and organizing fun BDC events.

I also want to say thank you to my friends who supported me through the past 8 years and being my anchors through all the ups and downs. To my BU cohort friends—it's been a privilege to get to know fun, intelligent, and kind people like you. It is truly inspiring watch you all achieve amazing things in your post-Ph.D. journeys. To my college friends, Liz and Clair, and high school friends, Jiawen, Xiaomei, Yucong and Jingwen, thank you for a decade of love, support and laughter. Our friendships mean the world to me. Thank you, Jim Li, for making me fall in love with nature and travels, and editing all my writing in pre-ChatGPT time.

Special shoutouts to Colin Kunze, who have played every possible supporting role in my life. You have been my best friend since the beginning of graduate school. You are an amazing lab mate who takes genuine interest in other people's projects and has always been willing to help people in any possible way you can. You are the most kind, patient, tolerant, caring, empathetic partner and human I could imagine. I don't know who I would be today without you in my life.

Finally, I would like to thank my parents, for providing me love and support and always believing in me. I owe everything I am, I have, and I've accomplished today to you. Being stuck home for a year and half during graduate school was not ideal, but I

cherish every moment we've spent together and am forever grateful to being your daughter.

UNLOCKING MACROPHAGE ENGINEERING AND THERAPIES WITH SYNTHETIC POLARIZATION CIRCUITS

HANRONG (BELLE) YE

Boston University College of Engineering, 2025

Major Professor: Ahmad S. Khalil, Ph.D., Professor of Biomedical Engineering.

ABSTRACT

Macrophages are versatile immune cells capable of diverse functions, enabled by unique cellular properties such as inflammation scavenging, phagocytosis capability, and perhaps most interesting, their unparallel phenotype plasticity. In response to extracellular signals, macrophages activate distinctive functional programs and differentiate into two general subtypes: classically activated macrophages (M1) and alternatively activated macrophages (M2). M1 macrophages promote inflammation and show anti-tumor activity in synergy with T cells, while M2 macrophages play a vital role in wound healing and treating anti-inflammatory diseases. While macrophage phenotypic plasticity is essential for maintaining tissue homeostasis, in pathological contexts such as cancer, microenvironmental signals often skew macrophages towards phenotypes that exacerbate disease progression. Therefore, the ability to precisely control macrophage activation states in vivo could unlock new therapeutic strategies to restore immune function and halt disease mechanisms.

To leverage the diverse immune functions of macrophages—in both immune environments and pathological contexts, we developed a synthetic system for inducible macrophages polarization combining three synergistic innovations: (1) engineered STAT

effector proteins that can robustly drive constitutive and sustained macrophage polarization to M1 or M2 state, independent of cytokine induction. (2) synZiFTRs 2.0, an optimized human gene regulation toolkit built upon our previous work, enabling drug-inducible and enhanced transgene expression with minimal basal activity; and (3) monocyte-targeting nanoparticles for cell-specific delivery of synZiFTR induction agents. Central to this advance is the discovery of the IWS1 TIMs domain as a potent transcriptional synergizer, which enhances human transcriptional activators like p65 through stimulating transcriptional elongation, without compromising safety or inducibility. This work establishes a generalizable framework for macrophage reprogramming with spatiotemporal precision, offering a tunable and clinically translatable approach for diverse applications. By decoupling polarization cues from local signals and integrating polarization effectors with synthetic gene regulation switches, our platform allows robust macrophage polarization against microenvironmental inferences while minimizing off-target effects. These advances not only provide new tools for macrophage-based therapies but also illuminate broader principles for engineering immune cell behavior in therapeutic contexts.

TABLE OF CONTENTS

LIST OF TABLES

LIST OF FIGURES

LIST OF ABBREVIATIONS

4OHT	4-Hydroxytamoxifen
CAR	Chimeric Antigen Receptor
CCR2	C-C chemokine receptor type 2
DMSO	Dimethylsulfoxide
DSPE	1,2-distearoyl-sn-glycero-3-phosphoethanolamine
EGFP	Enhanced green fluorescent protein
EloA	Elongin A
ERT2	Human estrogen receptor T2
FDA	Food and Drug Administration
GZV	Grazoprevir
IFNγ	Interferon gamma
IL	Interleukin
LPS	Lipopolysaccharide
MCP1	Monocyte Chemoattractant Protein 1
NP	Nanoparticles
PEG	polyethylene glycol
PLGA	Poly Lactic-co-Glycolic Acid
PMA	Phorbol 12-myristate-13-acetate
PRO Seq	Precision nuclear run-on sequencing
RNAP2	RNA Polymerase 2
STAT	Signa Transducer and Activator Transcription Proteins

TAD	Transactivation domain
TAM	Tumor Associated Macrophages
TF	Transcriptional factor
TFIIS	Transcriptional factor IIS
TIM	TND interacting domain
TME	Tumor Microenvironment
TND	TFIIS N-terminal domain
TNFα	Tumor Necrosis Factor Alpha
ZF	Zinc finger

CHAPTER ONE: INTRODUCTION

1.1 Macrophage therapies: an overview

Macrophages are multifaceted immune cells capable of diverse functions, as evidenced by their central role in maintaining homeostasis across nearly all types of tissue, defending against various pathogens, and orchestrating inflammatory and reparative responses. This versatility is enabled by unique cellular properties of macrophages, including their tissue infiltration, inflammation scavenging, antigen presentation capacity, phagocytotic ability, and perhaps most interesting, unparalleled phenotypic plasticity. Derived from monocytes in the bloodstream or from embryonic precursors, macrophages are highly plastic cells capable of adopting diverse functional phenotypes in response to environmental cues. These phenotypes are broadly categorized into pro-inflammatory (M1) and anti-inflammatory (M2) states, though macrophages exist along a spectrum of activation states with overlapping functions (Strizova et al., 2023). M1 macrophages are typically involved in host defense and tumor suppression, producing pro-inflammatory cytokines and reactive oxygen species, while M2 macrophages promote tissue repair, angiogenesis, and immune suppression, making them key players in wound healing, fibrosis, and tumor progression.

The diverse and distinctive biological properties of macrophages, coupled with their remarkable tissue infiltration capacity, including penetration of privileged sites unattainable by other cell types, such as solid tumors and across blood brain barrier (Corraliza, 2014), has made them attractive targets for therapeutic intervention. Macrophage-based therapies leverage the innate capabilities of these cells to modulate

both innate and adaptive immune responses, remodel tissues, and restore balance in diseased environments. In this chapter, we will explore some state-of-art macrophage-based cell therapies using different design principles, each capitalizes on *distinct aspects of macrophage biology* while addressing specific pathological mechanisms.

1.2 Current macrophage-based therapeutic strategies

1.2.1 Macrophage Reprogramming and Polarization

Macrophage phenotype plasticity allows them to serve versatile roles in different immune environments and pathological contexts. However, in diseases such as cancer, chronic inflammation, and fibrosis, macrophages often adopt phenotypes that exacerbate pathology. The ability to reprogram these macrophages, to either enhance their protective functions or suppress their pathological roles, has emerged as a promising strategy to restore immune function and halt disease progression, offering new avenues for treatment. Reprogramming tumor associated macrophages (TAMs) from an M2-like, pro-tumorigenic state to an M1-like, anti-tumorigenic phenotype can be a promising approach to enhance anti-tumor immunity for cancer immunotherapy. For example, blocking the CSF-1/CSF-1R axis or delivering IFN-γ, a potent pro-inflammatory stimulator, to polarize TAMs toward an M1 phenotype has been shown to reduce tumor growth and improve responses to immunotherapy in preclinical models (Pyonteck et al. 2013, Shields et al. 2020). Similarly, in fibrotic diseases, the pro-fibrotic M2-like macrophage contribute to the excessive deposition of extracellular matrix proteins, and polarizing these macrophages towards M1 phenotype via delivering TLR7 agonist was shown to reduce collagen deposition and mitigate lung fibrosis (Zhang et al. 2020). The therapeutic

potential of M1 macrophages was further evidenced in liver fibrosis, where their infusion reduced fibrotic burden through matrix metalloproteinases (MMPs) secretion, which promotes collagen breakdown, while enhancing tissue regeneration via HGF-driven hepatocyte proliferation (Ma et al., 2017).

On the contrary, in many **chronic inflammatory diseases**, hyperactive macrophages can cause persistent immune activation and tissue damage through the release of inflammatory cytokines, reactive oxygen species (ROS), and matrix-degrading enzymes. Shifting macrophages towards M2 macrophages to perform anti-inflammatory and tissue-repair functions can help resolve inflammation and promote healing. In rheumatoid arthritis (RA), targeting M1 macrophages with liposomes and repolarizing them towards M2 phenotype with chemical compounds resulted in significantly reduced tissue damage and inflammation in a rat model (Zhou et al. 2021). In atherosclerosis, Ginsenoside Rb1 alleviates inflammation and enhances atherosclerosis plaque stability by promoting local macrophage M2 polarization (Zhang et al. 2017). In a treatment developed for inflammatory bowel diseases, Ca^{2+} and a ferroptosis inhibitor were delivered to colitis lesion sites to promote macrophage M2 polarization and help maintain their cellular activity, resulting in an increased local M2/M1 macrophage ratio and significant therapeutic efficacy.

1.2.2 CAR-M

Chimeric Antigen Receptor (CAR) Macrophages leverage the *phagocytic, inflammatory and antigen-presenting capabilities* of macrophages. Equipped with the precision targeting of CAR technology, engineered macrophages can direct their usually

non-specific, antigen-independent cellular activities against the targeted antigens on diseased cells (e.g. tumor cells). Upon antigen recognition, CAR M phagocytose target cells, secrete pro-inflammatory cytokines to recruit and activate other immune cells, and present antigens to T cells, bridging innate and adaptive immunity (Klichinsky et al. 2020). Compared to CAR-T therapies, CAR-M is emerging as a potential solution for **solid tumors** due to its ability to infiltrate and remodel the TME. However, while FDA has approved several CAR-T therapy products for B-cell malignancies (e.g., Kymriah, Yescarta), CAR-M therapies are still in preclinical or early clinical trials (Reiss et al., 2025, Abdou et al., 2024).

1.2.3 Macrophage Depletion

While macrophages play a key role in maintaining homeostasis and shaping the immune landscape, regulatory or inflammatory, dysregulated macrophages can trigger undesired immune responses and contribute to pathological progression, such as in **TME, fibrosis and chronic inflammation**. For these cases, macrophages depletion therapies were developed to target the pathological roles of macrophages and selectively eliminate or reduce the number of macrophages in specific tissues. Macrophage depletion can be achieved using several strategies, such as inducing apoptosis (Zeisberger et al. 2006), blocking macrophage survival signaling axis (e.g., CSF-1/CSF-1R axis) (Ries et al. 2014), and inhibiting their recruitment to the diseased sites (CCR2 inhibition) (Wu et al. 2019).

1.2.4 Challenges and Limitations

Despite successful development of numerous novel macrophage-based therapies for a wide array of diseases, their application in clinics still faces many key challenges. Macrophage plasticity and heterogeneity offers an opportunity to make macrophage reprograming a generalizable approach to address multiple disease models, but also makes it hard to predict and fully control their behaviors in therapeutic settings. Particularly in diseases like cancer and fibrosis, the immunosuppressive microenvironment can render macrophages resistant to reprogramming and therefore limiting the effectiveness of macrophage-based therapies. Moreover, generating large numbers of therapeutic macrophages ex vivo is technically challenging and costly due to the difficulty to expand primary macrophages compared to T cells, and maintaining their stability and functionality during manufacturing and storage is difficult. After infusion to patients, macrophages also have a relatively short lifespan in vivo, which limits the durability and persistence of macrophage-based therapies such as CAR-M or ex vivo reprogrammed macrophages. Finally, and perhaps most concerning, the ubiquity of macrophages in the body makes their off-target effects particularly dangerous. When lacking specificity or precise control over cell functions, macrophages therapies could lead to systemic immune activation, causing “cytokine storms” that non-specifically damage healthy tissues and organs. In macrophage depletion therapies, eliminating macrophages systemically can impair host defense and tissue repair. These limitations highlight the need for next-generation approaches that provide precise spatiotemporal control over macrophage activity while improving cell persistence and safety profiles—challenges that this thesis seeks to address through innovative engineering strategies.

1.3 Therapeutic advantages of macrophage reprogramming

Macrophage reprogramming represents a uniquely powerful therapeutic strategy compared to other macrophage-based interventions because it leverages the cells' endogenous plasticity rather than attempting to override or eliminate their native functions. Unlike CAR-M therapies—which are limited to specific antigen targets—or depletion approaches—which disrupt homeostatic macrophage populations—reprogramming works with the cells' inherent capacity to dynamically adapt to environmental cues. This approach preserves macrophages' critical tissue-homing abilities and allows for nuanced modulation of their functional output, enabling tailored responses to complex disease states. Moreover, by targeting polarization pathways that are often hijacked in pathology (e.g., STAT signaling in tumors or PPARγ in fibrosis), reprogramming can reverse disease-driven macrophage dysfunction while avoiding the systemic risks associated with adoptive transfer or broad depletion. The ability to intervene in situ also bypasses manufacturing challenges posed by ex vivo cell therapies, as reprogramming agents can be delivered directly to endogenous macrophage populations. Importantly, this strategy is inherently adaptable: the same core tools (e.g., polarization cytokines, epigenetic modifiers, or synthetic gene circuits) can be repurposed across diverse diseases by simply adjusting the reprogramming cues to match the pathological context. This combination of biological precision, translational practicality, and therapeutic versatility positions reprogramming as the most promising avenue for unlocking the full potential of macrophage-targeted therapies.

While macrophages demonstrate immense therapeutic potential, realizing this promise requires robust and precise control over their phenotypic states. To effectively reprogram macrophages in vivo, we must overcome a fundamental challenge: to reliably reprogram macrophage function within complex disease microenvironments. This longstanding obstacle in macrophage therapy has driven the development of innovative delivery systems or molecular tools designed to overcome the biological and technical barriers. In the following section, we examine conventional and emerging technologies that enable targeted phenotypic modulation of macrophages, searching for inspirations for precise spatiotemporal control of macrophage function across diverse disease contexts.

1.4 Technologies for in vivo Macrophage Reprogramming

1.4.1 Small Molecule Inhibitors and Agonists

Small molecules targeting polarization signaling pathways or receptors in macrophages have been used to modulate macrophage polarization in vivo. These molecules are designed to inhibit or activate key proteins involved in macrophage phenotype switching. For example, PI3Kγ inhibitors and TGF-βR1 kinase inhibitors shift TAMs from an M2 to an M1 phenotype (De Henau et al., 2016; Kim et al., 2023), while toll-like receptors TLR7/8 agonists promote M1 polarization by activating pro-inflammatory pathways (Rodell et al., 2018). Hydrogel-based local administration of a chemical compound, paeoniflorin, simultaneously deactivates M1 polarization protein STAT1 and activates M2-polarizting effector STAT6 proteins, resulting in a phenotypic transition towards M2 subtype in local macrophages in a cutaneous healing model to address impaired wound healing in diabetes (Yang et al., 2021). Small molecules are

typically administered systemically, either intravenously or orally. However, despite their ease of use, small molecules often lack specificity and potency due to poor stability, and usually require multiple admirations which can cause systemic side effects. They are often encapsulated in nanoparticles or hydrogel implants to improve targeting, enhance half-life, and reduce off-target effects (Rodell et al., 2018, Yang et al., 2021).

1.4.2 Cytokines and Signaling Peptides

Cytokines and signaling peptides/proteins are potent modulators of macrophage polarization and function. These molecules can directly bind to receptors on macrophages, activating or inhibiting specific signaling pathways to shift their phenotype. For example, interferon-gamma (IFN-γ) promotes M1 polarization by activating the JAK/STAT1 pathway and have been explored as a cancer immunotherapy (Shields et al. 2020). Interleukin-4 (IL-4) and interleukin-13 (IL-13) drive M2 polarization via the STAT6 pathway, and IL-4 conjugated gold nanoparticles were developed to shift macrophages towards anti-inflammatory phenotype to promote tissue regeneration (Raimondo and Mooney, 2018). A synthetic 10-mer peptide, RP-182, was shown to effectively induce a conformational change in CD206 receptor on TAMs and shift them towards M1 phenotype (Jaynes et al., 2020). Similar to small molecules cytokines and signaling proteins are typically delivered systemically (intravenously or subcutaneously) or locally (e.g., via hydrogels or nanoparticles) to enhance targeting and reduce systemic side effects. However, their rapid clearance requires frequent or high-dose administration, bearing risks of excessive cytokine activity which can lead to systemic inflammation. Recombinant cytokines are also expensive to produce and purify.

1.4.3 Antibodies

Antibodies are used to target specific surface receptors or ligands on macrophages to modulate their function. For instance, phosphatidylserine, a phospholipid normally exposed on the outer surface of apoptotic cells but constitutively expressed on some tumor cells and tumor vasculature, is recognized by macrophages and triggers their immunosuppressive signals in TME. Using phosphatidylserine-targeting antibody to block this interaction increased the presence of M1 macrophages and suppressed the growth of prostate tumors (Yin et al., 2013). Similarly, cancer immunotherapy using antibodies targeting integrin αvβ8, an activator for Transforming Growth Factor β (TGF-β), disrupts TGF-β's crucial role in enforcing the immunosuppressive environment in TME and significantly inhibited tumor growth by promoting immune cell infiltration and modulating TAM M1 polarization (Guo et al., 2025). Anti-CD47 antibodies block the "don't eat me" signal (CD47-SIRPα interaction), enhance macrophage phagocytosis and promote an M1 phenotype, now being investigated in clinical trials as a treatment for advanced cancers (Sikic et al., 2019). Antibodies are typically delivered via intravenous injection and can be conjugated to nanoparticles to enhance their targeting efficiency (Saha et al., 2024; Zhou et al., 2020). While antibody-based therapies are more specific, their production is expensive and their tissue penetration is more limited, such as into solid tumors and cross blood-brain barriers. In addition, antibodies can trigger immune-related adverse events such as cytokine release syndrome when encountering the innate immune system.

1.4.4 Oligonucleotides

In vivo oligonucleotides therapies, including RNA interference (RNAi), mRNA and oligonucleotides, offer versatile and precise approaches for macrophage reprogramming. RNAi utilizes siRNA or miRNA to silence specific genes involved in macrophage polarization, such as anti-TAK1 siRNA for M2-to-M1 switching (Zhao et al., 2024) or miRNA-155 and miRNA-99b for promoting M1 phenotypes in TAM (Wu et al., 2025; Wang et al., 2020). mRNA-based therapies, on the other hand, involve delivering mRNA encoding specific proteins to instruct macrophages to adopt desired phenotypes. For example, delivery of mRNA encoding Shisa3 gene or codelivery of interferon regulatory factor 5 (IRF5) mRNA with its activating kinase reverse TAMs to an anti-tumor pro-inflammatory phenotype (Zhang et al., 2024, Zhang et al., 2019), while interleukin-4 (IL4) mRNA drives M2 phenotype and accelerates diabetic wound healing (Wang et al., 2024). Oligonucleotide therapies, such as antisense oligonucleotides (ASOs), antagomir and aptamers, modulate gene expression or protein function by binding to specific mRNA sequences or receptors. For example, ASOs targeting STAT6 mRNA, RNA aptamers targeting SPP1 and antagomiR-182 are shown to reprogram TAM by inhibiting M2 polarization (Ma et al., 2021, Kamerkar et al., 2022, Wang et al., 2024). Oligonucleotide molecules are typically delivered using lipid or polymeric nanoparticles or exosomes to enhance stability and targeting. Lipid nanoparticles (LNPs) are commonly used for their delivery due to their amphiphilic nature, which enables them to hold positive charges that stably bind to the anionic backbone of RNA or DNA cargos. Their functionality has been demonstrated by the success of a few FDA approved liver siRNA

delivery systems and mRNA vaccines. Despite their relatively robust and sustained therapeutic effects, RNA-based therapies face challenges such as delivery efficiency, stability, and immune activation and are highly dependent on the delivery vehicles. Moreover, manufacturing stable and effective RNA-based therapies at scale is too challenging and costly for their broader applications.

1.4.5 Genetic Engineering

Genetic engineering involves modifying macrophage genes to alter their polarization state or function. Techniques such as CRISPR/Cas9 can be used to knockout M2-associated genes (e.g., Pik3cg) to stabilize M1 phenotype in TAM and inhibit tumor progression (Zhao et al., 2024). Viral vectors like adeno-associated virus (AAV) are commonly used to deliver genetic material such as IL-27 in vivo for M1 macrophage accumulation in tumors, while lentiviruses are employed for ex vivo engineering of macrophages for constitutive expression of polarizing factors like interleukin (IL)-12, which promoted IFN gamma inflammatory pathways and slowed down tumor growth (Zhu et al., 2024, Brempelis et al., 2020). Genetic engineering offers precise and durable effects but is limited by challenges such as immune responses to viral vectors and limited cargo capacity. Technical complexity of engineering macrophage ex vivo or in vivo can also be a limiting factor, given their resistant nature against transduction and virus infection.

1.5 Modulating macrophage phenotype with genetic circuits

The emerging field of macrophage therapy continues to evolve rapidly, with recent advances in genetic engineering, biomaterial science, and synthetic biology

opening new possibilities for therapeutic intervention. In particular, genetic circuits have emerged as powerful tools to program novel sense-and-response capabilities in human cells, enabling precise control over therapeutic functions in response to disease signals. These synthetic biological systems combine sensors (e.g., transcription factors activated by small molecules or disease biomarkers) with effector outputs (e.g., therapeutic transgenes or immune-modulatory signals) to create customizable cellular behaviors. In immune cell engineering, such circuits have been particularly transformative—for example, in T cells, synthetic receptors (CAR, TCR, SNIPR) and logic-gated gene switches have been used to enhance tumor targeting, improve safety, and dynamically regulate cytokine production (Baulu et al., 2023, Cho et al., 2021, Li et al., 2022, Zhu et al., 2022). In contrast, engineering macrophages through genetic and synthetic biology-based methods remains limited and technologically underdeveloped, despite the versatile and unique functions of these cells across diverse disease contexts. There is a clear need for *a focused, macrophage-centric engineering approach*, complete with optimized toolkits with which to install and tune macrophage genetic circuitry that will enable rapid progress in the field.

As highlighted in the previous section, traditional macrophage reprogramming approaches—including cytokine delivery, small molecule inhibitors, and adoptive cell transfer—often lack the specificity, durability, or safety profiles needed for clinical translation. Even when combined with advanced delivery systems to enhance targeting, these approaches often fail to sustain therapeutic effects against the dominant immunosuppressive signals present in disease microenvironments. In contrast, genetic

and synthetic biology tools offer the potential to fundamentally reshape macrophage behavior by directly reprogramming transcriptional networks, thereby creating durable phenotypic changes that resist microenvironmental interference. However, current implementations remain constrained by several factors: most systems target only single polarization pathways, leaving compensatory signaling cascades intact; while in vivo delivery of genetic circuits remains challenging, the potency of genetic reprogramming also raises concerns about uncontrolled immune activation when applied in vivo. These limitations underscore the need for next-generation solutions that *simultaneously address efficacy and safety*—engineered systems capable of modulating complex and robust polarization effectors to ensure efficient reprogramming, coupled with stringent control mechanisms to prevent aberrant immune responses.

In this work, we aim to develop a next-generation macrophage therapy through synthetic genetic programs enabling **precise, inducible control over macrophage polarization**. In Chapter 2 (Aim 1), we will engineer master regulators of polarization—STAT proteins—to achieve constitutive, cytokine-independent M1/M2 reprogramming by introducing gain-of-function modifications in their functional domains. Chapter 3 (Aim 2) leverages our previously developed drug-inducible synZiFTR platform to drive STAT protein expression with spatiotemporal control, incorporating a novel transcriptional activation domain (TAD) architecture to enhance transactivation potency for large payloads like STATs. Finally, Chapter 4 will integrate these advances, testing engineered STAT effectors and optimized synZiFTR 2.0 systems in primary macrophages to validate their ability to drive robust phenotypic switching. To ensure

translational relevance, we will also develop monocyte-targeting nanoparticle delivery systems for small-molecule inducers for synZiFTRs, adding a critical safety layer by restricting inducer delivery to target cell populations. Altogether, by integrating three synergistic innovations, we aim to address key translational challenges for macrophage therapies—**robust polarization and resistance to microenvironmental suppression, precise and inducible control, and safe in vivo delivery—while maintaining modularity for diverse diseases**. By combining transcriptional modulation, inducible regulation, and cell-specific targeting, this platform establishes a transformative strategy to overcome the durability, specificity, and adaptability limitations of current macrophage therapies. Beyond its immediate therapeutic applications, the system provides a modular framework for **probing fundamental questions in macrophage engineering**, offering new tools to bridge this knowledge and methodology gap, and help to usher in a new era of macrophage cell-based technologies and therapeutics. As our understanding of macrophage biology deepens, so too does our ability to harness these remarkable cells for broad applicability where immune modulation could provide clinical benefits.

CHAPTER TWO: MODULATING MACROPHAGE PHENOTYPE WITH ENGINEERED STAT PROTEINS

2.1 Introduction

Macrophage polarization is driven by complex signaling pathways that shape their activation states. Classical (M1) polarization is typically induced by stimuli such as interferon-gamma (IFN-γ) and lipopolysaccharide (LPS), which activate signaling pathways involving NF-κB, STAT1, and MAPKs (mitogen-activated protein kinases). These pathways drive the expression of pro-inflammatory cytokines, chemokines, and antimicrobial effector molecules, equipping macrophages to combat infections and promote inflammation. Conversely, alternative (M2) polarization is triggered by cytokines like interleukin-4 (IL-4) and IL-13, which activate STAT6, PPARγ (peroxisome proliferator-activated receptor gamma), and other signaling cascades. M2 macrophages are characterized by their anti-inflammatory, tissue-repair, and immunoregulatory functions, making them essential for resolving inflammation and promoting wound healing.

Within the complex signaling network for macrophage polarization, Signal Transducer and Activator of Transcription (STAT) proteins, a family of transcription factors, play an indispensable role in regulating macrophage immune responses. Upon activation by cytokines, STAT proteins are phosphorylated by receptor-associated kinases, such as JAKs (Janus kinases). This phosphorylation induces dimerization and nuclear translocation of STATs, where they bind to specific DNA sequences to regulate the transcription of a wide array of target genes involved in immune modulation, cell

proliferation, and apoptosis. Among STAT family members, STAT1 and STAT6 are particularly well-characterized in macrophages, mediating opposing functional outcomes. STAT1, activated by IFN-γ, promotes pro-inflammatory and antimicrobial responses, whereas STAT6, stimulated by IL-4 and IL-13, drives M2 polarization. Dysregulated STAT signaling contributes to chronic inflammation, autoimmune disorders, and cancer. As discussed in Chapter One, therapeutic strategies targeting STAT1 or STAT6 show promise in macrophage reprogramming, with a STAT6-degrading small molecule currently under investigation in a Phase 1 clinical trial for TH2-mediated inflammatory diseases. The ability to understand, utilize and manipulate these signaling pathways governing the broad spectrum of M1and M2 effectors not only elucidates immune regulation mechanisms but also offers opportunity to develop broadly applicable interventions across multiple disease models. Moreover, tunable and precise control in both directions of macrophage polarization is crucial to the safety of macrophage therapies, as excessive and insufficient activation can both lead to severe systemic side effects.

However, STAT protein activity is inherently dependent on cytokine signaling, rendering their functions susceptible to the local immune microenvironment and often skewing them toward pathological rather than protective roles in disease. Additionally, STAT proteins are tightly regulated by feedback mechanisms and inhibitory pathways under homeostasis, complicating sustained therapeutic modulation. In this chapter**, I propose to overcome these limitations by engineering constitutive STAT1 and STAT6 variants capable of robust and sustained induction of M1 and M2**

polarization, respectively. These engineered STAT proteins will be functionally validated in THP-1 monocytes across multiple levels—including DNA binding, transcriptional activity, protein expression, and downstream effector functions.

2.2 Designing and constructing constitutively active STAT1 and STAT6

Previous studies on STAT protein structure have identified the key phosphorylation sites and regions responsible for self-dimerization (Loh et al., 2019). With these insights, Sironi and Ouchi generated a mutant STAT1 protein, STAT1c, where two amino acids in the dimerization domain were replaced with cysteines, allowing cytokine-independent auto self-dimerization through disulfide bridge formation (Sironi and Ouchi, 2003). We drew inspirations from this study and the natural activation mechanisms of STAT proteins, and established two more variants of STAT1 proteins that can bypass other key steps in their activation. STAT1dp was generated by replacing the amino acids at two key STAT1 phosphorylation sites, Y701 and S727, with phosphomimetics (Y701F, S727D) to achieve a constitutively phosphorylated state (SadZak et al., 2008). STAT1-NLS fused the wild type STAT1 protein with a nuclear localization signaling domain (NLS) to force nuclear translocation. With the above three STAT1 protein variants, **I aim to engineer STAT1 proteins that are constitutively phosphorylated, or dimerized, or localized in the nucleus, even in the absence of cytokine induction.**

In another study, an extensive alanine scan mutagenesis of the STAT6 SH2 domain, the key region for STAT protein phosphorylation and dimerization, uncovered a gain-of-function mutation of STAT6 where the introduction of alanine at amino acid

position 547/548 altered STAT6 confirmation, rendering a constitutively active STAT6 (STAT6c) that can translocate to the nucleus and activate M2-related genes independent of external cytokine signaling (Daniel et at., 2000). In this study, we evaluated the functional impact of these engineered STAT1 variants alongside STAT6c in driving M1 and M2 polarization in THP-1 monocytes, respectively.

2.3 Characterization of STAT1 mutants-driven M1 phenotype

To assess and compare STAT1 mutants' activity, we first constructed a STAT1-responsive reporter to test their ability to access and bind to STAT1 DNA targets and activate downstream gene. We placed a fluorescent protein (iRFP) downstream 4x STAT binding sites that has been previously established (Satoh and Tabunoki, 2013) (**Figure. 1A**). All STAT1 mutants were fused with a N-terminal GFP and iRFP output was normalized to the GFP-STAT1 expression level. GFP-T2A-mCherry and wild type STAT1 (STAT1wt) were used as control to assess transduction-induced macrophage activation.

The STAT1-responsive reporter was lentivirally integrated in THP1 cells to generate a reporter cell line. The reporter cells were then transduced with STAT1 protein variants using lentivirus and the resultant reporter signals were measured on flow cytometer. All three STAT1 mutants drove higher reporter expression compared to the control groups. Notably, the expression of a wild type STAT1 protein (STAT1wt) also led to increased signal output, possibly due to activation of innate inflammatory pathways in response to PMA treatment and viral infection (**Figure. 1A, left**). However, when THP1 cells were cytokine-induced to M2 state, STAT1wt activity was partially

suppressed, while STAT1 mutants were able to maintain their functions, suggesting that wild type STAT1 proteins are susceptible to negative regulation by endogenous signaling pathways in a M2-polarizing environment (**Figure. 1A, right**). These findings underscore the need for engineered STAT1 variants that are potent, resilient, and capable of functioning independently of native regulatory mechanisms, particularly in pathological contexts where opposing polarization signals may dominate.

Next, we tested if STAT1 mutants can produce transcriptional and subsequent phenotypic level changes in THP- 1. Due to the inherent heterogeneity of macrophages, specific polarization markers and their transcriptome profiles can vary significantly depending on the cell line, the origin, the activation state and the environmental context (Nascimento et al., 2022,). Moreover, THP1 macrophages are generated by PMA treatment, followed by a resting period and further cytokine-induction to become M1 or M2 macrophages. The specific PMA concentration, PMA induction time, resting period duration, cytokine concentration and cytokine treatment time have all been shown to influence THP1 cell state (Baxter et al., 2019). To mitigate variability, we carefully selected an array of M1 cellular markers that are (1) previously established in THP1 cell lines and (2) consistently present across different differentiation conditions (Genin et al., 2015, Yasin et al., 2022, Yuan et al., 2015). We further validated the functionalities of STAT1 mutants under different PMA concentration (25nM and 150nM) to ensure M1 responses were cell state-independent. IFNg and LPS induced wild type THP1 cells (M1) were used as the positive control and PMA-treated wild type M0 THP1 cells were used as the reference state. qPCR analysis revealed that all three STAT1 mutants upregulated M1

effector genes following 150 nM PMA treatment, with some reaching levels comparable to IFN-γ/LPS-induced M1 controls (**Figure 1B, top**). However, STAT1-NLS and STAT1wt exhibited reduced activity under low PMA conditions, indicating sensitivity to cellular differentiation states **(Figure 1B, middle**). Upon M2 polarization with IL-4, M1 markers were downregulated across all groups, but STAT1c and STAT1dp demonstrated greater resistance to suppression compared to STAT1-NLS and STAT1wt (**Figure 1B, bottom**).

To further examine STAT mutants-driven phenotype, we investigated protein level M1 marker expression, such as cytokine production and surface receptor expression. TNFα, a universal and classic inflammatory factor secreted by M1 macrophages across essentially all cell line and species, was collected in cell culture supernatant and quantified using ELISA assay. All groups exhibited elevated and saturating level of TNFα secretion compared to untransduced M0 cells, including STAT1wt—likely due to the PMA and lentiviral effects (Figure. 1C). Notably, CD38, a pro-inflammatory surface marker that has been identified as positive prognosis marker in hepatocellular carcinoma (Lam et al., 2019), was significantly upregulated in STAT1 mutants-expressing cells compared to both untransduced M0 cells and STAT1wt expressing cells (Figure. 1D). These data demonstrate that STAT1c and STAT1dp, in particular, drive robust M1 polarization at the phenotypic level. However, despite these promising results, our experiments revealed inherent limitations. The reliance on PMA for THP-1 differentiation and lentiviral transduction for STAT1 delivery complicates the isolation of STAT1-specific effects from background activation. Additionally, constitutive M1 effector expression imposed

fitness costs on engineered macrophages, suggesting that inducible activation systems may be necessary to optimize cell longevity in vivo.

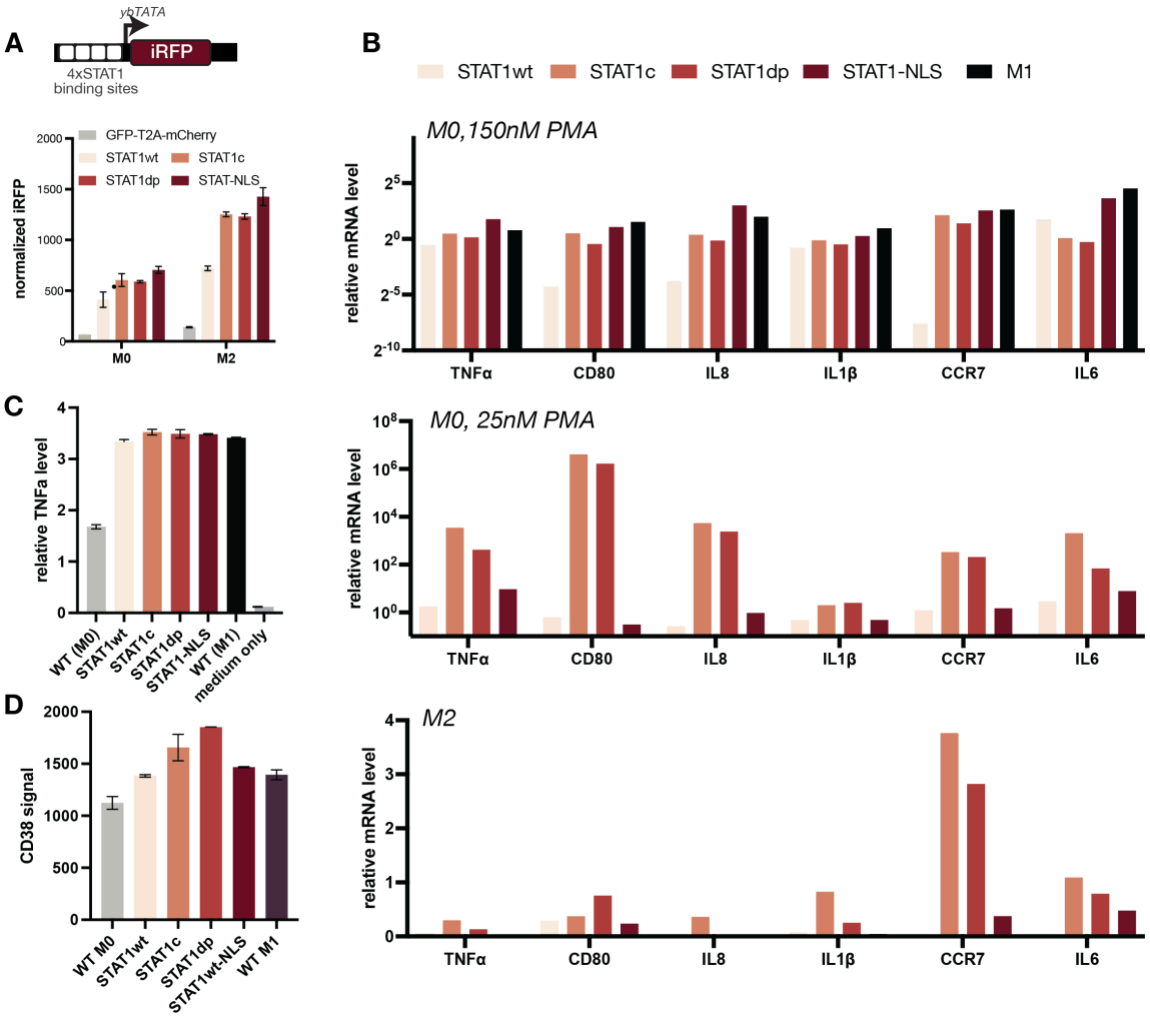

Figure 1. Characterization of STAT1 mutant protein-driven cell responses.

(A) iRFP fluorescent reporter was placed under 4x STAT1 binding sites and used to assess the DNA target-binding abilities of STAT1 mutants. All variants induced reporter expression across M0 and M2 states.

(B) Transcriptome analysis of selected M1 marker genes at different cell activation states, including high-level PMA-treated M0 state (top), low-level PMA-treated M0 state

(middle) and M2 state (bottom). STAT1-NLS only drives strong M1 gene expression with 150nM PMA treatment; STAT1c and STAT1dp sustain robust M1 responses with 25nM PMA treatment and even with M2 induction.

(C) Phenotypic characterization of M1 phenotype with TNFalpha secretion. All mutant proteins induce signal-saturating level of TNFalpha production.

(D) Phenotypic characterization of M1 phenotype with a M1 surface marker, CD38. STAT1c and STAT1dp upregulate CD38 expression compared to wild type STAT1 or STAT1-NLS.

2.4 Functional testing of STAT1 mutants in a 3D spheroid co-culture system

While in vitro characterization demonstrated the ability of STAT1 mutants to induce global M1 activation in THP-1 cells, their activity was partially diminished by M2 cytokine treatment (Figure 1). Although IL-4-induced M2 polarization in 2D culture represents an oversimplified model due to concentration- and duration-dependent effects, these observations prompted us to evaluate STAT1 mutant functionality in a more physiologically relevant tumor microenvironment (TME). To this end, we established a 3D spheroid co-culture system using THP-1 macrophages and MCF10A epithelial cells expressing either PI3K or ERbB2 oncogenes. Using this model, we explored how the interaction between macrophages and tumor cells affects their respective phenotypes and if STAT1 mutants were able to drive a robust M1 phenotype in TME, that we could exploit for therapeutic benefits.

To understand if macrophage polarization can drive functional changes in the tumor spheroid and if the changes are dependent on the tumor cell phenotypes induced by

different oncogenes, we first co-cultured PI3K MCF10A and ERbB2 MCF10A cells with cytokine induced M1 THP1 cells. M1 cells completely inhibited the formation of spheroids for both types of tumor cells across 7 days, by which time spheroids started to naturally disintegrate. In contrast, in the THP1 monocytes and tumor cells cocultures, spheroids emerged within 24h with their hallmark rounded shapes and necrotic central cores formed by the oxygen and nutritional gradients across the structure (**Figure. 2A**). Encouraged by these results, we next tested STAT1 mutants-expressing THP1 cells in the same spheroid models. In the 7-day co-culture, STAT1 mutant-expressing cells were not able to inhibit the initial formation of spheroids. However, by day 3, clear morphological disruptions were observed in cultures with both tumor cell types. In PI3K spheroids, spheroids lost the roundness of their shapes and exhibited more irregular architectural structure, a hallmark for loss in cell viability (**Figure. 2B**). While ERBb2 spheroids, maintained their overall shape, quantitative analysis revealed STAT1c- and STAT1dp-expressing macrophages significantly increased the necrotic core-to-total area ratio (**Figure. 2C**), with corresponding amorphous cell debris observed in culture wells. These results demonstrate the tumor-suppressive effects of STAT1-engineered macrophages in an oncogene-specific manner.

As macrophages in TME are known to be reprogrammed towards a less proinflammatory M1-like, more pro-tumorigenic M2-like phenotype, here we examined the loss of M1 response in macrophages using the STAT1-responsive reporter to explore if STAT1 mutants could maintain activity in the immunosuppressive TME. We compared reporter signal intensity between macrophages in monoculture versus those extracted

from disintegrated spheroids for the two best-performing STAT1 mutants, STAT1c and STAT1dp. Reporter cells with no integration of engineered STAT1 proteins were used as the negative control (reporter only). While the non-tumorigenic, wild-type MCF10A cells did not cause significant loss in reporter signal, both PI3K and ERbB2 cells sequestered the M1 response in THP1 cells, particularly prominent in the reporter only group. Notably, STAT1c and STAT1dp exhibited significant resistance to this suppression, with each variant showing preferential activity against PI3K- or ERbB2-driven tumors, respectively (**Figure 2D**). This sustained M1 activation correlated with observed tumoricidal effects, supporting their therapeutic potential in solid tumors.

One particularly appealing cell function of macrophages in TME is their recruitment and infiltration into solid tumors. To test if our spheroid model can recapitulate this cell activity and more importantly, if STAT expression negatively impacts cell migratory ability, we designed a second spheroid model, the recruitment model, where we only added macrophages to spheroids after their initial formation. We fluorescently labeled macrophages and tracked their localization in the co-cultures. STAT1-engineered macrophages displayed distinct infiltration patterns depending on tumor genotype: by day 3, both STAT1c and STAT1dp variants fully penetrated PI3K spheroids, while ERbB2 spheroids remained largely intact through day 5, with macrophages accumulating peripherally (**Figure 2F**). This divergence likely reflects fundamental differences in tumor biology rather than macrophage function—ERbB2 signaling enhances cell-cell adhesion and epithelial-mesenchymal transition (EMT) (Guo et al., 2006, Brix et al., 2014), resulting in more cohesive, invasive tumors that may

physically impede macrophage infiltration.

Altogether, our studies demonstrates that engineered STAT1 mutants (STAT1c and STAT1dp) drive robust and sustained M1 macrophage polarization, overcoming the immunosuppressive signals present oncogenic tumor spheroids. These variants disrupted spheroid integrity and induced tumor cell death, while showing resistance against TME-mediated reprogramming, maintaining M1 activity even in immunosuppressive conditions. While macrophage infiltration patterns varied depending on tumor cell adhesion properties, the anti-tumor effects of STAT1-engineered macrophages highlight their therapeutic potential for solid cancers. These findings validate the utility of constitutive STAT1 variants for macrophage-based therapies and underscore the importance of context-specific design for overcoming TME-driven immune evasion.

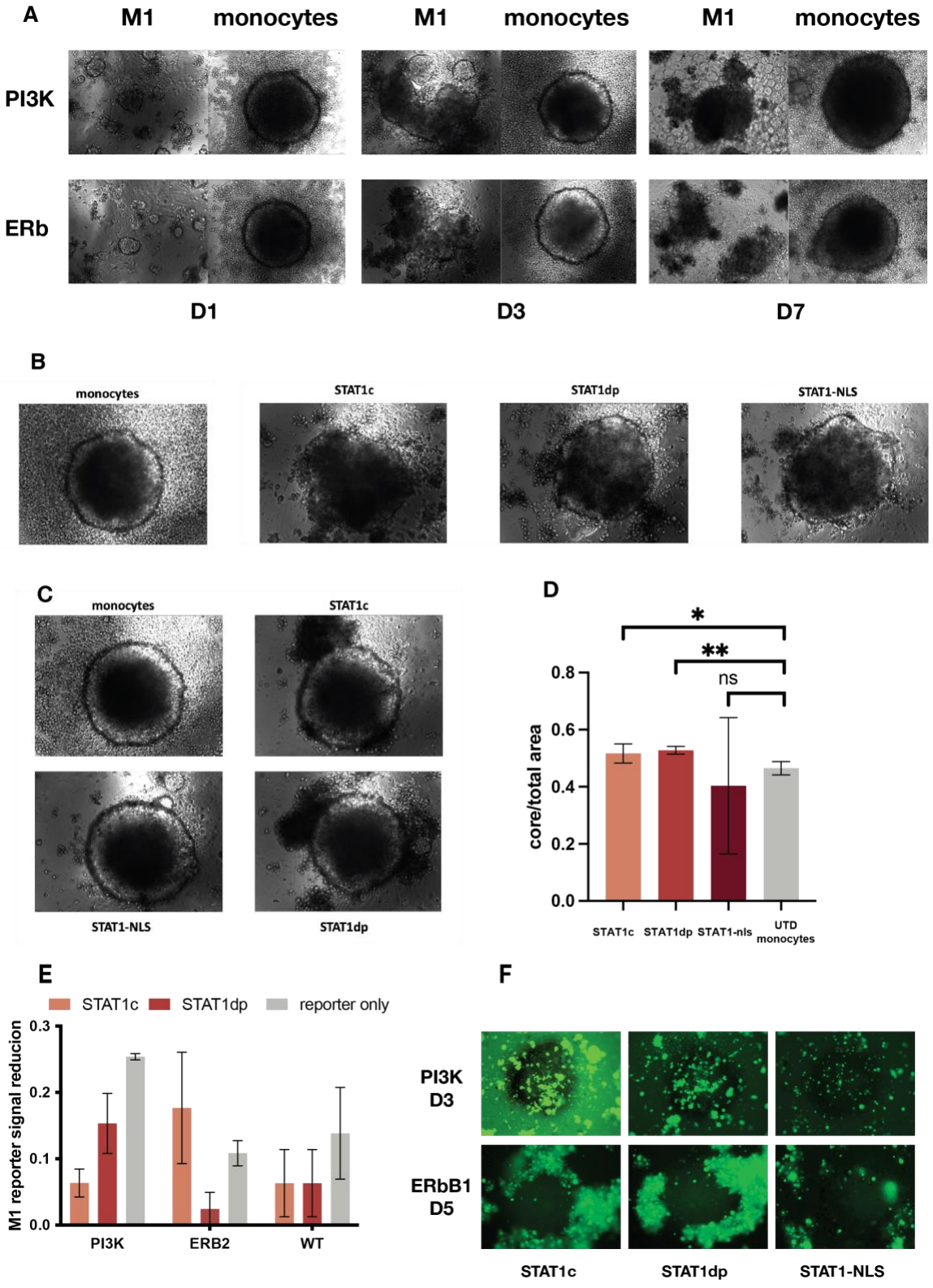
A
M1
monocytes
M1
monocytes
M1
monocytes
PI3K
ERb
D1
D3
D7
B
monocytes
STAT1c
STAT1dp
STAT1-NLS
C
monocytes
STAT1c
STAT1-NLS
STAT1dp
D
*
**
ns
core/total area
0.8
0.6
0.4
0.2
0.0
STAT1c
STAT1dp
STAT1-nls
UTD monocytes
E
STAT1c
STAT1dp
reporter only
M1 reporter signal reducion
0.3
0.2
0.1
0.0
PI3K
ERB2
WT
F
PI3K D3
ERbB1 D5
STAT1c
STAT1dp
STAT1-NLS

Figure 2. Functional characterizations of STAT1 effectors-driven M1 polarization in 3D spheroid models.

(A)Cytokine-induced M1 macrophages inhibit the formation of spheroids, validating the model for assessing STAT1-mutant-induce M1 responses and therapeutic potential.

(B)Engineered STAT1 effectors caused phenotypic disruptions in PI3K spheroid morphology by day 3, indicated by the loss in their round shapes and diffuse necrotic core.

(C)-(D) Engineered STAT1 effectors did not significantly affect the morphology of ERbB2 spheroids, but increase necrotic cores ratios by day 4, suggesting tumor-killing activity by STAT1c and STAT1dp.

(E)STAT1c and STAT1dp sustained their M1-polarization capabilities and drove persistent M1 responses in TME, as shown by stable M1 reporter signal with minimal decay.

(F) Recruitment spheroid models reveal that STAT1c and STAT1dp-expressing macrophages were able to infiltrate PI3K spheroids into necrotic cores, but ERbB2 spheroids are resistant to macrophage invasion.

2.5 Characterization of STAT6 mutant-driven M2 phenotype

STAT6 reporter was constructed by modifying a previously established luciferase reporter, replacing the luciferase domain with mCherry fluorescent protein. 4 tandem copies of STAT6/cEBP binding sites were placed upstream mCherry and a minimal promoter (ybTATA). A STAT6-responsive reporter cell line was established using lentiviral transduction.

STAT6c and wild type STAT6 protein (STAT6wt) were integrated in reporter cell lines and the resultant reporter outputs were measured on flow cytometer. STAT6c drove significantly higher reporter signal than STAT6wt in both resting M0 state and IFN gamma + LPS induced M1 states, demonstrating its robust transcriptional activity across cell states (**Figure. 3A**). To further assess STAT6c functionality, we took a similar approach as that for STAT1 mutants characterization. Transcriptional profiling of established M2 markers showed that STAT6c-expressing cells upregulated M2-associated genes to levels comparable to IL-4-induced M2 controls, despite the inherent pro-inflammatory bias imparted by PMA differentiation and lentiviral transduction (**Figure 2B**). At the protein level, STAT6c specifically induced secretion of the anti-inflammatory cytokine IL-10 and surface expression of the characteristic M2 marker CD206, effects not observed in control cells (**Figures 2C, 2D**). These findings collectively demonstrate that STAT6c effectively reprograms macrophages toward an M2-like phenotype and maintains this polarization even in the presence of conflicting M1-polarizing signals.

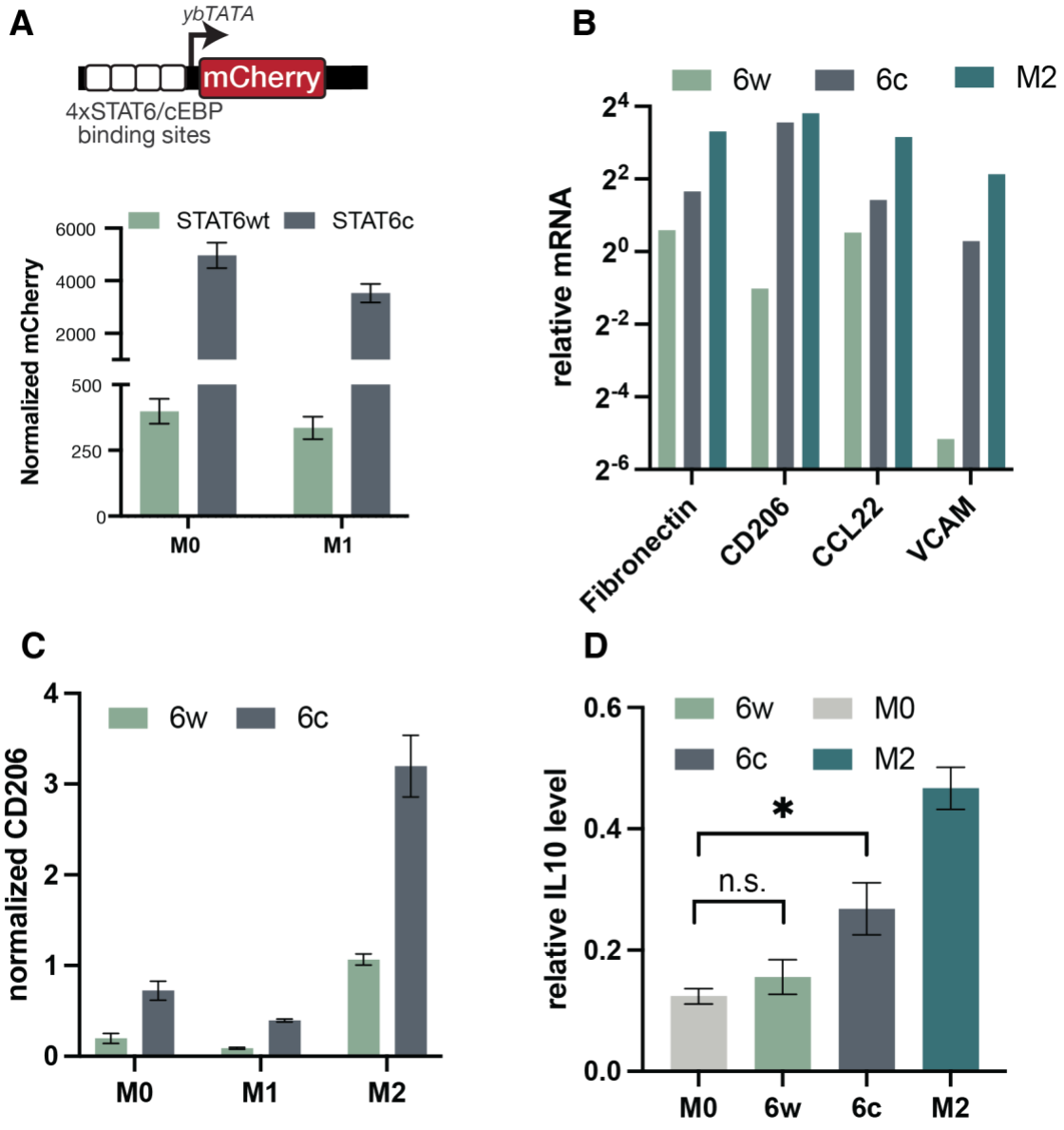

Figure 3. Characterization of STAT6c-driven M2 cell responses.

(A) DNA-binding activity of STAT6c assessed using an mCherry reporter under control of 4× STAT6 binding sites. STAT6c activated reporter expression in both M0 and M1 states.

(B) Transcriptional upregulation of M2 markers by STAT6c, reaching levels comparable to cytokine-induced M2 macrophages.

(C-D) STAT6c enhanced expression of the M2 surface marker CD206 (C) and secretion of the M2-associated cytokine IL-10, measured by ELISA (D).

2.6 Discussion and future perspectives

In this chapter, we investigated **distinct engineering strategies to develop constitutively active STAT protein variants capable of driving macrophage polarization independently of cytokine signaling**. We evaluated two previously characterized constructs (STAT1c and STAT6c) alongside two novel designs (STAT1dp and STAT1-NLS), systematically assessing their functionality across multiple targets, cellular states, and microenvironmental contexts. For M1 polarization, STAT1c and STAT1dp demonstrated consistent and robust activity, even under opposing polarization signals such as M2 cytokines and tumor microenvironment (TME) conditions. In contrast, STAT1-NLS, while capable of inducing measurable M1 responses, frequently lost activity under these challenging conditions, mirroring the behavior of wild-type STAT1 (STAT1wt).

Existing literature provides mechanistic insights into these observed differences. The STAT1-NLS variant operates through nuclear localization without dimerization, whereas native STAT1 typically forms dimers upon activation, binding to palindromic gamma-activated sequence (GAS) elements in DNA. Dissociation of STAT1 dimers from DNA and subsequent dephosphorylation require extensive spatial reorganization of the monomeric units (Mertens et al., 2006). Furthermore, multiple STAT dimers can cooperatively stabilize DNA binding through N-terminal interactions at adjacent GAS sites, reducing dissociation and dephosphorylation rates - features absent in monomeric

STAT1 configurations (Wenta et al., 2008; Riebeling et al., 2014). Although STAT1 monomers retain some DNA-binding capacity and can activate certain M1-associated genes (Yang and Stark, 2008), their simplified structural organization renders them more prone to dissociation, nuclear export, and subsequent inactivation. Future studies employing fluorescently tagged STAT1 variants for intracellular tracking or dimerization analysis by western blot could further test this hypothesis.

While our primary focus centered on STAT1 engineering and M1 macrophage polarization - given their emerging therapeutic potential for tumor microenvironment modulation - similar design principles could be productively applied to STAT6 proteins. We established a comprehensive framework for evaluating both M1 and M2 polarization responses in vitro, providing a generalizable approach for future investigations. To further characterize M2 macrophage functionality, we are developing a scratch wound-healing assay to examine anti-inflammatory and tissue-repair responses in a physiologically relevant context.

A significant limitation of this study relates to the THP-1 cell model. As noted previously, macrophages exhibit considerable functional heterogeneity, with responses highly dependent on cellular context. While THP-1 cells remain widely used due to their ease of culture, proliferation, differentiation, and genetic manipulation— and demonstrate core macrophage functions including phagocytosis, polarization, and inflammatory responses comparable to primary macrophages in some instances (Madhvi et al., 2019) - they represent an oversimplified model with restricted functional diversity relative to primary cells for polarization and phagocytosis studies (Tedesco et al., 2018;

Hoppenbrouwers et al., 2022). Additionally, as described earlier, the differentiation and transduction protocols themselves induce THP-1 activation, potentially biasing results toward M1 responses. Genetic ablation of endogenous STAT1 could mitigate baseline M1 activation, though this may concomitantly reduce global pro-inflammatory signaling capacity.

In summary, our preliminary investigations demonstrate **the functional efficacy of engineered STAT proteins**, with STAT1c and STAT1dp emerging as particularly potent M1-polarizing factors suitable for integration into drug-inducible macrophage polarization systems. Future work will focus on validating these constructs in primary human macrophages and conducting more comprehensive phenotypic characterization to further establish their therapeutic potential.

2.7 Materials and Methods

2.7.1 Mammalian Cell Culture

All cells were maintained in 10 cm treated dishes, 75mL flasks or 175mL flasks at 37 °C and 5% CO_2. Cells were passaged every 3-4 days when they reached 70-80% confluency or ~1million cells/mL.

HEK293FT cell lines (Thermo Fisher Scientific R700-07) were cultured in Dulbecco's Modified Eagle's Medium (Corning 10-013-CV) supplemented with 10% Fetal Bovine Serum (Takara Bio 631367), 1% GlutaMAX (Thermo Scientific 35050061), 1% Non-Essential Amino Acids (Thermo Scientific 11140050), and 1% Penicillin-Streptomycin (Thermo Scientific 15140122). Jurkat cell lines (ATCC TIP-152) were cultured in RPMI 1640 Medium (Corning 10-040-CV) supplemented with 10% FBS, 1%

GlutaMAX, and 1% Pen-Strep. THP1 cell lines (ATCC TIB-202) were cultured in RPMI 1640 Medium supplemented with 10% FBS, 1% GlutaMAX, 1% Non-Essential Amino Acids, 1% Sodium Pyruvate (Thermo Scientific 11360070) and 1% Pen-Strep. NALM6 target cell lines were cultured in RPMI 1640 Medium supplemented with 5% FBS, 1% GlutaMAX (Gibco A2916801), and 1% Pen-Strep. MCF10A target cell lines were cultured in DMEM/F-12 (Gibco 11320033) supplemented with 5% Horse Serum (Gibco 16050130), 1% Pen-Strep, 20ng/mL EGF (Peprotech), 0.5 mg/mL hydrocortisone (Sigma H-0888), 100ng/mL Cholera Toxin (Sigma C-8052), and 10ug/mL Insulin (Sigma I-1882).

2.7.2 Lentiviral Transduction of Cell Lines

Cassettes cloned into lentiviral donor plasmids were integrated into THP1 and Jurkat cell lines using lentiviral infection. Lentivirus was harvested from transfected CRISPRed HEK293T to Disrupt Antiviral Response (CHEDAR) cells (Han et al.,2021) 700,000 CHEDAR cells were seeded into 6-well treated plates for 24 hours and subsequently transfected with 2 ug total DNA using TransIT-Lenti Transfection Reagent (Mirius Bio MIR 6600). 1 ug of the donor plasmid was co-transfected with 700 ng of the pCMVR8.74 plasmid (Addgene #22036), 100 ng of the pAdVantage plasmid (Promega), and 200 ng of the pMD2.G VSVG plasmid (Addgene #12259). Upon transfection, cells were incubated for 72 hours prior to harvesting media containing lentiviral supernatant. Lentiviral media from each well was centrifuged for 5 minutes at 400 g to remove cell debris and concentrated using Lenti-X Concentrator (Takara Bio 631232) at a 3:1 volume ratio. Lentiviral-concentrated media was incubated at 4C overnight, prior to

centrifugation at 4C at 1600 g for 60 minutes and resuspension in 100uL Opti-MEM I Reduced Serum Medium (Thermo Scientific 31985062).

500,000/well THP1 cells were seeded into 24-well treated plates in 800uL media. 8ug/mL Polybrene Infection Reagent (EMD Millipore TR-1003-G) was added to each well prior to adding 100uL of each concentrated lentiviral solution. Cells were transduced by lentiviral spinfection by being spun 800g for 45 mins. Infected cells were incubated overnight prior to removal of lentivirus. Cells were washed by centrifugation at 300g for 5 mins three times. Transduced cells were subsequently used for downstream induction measurements.

2.7.3 Flow Cytometry

All flow cytometry measurements were performed on an Attune NxT Flow Cytometer (Thermo Fisher Scientific). Live cells were gated by forward scatter (FSC) and side scatter (SSC). Fluorescence data was collected for GFP (excitation laser: 488nm, emission filter: 530/30nm), iRFP-720 (excitation laser: 640nm, emission filter: 720/30nm), BFP (excitation laser: 405nm, emission filter: 440/50nm), and mCherry (excitation laser: 561nm, emission filter: 620/15nm). A minimum of 10,000 live cells were collected for each sample in triplicates. Flow cytometry data was analyzed using FlowJo (Treestar Software). Data was further analyzed using the Prism 8 software (GraphPad).

2.7.4 THP1 Differentiation

THP1 cells are differentiated with 25nM or 150nM (if specified) phorbol 12-myristate-13-acetate (PMA) (EMD Millipore) for 48h and then rested in PMA-free

medium for 24h to generate M0 macrophages. M0 cells were treated with 10ng/uL of human recombinant IFNγ (Peprotech) and 10ng/uL LPS (Fisher Scientific) for 24h to generate M1 macrophages or 10ng/uL recombinant human IL4 (R&D Systems) for 24h for M2 macrophages. Unless reported otherwise, all transduced cells were assessed at M0 states.

2.7.5 qPCR

Total RNA from 0.5-1 million of THP1 macrophages are extracted using RNeasy mini kit (Qiagen 74104) and treated with DNase (Qiagen 79254) following recommended protocols provided by the kit. RNA was reverse transcribed to cDNA using Maxima First Strand cDNA Synthesis Kit for RT-qPCR (Fisher Scientific FERK1641). PCR reactions were set up with 0.5uL cDNA, 1uL primer mix, 3.5uL DI water and 5uL LightCycler480 SYBR Green Master Mix (Roche 04887352001). Reactions were run at 95°C for 5 mins, and 45 amplification cycles of 10s at 95°C, 10s at 60°C, 10s at 72°C. Melting curve was generated with temperature raise from 65°C to 97°C at a rate of 0.11°C/second. RPS9 was used as the reference gene for all samples and relative mRNA expression levels were calculated as $2^{-\Delta\Delta Ct}$ using untransduced M0 macrophages as the baseline. The primer sequences used in this study are listed in Table 1.

Table. 1 qPCR primers sequences used for M2 and M2 phenotype characterization

Target gene	Forward primer	Reverse primer
TNFα	CTGCACTTTGGAGTGATCGG	TCAGCTTGAGGGTTTGCTAC
CD80	ACGCCCTGTATAACAGTGTCC	GAGGAAGTTCCCAGAAGAGGTC
IL-8	TCTGTGTGAAGGTGCAGTTTT	GGGGTGGAAAGGTTTGGAGTA
IL-1β	GCCCTAAACAGATGAAGTGCTC	GAGATTCGTAGCTGGATGCC
CCR7	CAG ACA GGG GTA GTG CGA GGC	CCA GCA CGC TTT TCA TTG
IL6_2	TCTCCACAAGCGCCTTCG	CTCAGGGCTGAGATGCCG
Fibronectin	TGTGGTTGCCTTGCACGAT	GCTTGTGGGTGTGACCTGAGT
CD206	GCTAAACCTACTCATGAATTACTTAC AACAA	GAAGACGGTTTAGAAGGGTCCAT
CCL22	TGTGGTTGCCTTGCACGAT	GCTTGTGGGTGTGACCTGAGT
VCAM	CAGGCTAAGTTACATATTGATGACAT	GAGGAAGGGCTGACCAAGAC
RPS-9	GGCGCAGACGGTGGAAGC	GGTCTCCGCGGGGTCACAT

2.7.6 ELISA

M0, M1 or M2 macrophages are plated at 50,000-100,000/well in RPMI medium and cultured for 48-72h. Supernatant from the cultures of specific volumes required by each ELISA kit were harvested and spun at 400g for 5 mins to eliminate cell debris. R&D Human TNF alpha Qunatikine ELISA Kit (Fisher Scientific DTA00D), Human IL-10 Qunatikine ELISA Kit (Fisher Scientific D1000B) were used to quantify the amount of TNF alpha and IL10 in M1 and M2 macrophage culture, respectively, following vendor's protocols.

2.7.7 Antibody Staining

Differentiated THP1 cells were lifted from plates with 20 mins of TrypLE Express Enzyme (Fisher Scientific) treatment under 37°C. Lifted cells were spun down at 300g for 5 mins and treated with Fc block (Fisher Scientific) for 10 mins then stained with Pacific Blue Anti-Human CD206 Antibody (BioLegend 321151) or CD38 Mouse

Anti Human, Brilliant Violet 405 Antibody (Fisher Scientific, BDB562665) for 20 mins under room temperature. Stained cells were washed with FACS buffer twice and run on flow cytometer.

2.7.8 Spheroid Model

ErbB2 (Her2+) or PI3K MCF10A cells were lentivirally transduced with BFP. THP1 cells were transduced with the STAT-1 responsive reporter and different GFP-tagged STAT1 variants. To generate 3D spheroids, 10,000 MCF10A cells and 5,000 THP1 macrophages were seeded into Corning 96-well Black/Clear Round Bottom Ultra-Low Attachment plates (Fisher Scientific). Spheroids morphologies were characterized using microscopy imaging and the necrotic core ratio was analyzed with ImageJ throughout day1-day7, when spheroids naturally start to disintegrate in culture. To assess macrophage responses to TME, spheroids were treated with Trypsin-EDTA (0.05%) for 30 mins and cells were run on flow cytometer. $BFP^{-}GFP^{+}$ cells were identified as macrophages, and the reporter signal levels were measured within this population.

CHAPTER THREE: SYNZIFTR 2.0—OPTIMIZING GENE REGULATION CIRCUITS FOR MACROPHAGE ENGINEERING

3.1 Introduction

Cells use networks of regulatory molecules to convert signals into appropriate output responses. Central to this process is transcriptional regulation, which enables cells to dynamically decode vast genomic information and mount precise responses to diverse stimuli. Synthetic biology exploits this paradigm by engineering artificial transcriptional circuits that mimic natural networks, empowering therapeutic cells with programmable decision-making capabilities. Such engineered systems hold immense potential for developing next-generation cell therapies that can reliably interpret physiological signals and precisely execute tailored, clinically relevant functions.

To enable this vision, Khalil lab developed synZiFTRs, a powerful set of synthetic transcriptional regulators that are fully humanized, modular, titratable and therefore clinically optimized for drug-inducible control of therapeutic human cell functions (Li, Israni, et al., 2022) (**Figure 4A)**. While synZiFTRs successfully programmed sophisticated sense-and-response capabilities in primary human T cells, their transactivation potency was insufficient to drive large cargos like STAT protein expression in THP1 cells (Figure 4B, left). Moreover, synZiFTRs development uncovered a fundamental design constraint: the trade-off between potency and safety. For example, replacing the human transcriptional activator domain (TAD) in synZiFTR, p65, with a viral-derived TAD, VPR, dramatically increased transactivation output, but abolished drug inducibility and raised concerns about potential in vivo toxicity (**Figure**

4B, right) (Yamagata et al., 2020, Ewen-Campen et al., 2017). This result highlights a grand challenge in synthetic transcriptional regulation in human cells—achieving high performance across diverse cell types and clinical contexts while relying exclusively on humanized components to ensure safety and controllability. Overcoming this hurdle is essential for translating engineered gene circuits into viable cell therapies, particularly for cells like macrophages that hold tremendous therapeutic potential but challenging to be genetically manipulated.

The efficacy of synthetic transcriptional regulators hinges on TAD performance, yet systematic understanding of TAD function across cell types remains limited. Recent efforts have addressed this gap through high-throughput pooled screening, in search for native, robust and compact transcriptional activator elements in the human genome, yielding novel and potent TAD such as NFZ (Tycko *et al.,* 2020, Mahata, *et al,* 2023, Alerasool *et al.,* 2022, Mukund *et al.,* 2023, Tycko, et al., 2024). To achieve the same goal, here we pursued an alternative strategy inspired by transcriptional cooperativity, a natural mechanism in human cells to enhance gene expression through synergistic TF interactions. Distinctive from our previous work that leveraged the physical TF-TF interactions (**Figure 4C, top left)** (Bragdon et al., 2023), we now focus on kinetic synergy, a less explored form of cooperativity that has only been tested in quantitative models, where two TFs can synergistically promote transcription by stimulating distinct steps in transcriptional cycle that are rate-limiting **(Figure 4C)** (Scholes et al., 2017, Martinez-Corral et al., 2023). By designing a targeted screen uniquely set up to identify TF elements that can kinetically synergize with p65, we built upon the original synZiFTR

architecture and engineered cooperative circuits, synZiFTRs 2.0, which demonstrated enhanced transcriptional output while retaining low basal leakiness and full inducibility. This approach represents a paradigm shift towards harnessing natural transcriptional principles such as kinetic cooperativity—rather than brute-force activation domains—to optimize the safety and efficacy of synthetic gene circuits for cell therapies.

3.2 Discovery of IWS1 TIMs domain as a strong transcriptional stimulator

In pursuit of human-derived components capable of kinetically synergizing with p65 to enhance synZiFTR activation potency, we performed a targeted screen of carefully selected, well-characterized protein domains from transcription factors known to modulate various stages of the transcriptional cycle. To optimize clinical translatability, we engineered these elements as fusions with p65 and ZF10, incorporating this fully humanized gene regulation cassette into a TetON-inducible system for evaluation in Jurkat cells as an immune cell model. Comparative analysis against p65 alone revealed that multiple domains enhanced reporter output. Most notably, the N-terminal TND-interacting motifs (TIMs) domain from the IWS1 elongation factor demonstrated superior performance, generating the highest induced-state signal output while maintaining minimal basal expression in the uninduced state (**Figure 4D**). The TIMs domain's compact size (43 amino acids) presents particular advantages for clinical implementation, as it substantially improves the system's dynamic range while adding minimal genetic payload - a crucial consideration for in vivo delivery of synthetic gene regulation tools.

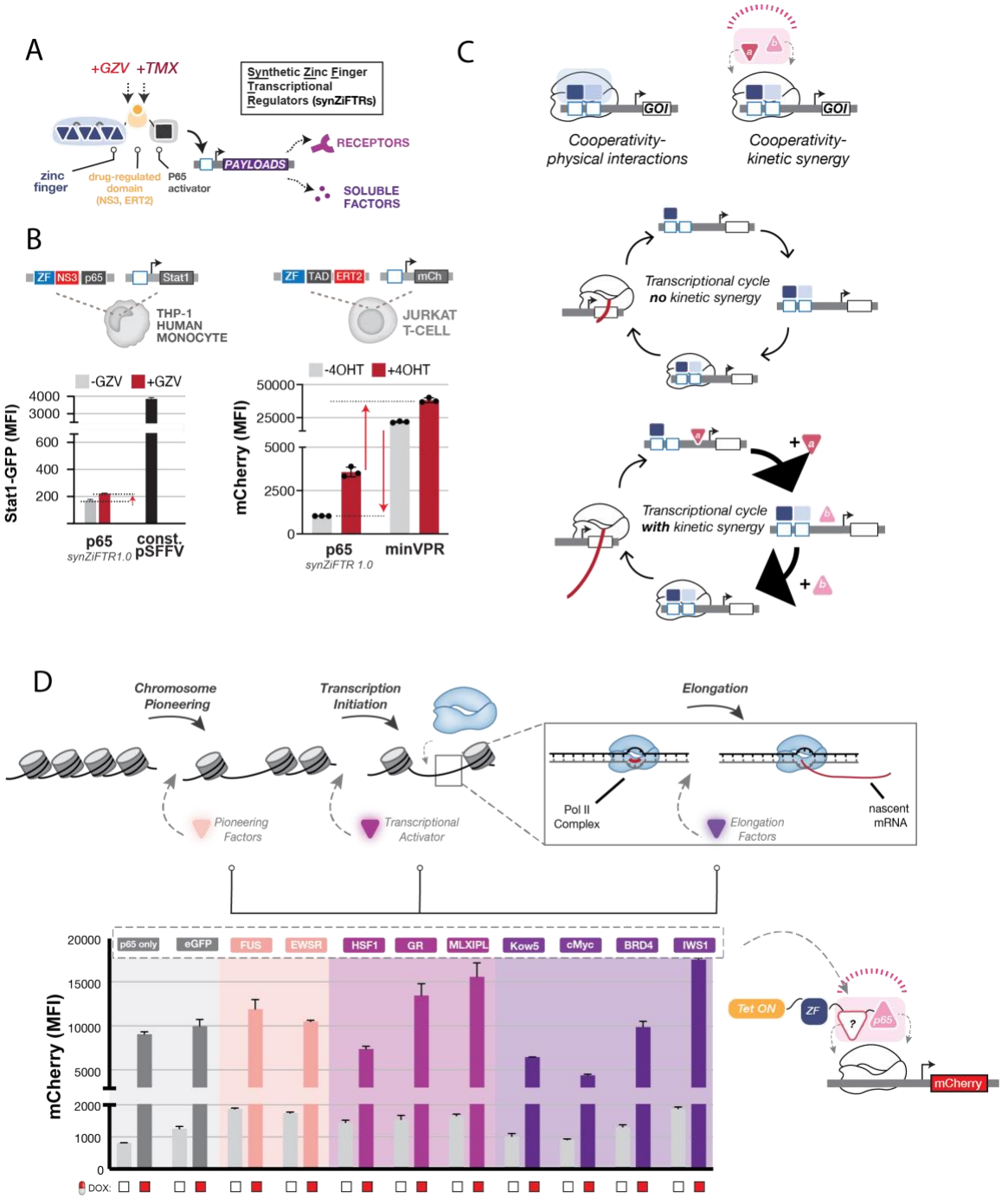

Figure 4. Optimizing synZiFTRs by TAD engineering and kinetic synergy.

(A) synZiFTR architecture features a compact, synthetic ZF-finger that's orthogonal to the human genome, the p65 transactivation domain and a drug inducible domain for

inducible regulation of therapeutic payloads such as CAR and proliferating cytokine IL2.
(B) synZiFTR-driven STAT expression in THP1 monocytes showed weak induction compared to the constitutive pSFFV promoter (left). Substituting p65 with VPR increased transactivation activity but abolished inducibility in ERT-synZiFTR (right), rendering it unsuitable for clinical use.
(C) Conceptual framework of kinetic synergy: unlike physical TF cooperativity, synergistic enhancement occurs when TFs stimulate distinct rate-limiting steps in the transcription cycle, resulting in higher level of transcriptional outputs.
(D) Targeted screen of transcriptional regulators, guided by kinetic synergy principles, identified the IWS1 TIMs domain as a p65 synergist that maximizes transactivation while minimizing basal leakage.

3.3 Development of synZiFTR2.0 with IWS1 TIMs

To test our newly discovered TAD architecture, we next imported the IWS TIMs (TIMs) into the GZV-inducible NS3 synZiFTR and 4OHT-inducible ERT synZiFTR. Through systematic screening of various TIMs-p65 domain arrangements (**Figure 5A)**, we identified that N-terminal TIMs integration significantly enhanced transcriptional output while maintaining tight control in both inducible systems (**Figure 5B)**. These results also highlight that TIMs functionality is independent of induction mechanism, as evidenced by its consistent and robust performance across three drug-inducible systems.

To leverage the compact size of TIMs, we investigated if multiple copies of TIMs could further boost the TAD transactivation potency. Remarkably, dual TIMs (2xTIMs)

exhibited synergy beyond simple additive effects, producing over 2x higher signal outputs compared to single-TIMs constructs (**Figure 5C)**. Addition of a third TIMs domain showed modest further enhancement, and the inclusion of a TIMs-size flexible linker also did not show transactivation benefits, indicating the observed synergy of 2xTIMs stems from intrinsic TIMs protein function rather than spatial organization or conformational differences (**Figure S1)**.

With these newly uncovered design principles and insights into TIMs function, we designed a novel TAD architecture by fusing 2xTIMs upstream of p65 in the original synZiFTRs and named these new constructs **synZiFTRs 2.0**. We tested synZiFTRs 2.0 performance in Jurkat cells and demonstrated that synZiFTRs 2.0 not only showed significant enhancement from synZiFTR 1.0, but also outperformed some of the most well-known and potent viral-derived TADs such as VPR and minVPR (**Figure 5C)**.. Notably, synZiFTRs 2.0 maintained crucial inducible system properties: (1) a strong transactivation output, (2) minimal basal leak, and (3) full retention of inducibility in both induction systems—features where viral TADs consistently failed. This work establishes proof-of-principle for our kinetic synergy-driven TAD engineering, yielding a novel TAD architecture and a potent, fully humanized second-generation human cell gene regulation toolkit optimized for next-generation cell therapies.

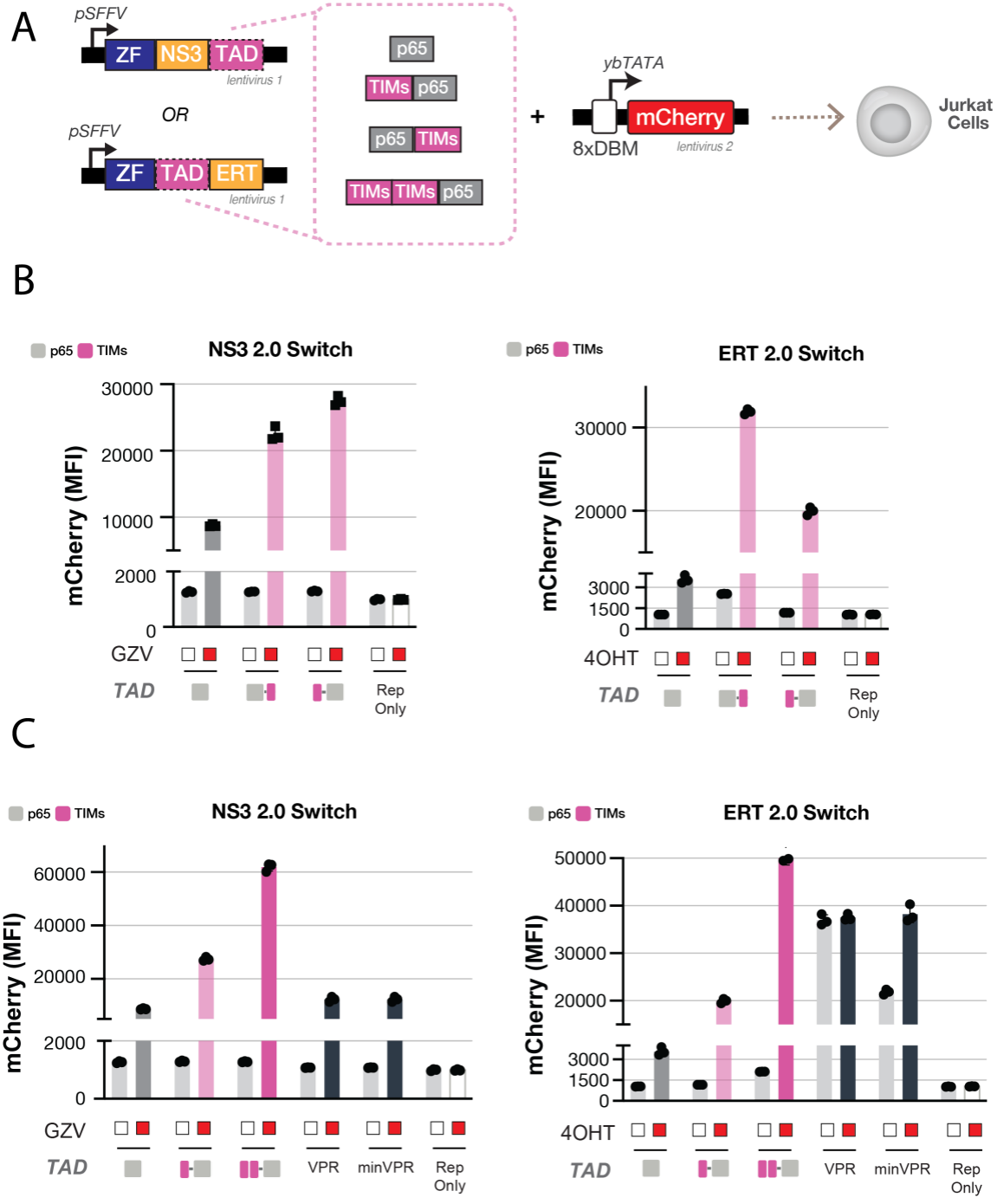

Figure 5. Optimization of TAD architecture in synZiFTR 2.0.

(A) Systematic evaluation of TAD configurations in both NS3- and ERT-synZiFTR platforms to identify optimal arrangements.

(B) The N-terminal TIMs domain demonstrated the optimal balance between transcriptional potency and baseline leakage.

(C) Dual TIMs copies exhibited synergistic enhancement, outperforming both VPR and minVPR in induction efficiency across systems. This optimized architecture (2xTIMs-p65) was designated synZiFTR 2.0.

3.4 Mechanistic insights into TIMs functions in synZiFTR 2.0 as an elongation stimulator

3.4.1 Functional roles of TIMs subdomains

How does such a small effector like TIMs so drastically improve the performance of synZiFTRs? To better understand TIMs and its role in transcriptional regulation, we investigated previously established knowledge in IWS1 and TIMs domains. TIMs domains are intrinsically disordered regions that are highly conserved and enriched among elongation factors. TIMs interacts with TFIIS N-terminal Domains (TNDs), and these binary reactions are ubiquitously throughout the elongation network. While TIMs domains are not exclusively found in IWS1, IWS1 TIMs is uniquely comprised of three subdomains, each interacting with a specific set of elongation factors, making IWS1 a central hub for organizing elongation machinery. Specifically, TIM1 subdomain binds with TFIIs or EloA, TIM 2 with PPP1R10 (PNUTS) and TIM 3 with LEDGF/HRP2 (Cermakova, K. et al., 2021). Each set of these elongation factors mediate distinctive steps in the elongation process. LEDGF and HRP2 are known epigenetic regulators that colocalize with H3K36me3 to assist RNAP2 overcome nucleosome-induced barriers to

productive transcription (LeRoy et al., 2019). TFIIs and EloA stimulate active elongation by functions like rescuing RNAP2 from backtracking to resume elongation, forming active RNAP2 preinitiation complexes (PIC) for elongation initiation and reinitiation, and regulating active RNAP2 conformation, while PPP1R10 plays a critical role in elongation termination and RNAP2 pause release (Zatreanu et al., 2019, Kim et al., 2007, Chen et al., 2023, Cartazar et al., 2019, Austenna et al., 2015, Landsverk et al., 2020, Kelley et al., 2024). Through these interactions, IWS1 and these other elongation factors collectively modulate RNAP2 activity and dictate the landscape of elongation kinetics and dynamics.

Seeing the clear structural and functional divisions among different TIMs subdomains, we first asked the question which one(s) of these TIMs subdomains enable and drive TIMs function in synZiFTRs 2.0. Using prior knowledge, we generated GZV synZiFTRs2.0 switches containing TIMs mutants that abolish the function of each of the TIMs subdomains (M1, M2, M3, M123), as previously described (Cermakova, K. et al., 2021). The mutagenesis studies revealed that TIM 2 was the critical TIMs subdomain for synZiFTR 2.0 performance, as its disruption completely diminished the improved signal output observed in synZiFTRs 2.0, to the original TIMs-less 1.0 level. These results imply that elongation factor PPP1R10 might play a key role underlying the transactivation mechanism employed by synZiFTRs 2.0. Furthermore, they serve as an important reminder to us that physical protein-protein interactions do not always predict functional relevance.

3.4.2 TIMs-dependent protein interactome

Inspired by the evidence that TIMs function through interactions with certain elongation factors, we next investigated if there are other uncovered interactions between IWS1 TIMs and other elongation factors that could contribute to its function. In collaboration with Professor Mikko Taipale, we employed the BioID technique, an established methods that have been widely used to study the interactome and mechanism of transcriptional regulators and co-activators (Alerasool et al., 2022, Piette et al., 2021). Using BioID, we were able to study the interactome of different TAD architectures and identify TIMs-dependent interacting partners. To confirm their functional roles beyond just the physical interactions with TIMs, we coupled RNAi studies with BioID to test if the knockdowns (KD) of these proteins have meaningful consequences in GZV synZiFTRs 2.0 switches. First and foremost, PPP1R10 emerged as the strongest TIMs-dependent interactor, with number of PPP1R10 recovered by BioID scaled with TIMs copy number. PPP1R10 KD further validated this result and emphasize the indispensable role of both components in this binary interaction. More excitingly, BioID also revealed novel TIMs interactions with some previously unknown targets, such as TOX4, a PPP1R10 interacting partner and an elongation regulator that promotes RNAP2 recycling and transcriptional initiation, restricts pause release and promotes productive late-stage elongation (Lee et al., 2010, Liu et al., 2022). Some proteins pulled down by BioID were excluded from the results due to the lack of evidence in their functional roles from RNAi studies, such as CC2D1A, HDGFL and TCEANC (**Figure S2B)**. While BioID indiscriminately searched for transcriptional factors that are in proximity to the target

protein, the enrichment of elongation factors in TIMs-dependent interactions strongly suggest that TIMs functionality is deeply entrenched with elongation machinery and modulations. Notably, there is a clear distinction between the groups of transcriptional regulators interacting with TIMs-containing TADs and with p65, NFZ or VPR, as elongation factors are exclusively found to react with TIMs but no other TAD elements (**Figure S2A)**, suggesting a mechanistic distinction between their transactivation functions. This suggests TIMs and p65 achieve kinetic synergy through complementary mechanisms—p65 recruits initiation/chromatin remodeling complexes (Lecoq et al., 2017; Jiang et al., 2003, Mukherjee et al., 2013, Schmitz et al., 1995, Burkhart et al., 2005), while TIMs enhances elongation efficiency.

3.4.3 TIMs effects on transcription and elongation landscape

To test our hypothesis and deepen our understanding in TIMs' role in remodeling elongation landscape, we performed Precision Run-on Sequencing (PRO-Seq) with synZiFTRs 1.0 and 2.0 for comparison. What distinguishes PRO-Seq from other sequencing techniques is that it uniquely focuses on the transcriptome of nascent RNA to investigate active and productive. During the process of elongation where many signature RNAP2 activities such as pausing, pause release, RNA synthesis and termination are rate-related and time-sensitive, PRO-Seq is particularly suitable for us to gain insights in TIMs' effects on not only stimulating transcriptional activity, but also mediating the kinetics of different stages of elongation. To that end, we analyzed the nascent RNA transcript profiles for the mCherry reporter induced by synZiFTR 1.0 (p65) or synZiFTR 2.0 (2xTIMs-p65). Mapping the 3' ends of the total transcripts was used as an indicator

of the RNAP2 presence along the gene body. By quantifying the average counts of 3' end reads in different regions on the gene body, such as promoter proximal, gene body, distal and post termination, we discovered a globally higher level of RNAP2 activity in the presence of 2xTIMs, indicating a higher level of active transcription, which would result in an elevated level of transcriptional outputs as we observed with the strong mCherry signal in previous experiments. Conveniently, a constitutively expressed puromycin selection marker (puro) was placed downstream the mCherry reporter for references, and we saw that its expression also benefited from the higher local concentration of RNAP2. To further explore the RNAP2 dynamics modulated by TIMs, we investigated the relative localization of RNAP2 on the reporter gene for each TAD, by normalizing the average counts of 3' end reads in each region with that of the gene body. This analysis revealed a striking difference in RNAP2 localization with and without TIMs, showing clearly faster clearance of RNAP2 post-termination. The same trend was not observed with the puro selection gene, suggesting this is a TIMs-dependent effect that is unique to TIMs-mediated genes. To interpretate these results, we combined insights we gained from BioID studies and hypothesize that TIMs modulates RNAP2 dynamics through recruiting elongation factors such as PPP1R10 or TOX4 that are crucial for efficient elongation termination and RNAP2 recycling, resulting in faster RNAP2 dissociation post termination and reloading on the promoter. The specific RNAP2 dynamics in each elongation stage and how these different rates are affected by TIMs is beyond the scope of this study. While other alternative factors might also contribute to or explain what we observed from PRO Seq results, we are confident to conclude that TIMs was able to

facilitate efficient elongation by increasing RNAP2 activity level across the gene body, modulating RNAP2 dynamics such as post-termination clearance, and thus enhancing the overall transcriptional output.

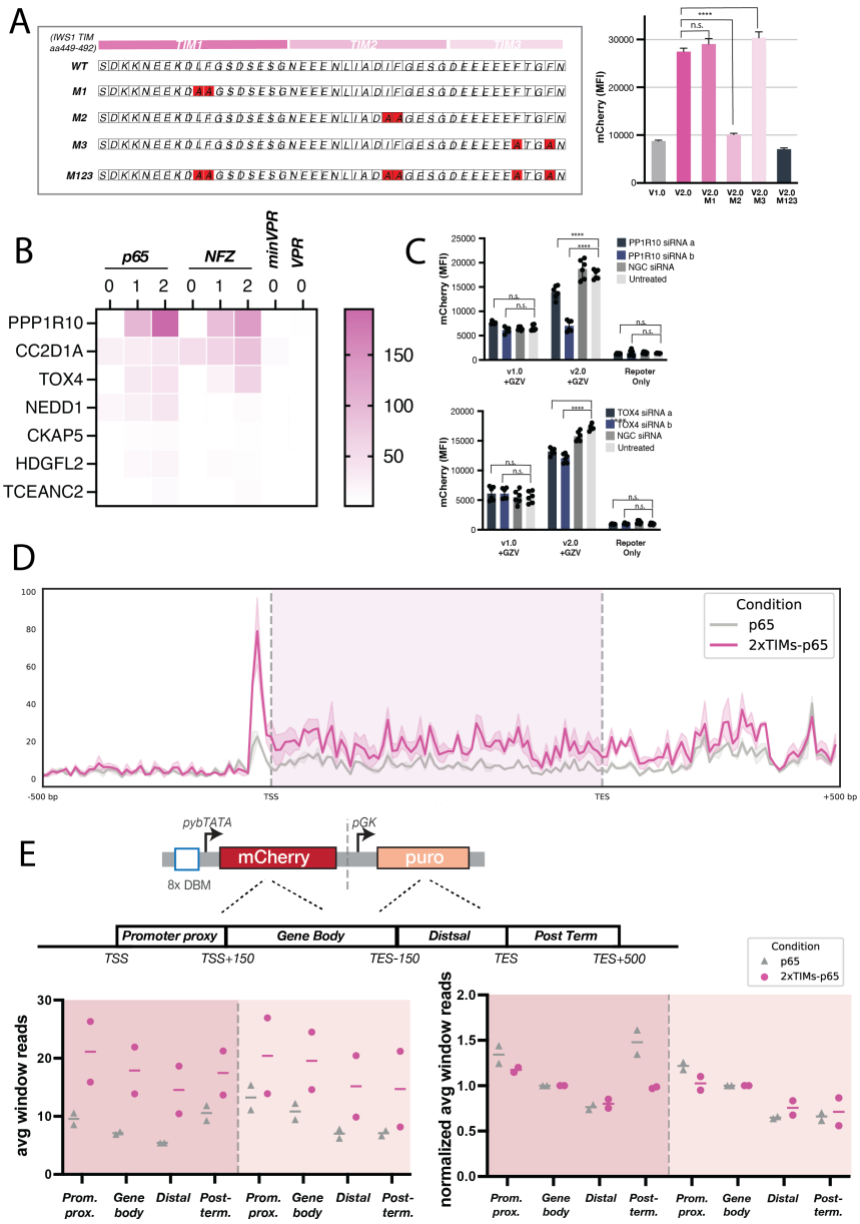

Figure 6. Mechanistic basis of TIMs-dependent enhancement in synZiFTR 2.0.

(A) Mutagenesis studies revealed that TIM2 subdomain is indispensable to TIMs functionality in synZiFTR 2.0.

(B) BioID validated that TIM2 binding partner, elongation factor PPP1R10, interacts with synZiFTR 2.0 and other TIMs-containing TADs, in a “dose-dependent” manner. BioID also revealed other novel TIMs-interacting proteins, such as elongation factor TOX4.

(C) RNAi knockdown studies confirmed functional requirements: PPP1R10 and TOX4 depletion specifically impaired synZiFTR 2.0 (but not 1.0) output, indicating a TIMs dependency in these interactions.

(D) 3’ reads from PRO Seq transcripts are plotted across the exogenous gene body to assess PolII activity. A globally higher RNAP2presence was observed with synZiFTR 2.0.

(E) Average 3’ reads in different sections on the TIMs-regulated reporter gene and TIMs-independent puromycin resistance gene were calculated and plotted. This quantitative analysis confirmed that RNAP2 activity and nascent transcription were enhanced in the presence of TIMs (left). Locating RNAP2 relative position on the gene body by normalizing average reads of each section with that of the gene body revealed fast RNAP2 clearance post termination, consistent with PPP1R10 and TOX4 elongation functions.

3.5 Therapeutic applications of synZiFTR 2.0

3.5.1 Enhanced CAR-T cell therapy with synZiFTR 2.0

To evaluate synZiFTR 2.0 in clinically relevant settings, we first validated its performance in primary human T cells. The system maintained VPR-comparable activation levels while exhibiting minimal basal leakage, consistent with Jurkat cell

results. Notably, fusion of 2xTIMs to a recently discovered, potent human TAD, NFZ , similarly enhanced its activity, demonstrating TIMs' function is not co-dependent with p65 and highlighting its potential as a universal TAD amplifier beyond p65-based systems (**Figure 7A)**.

Next, we set out to investigate if TIMs can enhance functional outputs in primary T cells, by using GZV synZiFTR 2.0 to drive anti-CD19 CAR and measure the resultant target tumor cell killing. In our previous work, we demonstrated that synZiFTR 1.0 enabled efficient anti-tumor CAR T activity both in vitro with NALM6 leukemia cells and in vivo with a xenograft blood tumor model (Li &Israni, et al., 2022). We therefore benchmarked synZiFTR 2.0 performances against its predecessor and CAR T activity driven by a constitutively strong promoter (pSFFV), and assessed the NALM cell killing efficiency in vitro. Compared to version 1.0 and constitutive pSFFV-driven CARs, synZiFTR 2.0 demonstrated superior CAR expression and NALM6 leukemia cell killing efficiency while maintaining tight control— showing potent activity only in the induced state and minimal activity in the uninduced condition (**Figure 7B**). These results build upon our previous work and establish synZiFTR 2.0 as an improved platform for controllable cell therapies.

3.5.2 Precise activation of endogenous VEGF for gene therapy

The modularity of the synZiFTR architecture enables development of gene switches for diverse application, particularly after overcoming the bottleneck of insufficient transactivation with the TIMs-enhanced synZiFTRs 2.0. The recent advancement in Zinc Finger (ZF) engineering and a deeper understanding in ZF designs

to target specific genomic sequences offer an unprecedent opportunity to expand synZiFTRs utilities beyond exogenous therapeutic payloads to endogenous targets. As a proof of concept, we integrated a customized ZF targeting the endogenous Vascular Endothelial Growth Factor (VEGF-A) gene in the 4OHT- synZiFTR 2.0 construct (Maeder et al., 2008), aiming to develop a gene therapy for diseases that can benefit from the pro-angiogenic function of VEGF, such as wound healing and neuron degeneration (Storkebaum et al., 2005, Rivard et al., 1999). The VEGF-targeting synZiFTR 2.0 achieved dose-dependent VEGF production with negligible basal activity (**Figure 7B**)—a critical feature given the observed fitness costs of unnatural VEGF secretion (**Figure S3A)**. This fitness costs became a detrimental defect in VPR-containing variants, which caused severe viability issues due to leaky expression, highlighting the importance of both high inducibility and tight control for therapeutic applications. These findings establish a critical design paradigm for transcriptional activator domains (TADs) in therapeutic applications: optimal performance requires both high inducible activation and stringent baseline control. Unlike viral-derived activators like VPR that compromise leakiness for potency, the TIMs domain uniquely enhances transcriptional output while maintaining tight regulation. This dual capability positions TIMs as an ideal component for engineering human-compatible gene regulation systems that meet the stringent safety and efficacy requirements for clinical translation.

3.5.3 synZiFTRs 2.0 enable optimization of specificity-activity balance

A key concern for using gene editing and gene regulation tools to drive cell and gene therapies is their specificity to the target genes. Precise targeting of specific DNA

sequences with minimal off-target edits and disruption in the native genomic background is essential for successful therapeutic outcomes and patient safety. In ZF-based regulatory systems, a common and effective strategy to reduce such off-target activity is through mutating the phosphate-contacting arginine on ZF to reduce the nonspecific affinity between ZF and DNA backbone (Khalil et al., 2012, Miller et al., 2019, Ichikawa et al., 2023). However, this improved specificity often comes at the cost of reduced on-target activity, an unaffordable price for synthetic gene regulators with limited transactivation capability and insufficient transcriptional outputs. Fortunately, the enhanced TAD potency in synZiFTRs 2.0 grants such trade-off to improve specificity while maintaining high level of gene expression. By introducing arginine mutations in all 6 fingers, we generated a mutant ZF10 that maximally reduced synZiFTR cross-activity with endogenous genes in primary T cells, as indicated by the decreased number of differentially expressed transcripts in both synZiFTR 1.0 and 2.0 compared to the original ZF10(**Figure 7D**). Despite the lower level of ZF contact with both on-target and off-target DNA and the resultant signal reductions in both v1.0 (13.15%) and v2.0 (23.47%), the reporter output by 2.0 was still significantly improved compared to 1.0 (**Figure S3B**). TIMs strong effect on stimulating transcription allows us to engineer ZFs with a full spectrum of activity levels by modifying the number of arginine mutations, at minimum cost of on-target gene expression. The optimal balance between transcriptional activity and ZF specificity can be finely tuned and determined for specific contexts, making synZiFTRs 2.0 a highly modular, adaptable yet powerful gene regulation toolkit for broad applications.

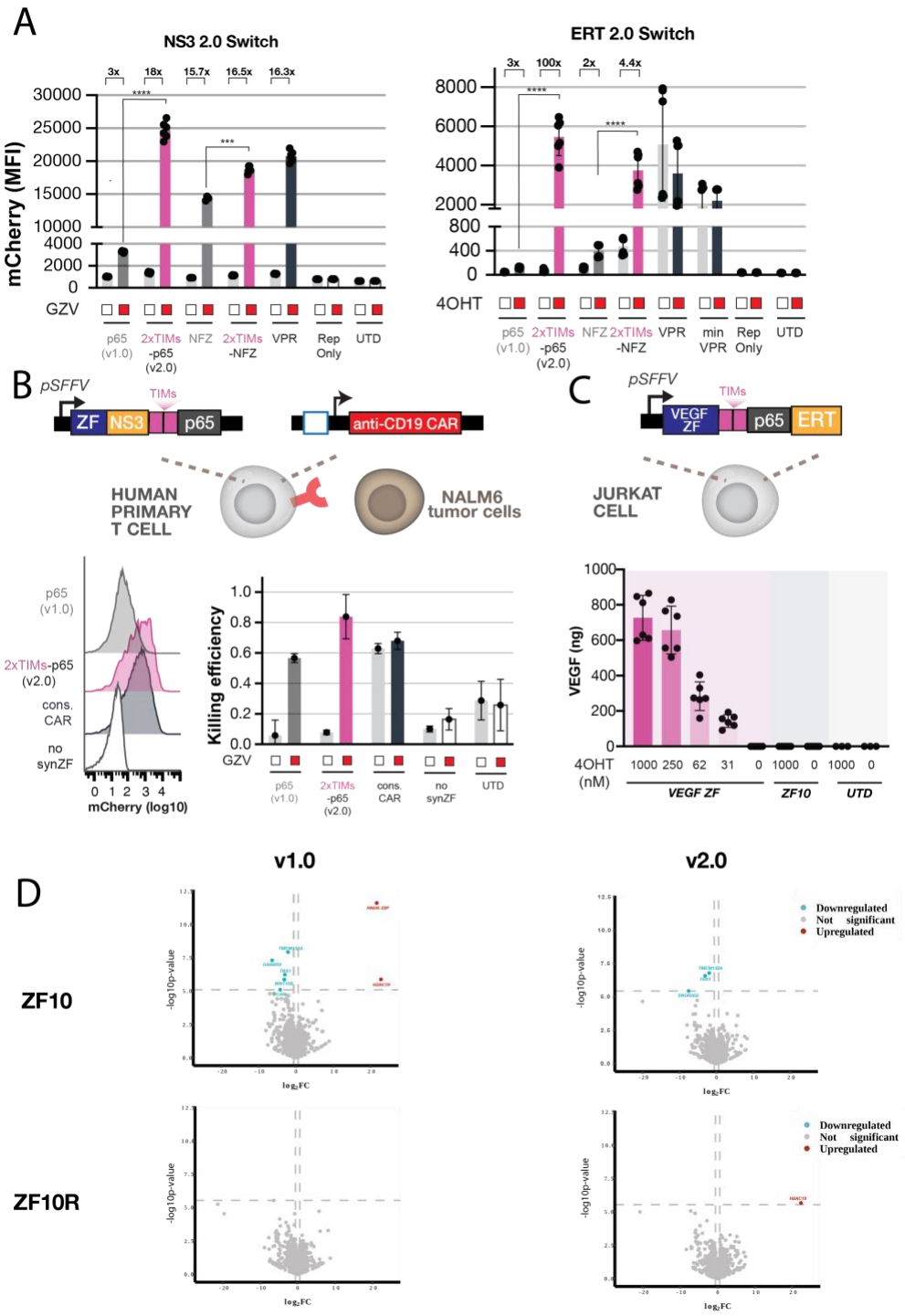

Figure 7. synZiFTR 2.0 enable versatile therapeutic functions.

(A) Both NS3 and ERT synZiFTRs 2.0 drive high reporter expression in primary T cells, outperforming VPR and minVPR with high transactivation potency and stringent control

in the uninduced state. TIMs also enhance NFZ performance, suggesting its potential role to be a generalizable TAD synergizer and enhancer.

(B) NS3 synZiFTR drives high level CD19 CAR expression and directs highly efficient CD8+ T cell killing of the target cells.

(C) ERT synZiFTR 2.0 coupled with zinc finger engineering enables robust activation of endogenous gene and titratable VEGF production.

(D) Differential analysis of primary T cells expressing different synZiFTR architectures demonstrates that Arginine mutations in ZF backbone increases target gene specificity and reduces off-target cross activity with the genomic background.

3.6 Discussion and future perspectives

In this chapter, we explored a novel strategy for TAD engineering by creating kinetic synergy between TAD elements to stimulate transcription. Under this principle, we identified a compact and humanized protein effector that functions as a potent elongation enhancer, IWS1 TIMs, to be a strong synergizer for previously established human TADs such as p65 and NFZ. This discovery led to the design of a novel TAD architecture (p65+2xTIMs) and the development of synZiFTR 2.0, a significantly enhanced human transcriptional regulator that exhibits robust transactivation activity (comparable to those strongest viral-derived activators), minimum basal expression and a wide range of inducibility—all crucial pre-requisites for precisely controlling therapeutic cell functions and driving next-generation cell therapies. SynZiFTR 2.0 demonstrated its robust performance across multiple clinically relevant contexts including CAR T cell activity and endogenous VEGF activation, while enabling zinc finger engineering

approaches that could further improve its safety profile for in vivo use.

Our mechanistic studies reveal that synZiFTR 2.0's enhanced performance stems from successful kinetic synergy between complementary activation mechanisms. While conventional TADs like p65, NFZ and VPR primarily interact with initiation-focused complexes (Mediator, p300/CBP, and BAF chromatin remodelers) (**Figure S2A**), TIMs uniquely engages the elongation machinery through its interaction with PPP1R10 (PNUTS). This division of labor allows simultaneous enhancement of distinct transcriptional processes - initiation/remodeling by classical TADs and elongation efficiency by TIMs - resulting in multiplicative rather than merely additive effects on transcriptional output. The generalizability of this synergy is evidenced by TIMs' ability to enhance both p65 and NFZ, suggesting broad applicability to other non-elongation-focused TADs.

The PPP1R10 interaction emerged as a critical node for TIMs-mediated elongation enhancement. Previous studies on PPP1R10 uncovered its diverse functions in regulating RNAP2 speed and elongation rate. Most well-known for its role in the termination zone, PNUTS-PP1 complex plays an irreplicable role in facilitating efficient termination by forming cleavage/polyadenylation (CPA) complexes, dephosphorylates Spt5 and consequently decelerates RNAP2 activity post Poly(A) signals (Shi et al., 2009, Cortazar et al., 2019). Disruption in PNUTS-PP1 integrity causes termination defects and results in synthesis of long extragenic transcripts and read-through transcripts (Austenna et al., 2015). In addition, PNUTS-PP1 complex promotes RNAP2 degradation and facilitates its turnover on chromatin, resolving transcription-replication conflicts

(Landvserk et al., 2020). Outside termination zone, PNUTS-PP1 regulates spliceosome assembly near TSS and modulates RNAP2 pausing on the gene body, controlling the overall elongation rate (Cossa et al., 2020, Cortazar et al., 2019). On the transcriptional level, PNUTS-bound genes are shown to display higher levels of expression (Cossa et al., 2020), and depletion of PNUTS reduced the fraction of RNAP2 bound to the chromatin and increased the level of free RNAP2 (Kelley et al., 2024). Our PRO Seq results are highly consistent with these studies, as evidenced by the transcriptional footprints of PPP1R10 when TIMs was present, such as the elevated level of RNAP2 presence and the enhanced post-termination RNAP2 clearance. One PPP1R10-related feature that we did not observe with TIMs was the faster pause-release rate in the promoter proximal region (**Figure S3C**), a newly discovered function of PNUTS that is dependent on its TND domain and its interactions with elongation factors including IWS1 (Kelley et al., 2024). The absence of enhanced pause release likely reflects fundamental differences between our synthetic recruitment approach and conventional loss-of-function studies. Specifically, Kelly et al demonstrated PNUTS depletion clearly limits pause release, but it remains unclear if higher level of PNUTS will proportionally promote pause release before/if ever reaching a steady state or maximal rate. Distinctive from the PNUTS disruption method, our system examines the consequences of localized PPP1R10 enrichment at a synthetic locus by indirectly recruiting more PNUTS to the target gene with higher copies of TIMs. In addition, our system's lack of native regulatory elements such as PolyA signals and intron-exon regions and boundary—while simplifying mechanistic interpretation—may also explain why we don't recapitulate certain PNUTS-

associated phenomena like splicing activation. This distinction highlights both the value and limitations of synthetic biology approaches for dissecting complex transcriptional regulation.

Overall, these findings collectively position PNUTS as a versatile transcriptional rheostat whose effects are highly context-dependent, while demonstrating how synthetic biology can repurpose native regulatory interactions to achieve predictable control over transcriptional output. Our work not only advances engineering principles for synthetic transcription systems, but also provides new experimental paradigms for studying dosage-sensitive effects of elongation factors that are difficult to probe through conventional genetic approaches.

3.7 Materials and methods

3.7.1 Mammalian Cell Culture

All cells were maintained in 10 cm treated dishes, 75mL flasks or 175mL flasks at 37 °C and 5% CO_2. Cells were passaged every 3-4 days when they reached 70-80% confluency or ~1million cells/mL.

HEK293FT cell lines (Thermo Fisher Scientific R700-07) were cultured in Dulbecco's Modified Eagle's Medium (Corning 10-013-CV) supplemented with 10% Fetal Bovine Serum (Takara Bio 631367), 1% GlutaMAX (Thermo Scientific 35050061), 1% Non-Essential Amino Acids (Thermo Scientific 11140050), and 1% Penicillin-Streptomycin (Thermo Scientific 15140122). Jurkat cell lines (ATCC TIP-152) were cultured in RPMI 1640 Medium (Corning 10-040-CV) supplemented with 10% FBS, 1% GlutaMAX, and 1% Pen-Strep. NALM6 target cell lines were cultured in RPMI 1640

Medium supplemented with 5% FBS, 1% GlutaMAX (Gibco A2916801), and 1% Pen-Strep.

3.7.2 Primary T cell isolation and culture

Primary T cells were obtained from whole peripheral blood from healthy donors at the Blood Donor Center at Boston Children's Hospital through a protocol approved by the Boston University Institutional Review Board (IRB). CD4+ primary T cells were isolated using EasySep Human CD4+ T Cell Isolation Kit (STEMCELL Technologies 17952). CD8+ primary T cells were isolated using EasySep Human CD8+ T Cell Isolation Kit (STEMCELL Technologies 17953). Primary T cells were cultured in X-Vivo 15 Medium (Lonza 04-418Q) supplemented with 5% human AB serum (Valley Biomedical, Inc. HP1022), 10mM N-acetyl L-Cysteine (Sigma A9165), 55 uM 2-Mercaptoethanol (Gibco), and 100-200 U / mL IL-2 (PeproTech 200-02).

3.7.3 Lentiviral Transduction of Jurkat cells

Cassettes cloned into lentiviral donor plasmids were integrated into Jurkat cell lines using lentiviral infection. Lentivirus was produced as previously described in 2.6.2. 500,000/well Jurkat cells were seeded into 24-well treated plates in 1mL media. 100uL of each concentrated lentiviral solution was added to the cells. Infected cells were incubated for 48-72 hours prior to removal of lentivirus. Cells were collected and centrifuged for 5 minutes at 300 g. Lentiviral media was removed and fresh media was added. Transduced cells were subsequently used for downstream induction measurements. When the puromycin selection marker is present, cells are selected with 1ug/mL puromycin (Thermo Fisher Scientific).

3.7.4 Lentiviral Transduction of Primary T Cells

Cassettes cloned into lentiviral donor plasmids were integrated into human primary T cells by activating and transducing primary CD4+ or CD8+ cells. First, lentivirus was generated by transfecting CHEDAR cells. 25,000,000 CHEDAR cells were seeded into T175 flasks in DMEM medium. Prior to transduction, DMEM medium was replaced with Opti-MEM I Reduced Serum Medium supplemented with 5% FBS, 1% GlutaMAX, 1% Non-Essential Amino Acids and 1% Sodium Pyruvate. Cells were transfected with 44 ug total DNA using TransIT-Lenti Transfection Reagent. 22 ug of the donor plasmid was co-transfected with 15ug of the pCMVR8.74 plasmid, 2ug of the pAdVantage plasmid, and 5ug of the pMD2.G VSVG plasmid. Cells were incubated for 72 hours prior to harvesting media containing lentiviral supernatant. Lentiviral-containing media from each flask was centrifuged for 5 minutes at 400 g to remove cell debris, and then concentrated at a 3:1 ratio using Lenti-X Concentrator. Lentiviral-concentrated media was incubated at 4C overnight, prior to centrifugation at 4C 1600 g for 60 minutes and resuspension in 200uL Opti-MEM I Reduced Serum Medium.

Primary CD4+ or CD8+ cells were thawed 72 hours prior to spinfection, and then activated using Human T-activator CD3/CD28 Dynabeads (Thermo Fisher 11131D) with 100U/ml IL-2 media 24 hours prior to spinfection. T cells were seeded at 0.25-0.5 million cells/well in a 24-well plate and 100uL of each concentrated lentiviral solution was added to cells. Cells were spun at 2000g for 90 minutes and incubated with virus for 48-72h prior to removal of lentivirus and Dynabeads. Transduced cells were occasionally supplemented with 25uL/mL ImmunoCult Human CD3/CD28 T Cell Activator

(STEMCELL Technologies, 10971) to stimulate proliferation. When the puromycin selection marker is present, cells are selected with 5ug/mL.

3.7.5 BioID sample preparation

Cells expressing synZiFTRs with different TAD architectures were grown to 70% confluence in 150 mm dishes before inducing gene expression with 1mM GZV for 72h. 50 µM biotin was then added to each plate for 6 hours. Cell pellets were collected as for AP-MS, and resuspended in lysis buffer (50 mM Tris-HCl pH 7.5, 150 mM NaCl, 0.1% SDS, 1% Igepal CA-630, 1mM EDTA, 1 mM $MgCl_2$, protease inhibitor cocktail (Sigma-Aldrich P8340, 1:500), and 0.5% sodium deoxycholate) using a 1:10 pellet weight:volume ratio. After sonication, each sample was treated with 250U Turbonuclease (BioVision 9207-50KU) and 1 µL RNase A solution (Sigma-Aldrich R6148) and incubated for 30 minutes at 4°C. SDS was then added to a final concentration of 0.25% and after mixing the samples were incubated for another 10 minutes at 4°C followed by centrifugation at 20,000g for 20 minutes. The supernatant was transferred to a tube containing 30 µl of pre-washed packed streptavidin beads (GE Healthcare, 17-5113-01). Streptavidin pulldown was done for 3 hours at 4°C. Beads were washed once in 1 ml of SDS buffer (2% SDS/50 mM Tris-HCl pH7.5), once in 1 ml lysis buffer, and once in TAP buffer (50 mM HEPES-KOH pH 8.0, 100 mM KCl, 10% glycerol, 2 mM EDTA, 0.1% Igepal CA-630), followed by three 1 ml washes with 50 mM ammonium bicarbonate pH 8.0. After the washes, beads were resuspended in ABC buffer containing 1 µg trypsin and incubated overnight at 37°C. The following day, the supernatant was collected and the streptavidin beads were washed with 50 µl water, which was combined

with the first supernatant fraction. 0.5 µg trypsin was added to the combined supernatant sample, which was then incubated at 37°C for 4 hours. Beads were then spun down and the supernatant recovered. Beads were rinsed twice using ABC buffer and these rinses were combined with the original supernatant. Combined supernatants were dried by centrifugal evaporation.

3.7.6 Mass spectrometry data acquisition and analysis

Samples were analyzed on a TripleTOF 5600 instrument (AB SCIEX, Concord, Ontario, Canada) using Data-Dependent Acquisition (DDA). AB SCIEX WIFF MS files were converted to mzXML format using Proteowizard (Adusumilli and Mallick, 2017) as implemented in ProHits v4.0 (Liu et al., 2016). Searches were performed with Mascot version 2.3.02 and Comet version 2012.02rev.0 (Eng et al., 2013) against the NCBI RefSeq database (version 57, January 30, 2013). The results from each search engine were subsequently analyzed through the Trans-Proteomic Pipeline (version 4.6 Occupy rev 3) using the iProphet pipeline (Shteynberg et al., 2011), and proteins with an iProphet probability ≥ 0.95 were further analyzed. Significant interactors were identified with SAINTexpress (Teo et al., 2014). EGFP-BioID2-FLAG and EGFP-BioID2-FLAG were used as negative controls. SAINTexpress analysis used default parameters (using 2-fold compression for stringency; (Mellacheruvu et al., 2013)), and prey proteins were considered significant if they passed calculated Bayesian FDR cutoff of ≤5%. Dot plot figures were generated with ProHits-viz webserver (Knight et al., 2017).

3.7.7 RNAi KD

Transduced HEK cells were treated with siRNA and Lipofectamine RNAiMAX transfection reagent (Thermo Scientific) for 72h following the recommended protocols by the manufacturer. KD cells were harvested and replated with 1mM GZV or DMSO for 72h. The reporter signal was measured on flow cytometer. The siRNA kits used in this study is listed in **Table.2**

Table.2 Source of siRNA for RNAi KD in TIMs mechanistic studies

Target	Manufacturer	Product
PPP1R10	OriGene Technologies	SR303681
TOX4	OriGene Technologies	SR306624
CC2D1A	OriGene Technologies	SR310295
TCEANC	OriGene Technologies	SR314980
PSIP1	OriGene Technologies	SR307657
HDGFL2	MedChem Express	HY-RS06095

3.7.8 PRO Seq

PRO Seq samples were prepared following published protocols (Mimoso & Goldman, 2024). In short, Jurkat reporter cells transduced with synZiFTR 1.0 or 2.0 were treated with 1mM GZV for 10h. Cells were harvested by centrifugation and kept in ice cold buffer to halt transcription. Harvested cells were then permeabilized with mild detergent, washed and counted in freezing medium. Permeabilization rate and permeabilized cell count was determined with trypan blue. Freezing medium volume was adjusted to 25M permeabilized cells/mL. Cells were stored in -80 ºC until submission to Harvard Medical School Nascent Transcriptomics Core were subsequent library preparation and sequencing. All sample groups were prepared in duplicates with a

permeabilization rate >90%.

Raw PRO-seq reads were trimmed using *cutadapt* (-a TGGAATTCTCGG -A GATCGTCGGACT -m 26 -q 10) to remove Illumina primers, and *UMItools extract* (-p NNNNNN --bc-pattern2=NNNNNN) to extract the 6nt Unique Molecular Identifiers (UMIs). Trimmed reads were aligned to the reference sequence using *Bowtie2* (--very-sensitive). *Samtools sort* was used to sort and compress the *Bowtie2* output. *bedtools bam2bed* was used to create bed files for the reference sequence. The bed files were read into Python (ver.3.10.12) for further processing. Since PRO-seq's R1 contains the RNA 3' end, reads aligning to the "-" strand were the reads aligned to the reference sequence. The first base of each R1 read aligned to the "-" strand were counted and plotted to generate RNA Pol II traces. The traces were binned every 10nt to reduce noise and were plotted with 95% confidence intervals.

RNA Pol II pausing indices (PI) were also calculated using the 3' end data, where PI is the ratio of total 3' reads in [TSS-50 – TSS+50] and in [TSS+50 – TSS+250]. Average read is defined by total counts in a window, divided by window size and was calculated for the following windows for the reporter gene: TSS–TSS+150, TSS+150–TES-150, TES-150–TES, TES–TES+150, and TES+150–TES+500. Normalized average reads were calculated by normalizing average reads in each window by average reads in [TSS+150 – TES-150] window.

3.7.9 In vitro co-culture experiment

Transduced primary CD8 cells were puro selected then treated with 1mM GZV or DMSO for 72h. 100,000 T cells were co-cultured with NALM target cells transduced

with BFP at a 1:1 effector to target (E:T) ratio overnight at 37 ºC. Following 16 hours of incubation, cells were analyzed using flow cytometry to count live NALM6 cells via gating for BFP+ cells. Killing efficiency was calculated as the percentage of cells killed compared to control wells containing NALM6 cells without T cells.

3.7.10 VEGF activation

100,000 transduced and puro selected Jurkat cells were plated in 25uL medium in 96-well plates with varying concentrations of 4OHT or DMSO control. After 72h incubation, cells were spun down at 300g for 5 mins and the supernatant was collected to quantify the VEGF secretion level with Human VEGF Quantikine ELISA kit (R&D system, DVE00), and the cells were collected for cell count with CellTiter-Glo Luminescent Cell Viability Assay (Promega G7570).

3.7.11 Fluorescence Activated Cell Sorting (FACS)

FACS was performed for primary CD4 cells integrated with synZiFTR or GFP and reporter cassettes after 72h 1mM GZV treatment and puro selection on a SH800 Cell Sorter (Sony Corporation). Cell samples were suspended in 0.5 mL HBSS buffer (Cytiva SH30030) supplemented with 1% Fetal Bovine Serum and passed through a 0.45 um filter to filter out cell clumps. Live cells were gated by forward scatter (FSC) and side scatter (SSC) and singlets were gated by FSC-area and FSC-height. Fluorescence data was collected for GFP (excitation laser: 488nm) and mCherry (excitation laser: 561nm) and gated with untransduced CD4 cells. GFP or mCherry expressing cells were collected in 0.5mL of the fresh primary T cell culture medium. Sorted cells were immediately spun down, lysed and processed for total RNA extraction using the RNeasy Mini Kit as

previously described in 2.6.7.

3.7.12 RNA Sequencing

All RNA sequencing preparation steps and measurements were performed in triplicates. RNA samples were submitted to the Boston University Microarray & Sequencing Resource for subsequent library preparation and sequencing. Sample purity and quality was measured using an Agilent Bioanalyzer; cDNA synthesis and libraries were prepared using total RNA library Prep with rRNA reduction (Illumina). Libraries were sequenced as 100 bp Single End reads using Illumina XLEAP sequencing chemistry and a NexSeq2000 instrument (Illumina).

RNA-seq reads had 6nt UMIs removed with *UMItools extract* (-p NNNNNN --bc-pattern2=NNNNNN). Reads were input into *Salmon* (quant --validateMappings --seqBias --gcBias) to estimate transcript abundances. The *Salmon* index necessary for estimation was created using the GENCODE human transcript file gencode.v47.transcripts.fa.gz and -k 19. *tximport* was used to import the transcript abundance files into RStudio (R ver.4.4.0). *DESEQ2* was used for differential gene expression analysis (DGE). The wildtype sample was set as the reference level for the DGE analysis, and the sample condition was defined as the independent variable. Genes which had less than 10 counts in 3 or less samples were filtered out before analysis. P-values were corrected for multiple testing using the Benjamini-Hochberg method, and all genes with adjusted p-values below 0.05 were considered significant. Volcano plots were created by plotting pre-adjusted p-values but only coloring genes which were significant with adjusted p-value. Significance cutoffs were drawn on the y-axis using the p-value of the sample with the adjusted p-value closest to 0.05.

CHAPTER FOUR: DEVELOPMENT OF A DRUG-INDUCIBLE POLARIZATION-BASED MACROPHAGE THERAPY

4.1 Introduction

In the preceding chapters, we developed the core components and toolkits necessary for achieving inducible macrophage polarization in vivo. In this chapter, we integrate engineered STAT effector proteins with the enhanced synZiFTR 2.0 system to establish a proof-of-concept for drug-controllable, polarization-based macrophage therapy. To enable efficient delivery of polarization inducers, we will design nanoparticle carriers targeting circulating monocytes—highly plastic macrophage precursors that are readily recruited to pathological or physiological sites, where they differentiate into macrophages and execute context-dependent functions. As outlined in Chapter 1, nanoparticles offer distinct advantages for delivering polarizing effectors to macrophages in vivo, including cargo stabilization and cell-specific targeting, which collectively minimize systemic toxicity and off-target effects.

To validate our system, we focus on solid tumors as a prototype disease model due to their physiological relevance to macrophage biology, particularly M1-polarized effector functions. Tumor-associated macrophages (TAMs) dominate the tumor microenvironment (TME) and their polarization state directly correlates with disease progression, making them a clinically compelling target for reprogramming strategies (Bill et al., 2023, Lam et al., 2019). In particular, STAT1 protein was found to play an indispensable role in the reprogramming of TAM (Ma et al., 2023). Successful TAM conversion to an M1 phenotype could not only revolutionize cancer treatment but also

provide mechanistic insights into macrophage roles in tumor immunity. Moreover, the growing arsenal of TAM-directed therapies—such as CAR-M—provides well-characterized benchmarks for evaluating our system's performance. Conveniently, nanoparticles are also found to be accumulated more in the solid tumors compared to other organs, due to the leaky vascularization in TME and the enhanced permeability and retention (EPR) effect.

4.2 synZiFTR 2.0 drives STAT expression and M1 polarization in macrophages

While our initial synZiFTR 1.0 system showed limited capacity to drive STAT expression in THP1 cells—constrained by both the large size of STAT proteins and the intrinsic challenges of macrophage transduction—the enhanced synZiFTR 2.0 platform successfully overcame these transcriptional and delivery bottlenecks. To evaluate its efficacy, we engineered THP1 cells with a GZV synZiFTR 2.0 cassette driving expression of a GFP-STAT1c fusion protein and quantified both GFP levels and the M1 marker CD38. SynZiFTR 2.0 mediated robust induction of GFP-STAT1c, which correlated with significant upregulation of CD38, confirming functional M1 polarization. Importantly, in the uninduced state, CD38 expression remained at baseline levels comparable to untransduced (UTD) M0 macrophages, demonstrating stringent off-state control. This tight regulation is critical for mitigating risks of systemic inflammation or hyper-immune activation due to leaky polarization. Collectively, these results validate synZiFTR 2.0 as a potent and precisely controllable system for inducible macrophage reprogramming, while highlighting the functional synergy between optimized transcriptional regulation and STAT effector delivery.

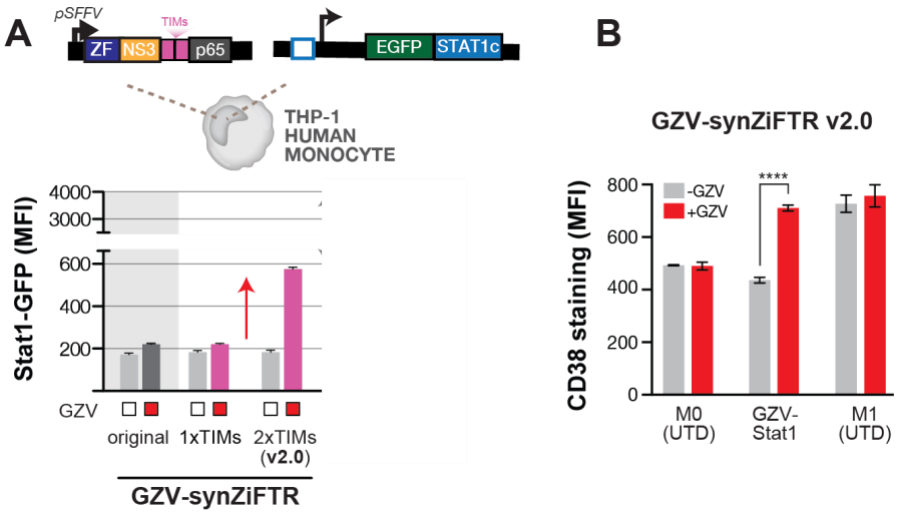

Figure 8. synZiFTR 2.0 drives STAT1c expression and CD38 upregulation in THP1 cells.

(A) synZiFTR 2.0 significantly boosted STAT1c expression in THP1 cells, showing clear inducibility and improved output level.

(B) Subsequently, synZiFTR 2.0-driven STAT1c expression upregulated CD38 M1 surface marker, with a dynamic range that aligns well with that of the natural cytokine induction mechanism.

4.3 synZiFTRs 2.0 exhibit robust activity in primary macrophages

Recognizing the cell line- and protocol-dependent phenotypic variability observed in THP1 cells, we sought to evaluate the performance of synZiFTR 2.0 and engineered STAT proteins in the more physiologically relevant context of primary human macrophages. This transition presented significant technical challenges, as primary macrophages are notoriously difficult to genetically manipulate due to their limited proliferative capacity and resistance to lentiviral transduction. These inherent limitations have resulted in a lack of thorough understanding and characterization of how genetic elements and synthetic circuits interact with macrophage biology. To address this gap, we

used a mCherry reporter and conducted a comprehensive screen of synZiFTR variants containing different transcriptional activation domains (TADs) to identify optimal architectures for macrophage applications. While we observed cell-type-specific variations in TAD performance in primary macrophages and monocytes compared to our previous studies in primary T cells, the synZiFTR 2.0 configuration incorporating TIMs-enhanced p65 (2xTIMs-p65) consistently emerged as the most effective activator, demonstrating both high potency and minimal basal activity across multiple induction platforms. These findings not only validate synZiFTR 2.0 as a robust transcriptional regulator in primary human macrophages, but also underscore the remarkable cell-type versatility of TIMs-mediated transactivation enhancement.

4.4 synZiFTRs 2.0 drives high level of STAT expression in primary human macrophages

To systematically evaluate synZiFTR 2.0's capacity to drive both reporter genes and large effector proteins like STAT1c, we selected top-performing TAD variants for comparative analysis. Using a T2A self-cleaved peptide-linked mCherry reporter system (STAT1c-T2A-mCherry), we assessed transcriptional output and STAT1c expression levels through mCherry fluorescence while maintaining native STAT1c functionality. Our results demonstrated that TIMs-mediated enhancement consistently improved the performance of both p65 and NFZ activation domains, enabling the highest levels of STAT1c expression. These findings confirm synZiFTR 2.0 as the optimal architecture for driving macrophage reprograming with our polarizing transgenes and highlight its reliable performance independent of cargo size and type.

4.5 synZiFTR drives CAR expression and CAR-M tumor killing activity

To rigorously evaluate synZiFTR 2.0 with a clinically relevant payload, we engineered a CD19-targeting CAR-M system using the same anti-CD19 CAR construct previously validated in primary T cells. We quantitatively assessed tumoricidal activity against both CD19+ NALM cells and isogenic CD19-knockdown (CD19-KD) controls through coculture assays. Importantly, our endpoint measurement of residual tumor cell numbers intentionally integrated all macrophage-mediated cytotoxic mechanisms—including phagocytosis, trogocytosis, and secretory killing—to capture the net therapeutic effect. SynZiFTR 2.0-regulated CAR-Ms achieved tightly inducible tumor cell killing comparable to constitutive CAR expression systems, specific killing as evidenced by selective activity against CD19+ (but not CD19-KD) targets, and no baseline activation in uninduced conditions, confirming CAR-dependent functionality. These results further validate synZiFTR 2.0's capacity to drive complex therapeutic payloads to functional levels in primary macrophages, highlighting its versatility as a platform adaptable to diverse cell therapy applications.

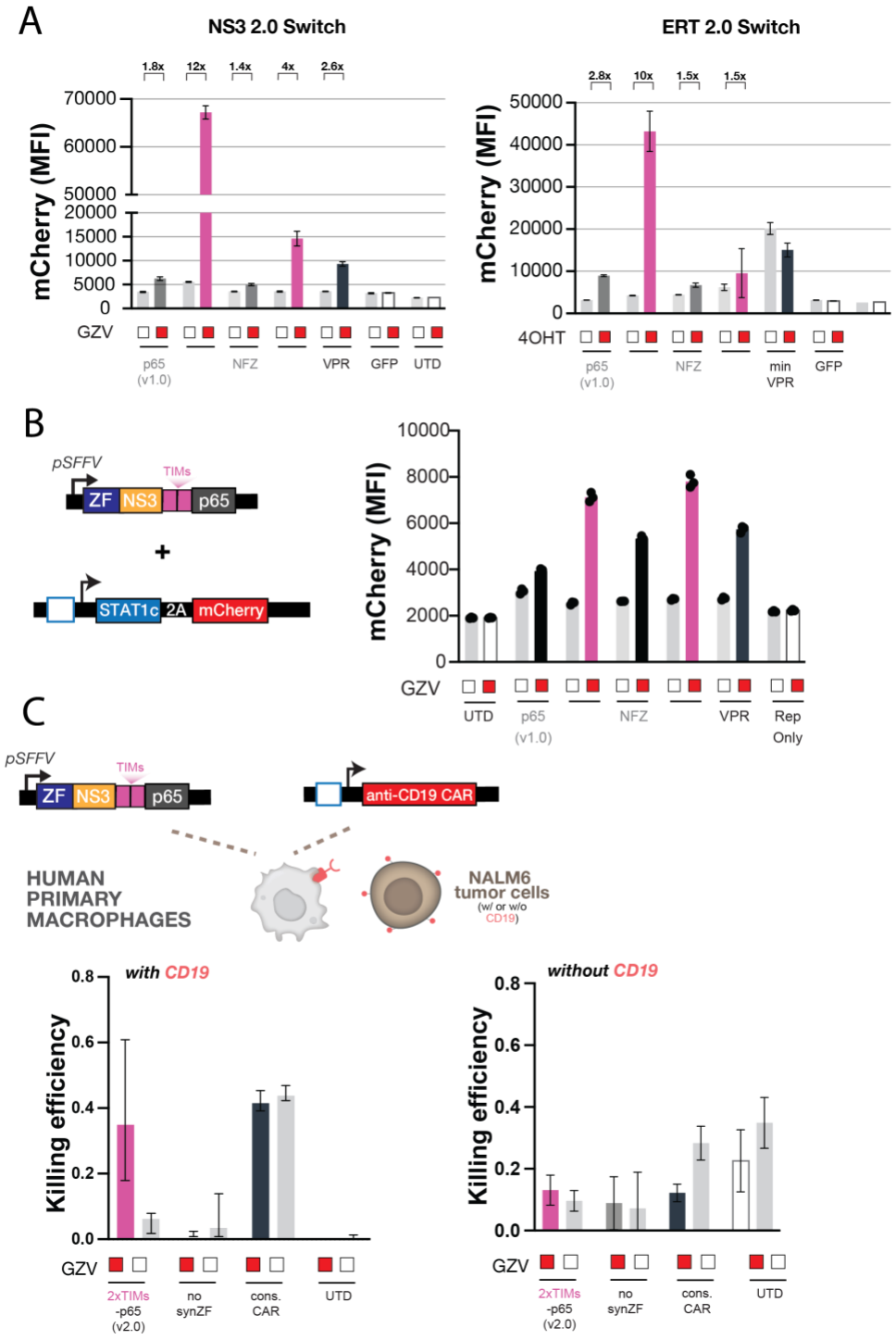

Figure 9. synZiFTR 2.0 exhibits robust activity in primary macrophage.

(A) NS3 and ERT switches with different TADs were tested in primary macrophages. synZiFTR 2.0 demonstrated consistently potent and stringent control, highlighting its

functionality for macrophage engineering.

(B) synZiFTR 2.0 drive high level of STAT1-mcherry expression, overcoming the transactivation bottleneck previously observed in synZiFTR 1.0.

(C) Using synZiFTR 2.0 to regulate CD19 CAR expression in CAR-M system, we achieved efficient and specific killing of the target cells.

4.6 Development of monocyte-targeting nanoparticles

To leverage macrophages' inflammation scavenging ability and recruitment to disease sites that are inaccessible to any other immune cell types, we designed nanoparticles to target macrophage precursor cells, monocytes, before their differentiate in macrophages, a process that diminishes their migratory capacity (Cui et al., 2018, Hind et al., 201). Our NP system features a biocompatible PLGA backbone and PEG surface decoration which will improves NP circulatory stability through its hydrophilic "stealth effect" that naturally repels hydrophobic biomolecules (Salmaso& Caliceti, 2013). For the maximal phagocytic uptake by macrophages, we optimized NPs' physiochemical properties, such as high lipid content (by adding DSPE and lecithin), a controlled size between 100-500nm, negative surface charges and a PEG chain length of 3.4k and 2k to balance stealth properties and cellular update (Getts et al., 2014, Alexis et al., 2018, Ahsan et al., 2002). The incorporated lipids components form a hydrophobic core that can stabilize our inducers. To actively target monocytes, we functionalized the NP surface with mcp1 peptide (derived from monocyte chemoattractant protein-1 MCP1), which specifically targets the chemoattractant receptor 2 (CCR2), the most characteristic surface marker of circulating monocytes (Phillips et a., 2005) (**Figure 10A**).. Through

extensive formulation optimization, we achieved maximal mcp1 surface coverage while maintaining particle stability (**Figure S4)**.

To validate our active targeting strategy, we used NPs decorated with a scramble peptide as controls and examined NP-cell interactions under different conditions—at 4ºC to investigate binding of NPs to cells (no internalization) and 37 ºC to study the active cellular uptake. NPs decorated with high level of mcp1 peptide exhibited consistently higher uptake by THP1 cells across different temperatures and FBS concentrations (**Figure 10B**). In high FBS conditions, which promote protein corona formation on the NP surface and block the binding between targeting motifs and their intended targets, lower mcp1 density showed improved performance, highlighting PEG's role in blocking nonspecific protein interactions (**Figure 10B, right**) (Partikel et al., 2019). While in vitro conditions cannot fully recapitulate in vivo complexity, our modular NP design allows customization for diverse physiological environments, by balancing optimized active targeting and minimal nonspecific interactions.

To further test the CCR2 targeting specificity, we conducted a competition assay by co-treating THP1 cells with full-length CCR2-binding protein MCP1 and NPs. Under 4 ºC condition, while scramble NP binding remained low and unaffected by MCP1 addition, mcp1 NPs showed significant binding reduction due to the reduced interaction with CCR2 in the presence of MCP1 (**Figure 10C, left**). Under 37ºC, while after 2h we observed a similar trend as in 4 ºC condition, mcp1 NP maintained higher uptake despite competition, suggesting addition phagocytosis mechanisms that are not CCR2-related. At the 24h time point, the cellular uptake becomes predominantly CCR2-independent, even

though mcp1 NPs still show a higher uptake rate than scramble NPs (**Figure 10C, right**). This result is consistent with previous studies showing that macrophage phagocytosis is a relatively fast process, with a plateau in cell uptake rate within the first 4h (Kapellos et al., 2016). In a long culture period as 24h, macrophages most likely have reached a saturating level of phagocytosis even without relying on active targeting.

Finally, to conclusively validate the targeting specificity of mcp1 NPs, we performed ex vivo uptake assays using freshly isolated mouse peritoneal immune cells. Using immunostaining and flow cytometric analysis, we identified that local monocytes and macrophages, blood monocytes and granulocytes all non-specifically adsorb scramble NPs at a high level. On the other hand, mcp1 NPs showed selective accumulation only with monocytes (tissue-resident and circulating) and macrophages, but not in granulocytes or other non-myeloid cells (**Figure 10D**). While mcp1 decoration appeared to moderately reduce overall monocyte/macrophage binding compared to scramble NPs (potentially due to competition with endogenous MCP1), the complete exclusion of granulocytes demonstrates significantly improved cellular specificity. These results confirm that CCR2 targeting via mcp1 effectively directs NPs to monocyte-lineage cells and minimizes off-target uptake by other phagocytes. The strategy can potentially enhance the therapeutic window for our drug-inducible systems by increasing delivery efficiency to target cells and reducing potential side effects from non-specific uptake. This cellular specificity profile, combined with our previous in vitro characterization, establishes mcp1-NPs as a robust platform for precision delivery to monocytic cells in therapeutic applications.

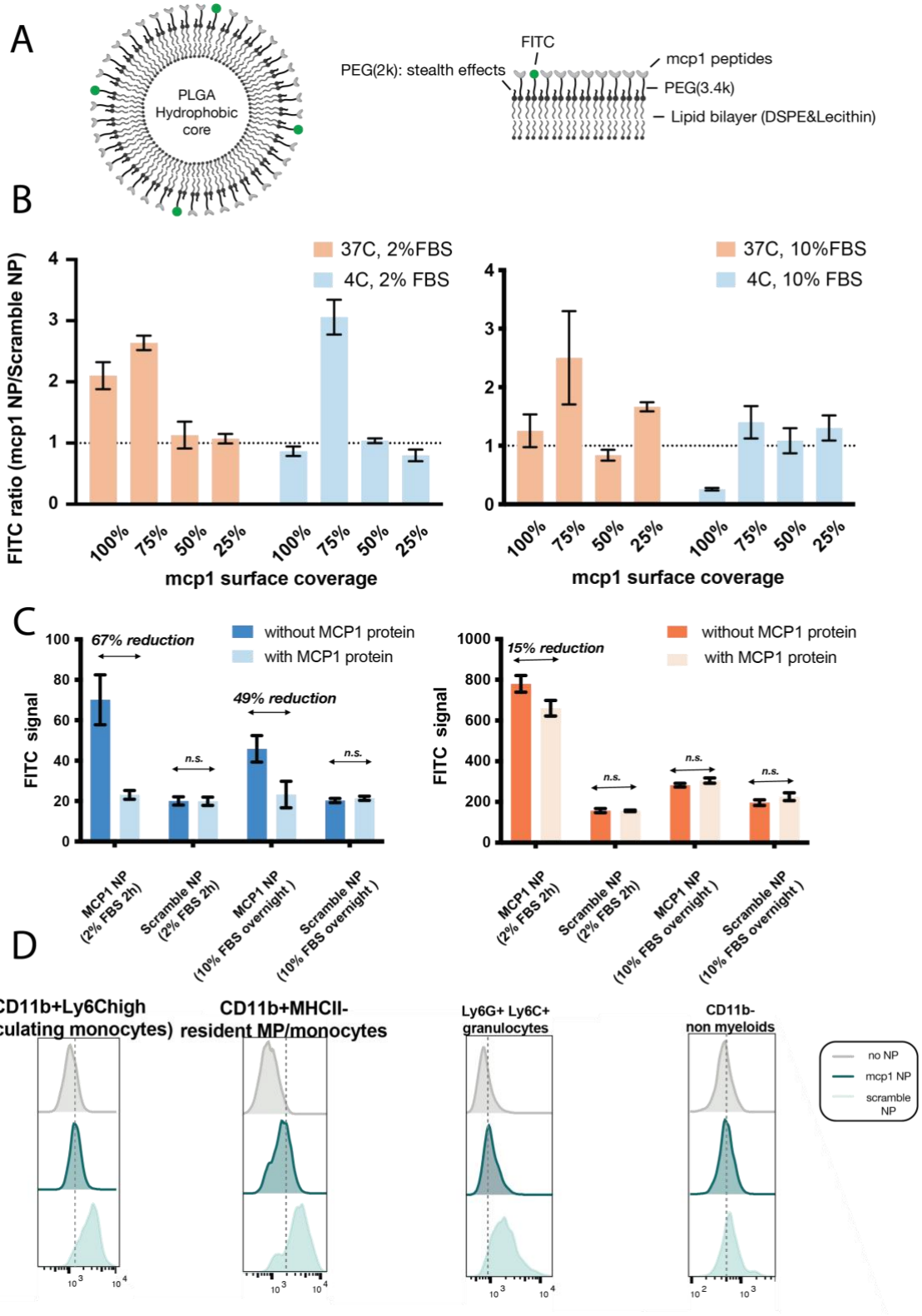

Figure 10. mcp NPs enable CCR2 binding and specific monocyte/macrophage targeting.

(A) NP design consists of: (i) PLGA hydrophobic core for drug stabilization, (ii) lipid bilayer to enhance cell penetration, (iii) long PEG 3.4k chains conjugated to MCP1 targeting peptides for optimal surface presentation, and (iv) short PEG 2k chains for stealth properties in biological environments, with FITC labeling for visualization.
(B) THP1 uptake studies under physiological conditions identified 75% MCP1 surface coverage as optimal for specific targeting (dotted line indicates threshold for preferential MCP1-NP uptake versus scramble controls).
(C) Competitive binding assays demonstrate CCR2-dependent uptake at 4°C (left panel), while 37°C studies (right panel) show CCR2-mediated phagocytosis dominates within 4 hours before transitioning to receptor-independent mechanisms.
(D) Peritoneal immune cell profiling confirms MCP1-NPs selectively target CCR2+ monocytes and macrophages, while scramble NPs exhibit non-specific adsorption across cell types including granulocytes.

4.7 Discussion and future perspectives

In this chapter, we have established key functional validations of our inducible macrophage-polarization system, demonstrating its potential as a novel platform for macrophage-based therapies. Our results show that: (1) synZiFTR 2.0-driven STAT1c expression effectively induces M1 polarization in THP1 cells, as evidenced by CD38 upregulation, while maintaining tight control in the uninduced state; (2) synZiFTR 2.0 exhibits remarkable versatility in primary monocytes and macrophages, capable of driving diverse payloads ranging from reporter proteins to complex therapeutic cargos like CARs and STAT proteins; (3) these engineered systems maintain functional

integrity, as demonstrated by CAR-mediated tumor cell killing. These findings collectively validate synZiFTR 2.0 as a robust platform for precisely controlling macrophage activation states through drug-inducible mechanisms.

Looking forward, several critical validations will strengthen the therapeutic potential of this system. We will utilize previously established methods in THP1 cells to conduct comprehensive phenotype characterization on the induced M1 phenotype, incorporating both classic M1 markers and newly identified signatures correlated with anti-tumor activity or TAM functions (such as CXCL9, SPP1, PDL1, etc.). We will examine the functional outcomes by measuring subsequent tumor cell killing using in vitro 2D or 3D co-culture systems. Furthermore, upon the successful development of our GZV inducible-M1 polarization system, we can readily integrate the STAT6c protein effector with the 4OHT synZiFTR 2.0, achieving orthogonal and precise control over the full spectrum of macrophage polarization.

The implementation of macrophage-based circuits opens exciting possibilities to program “collaborative functions” with other cell types, such as T cells which we now readily engineer. In principle, this would allow us to create synergistic anti-tumor responses that capitalize on each cell type's unique strengths. For instance, M1-polarized macrophages could enhance T cell activity through localized cytokine production, while T cells could in turn sustain macrophage activation, creating a positive feedback loop particularly valuable in solid tumor microenvironments. The compatibility of synZiFTR systems across cell types offers unprecedented opportunities to distribute therapeutic roles optimally throughout the immune systems, allowing us to simultaneously induce

their distinctive cellular functions and enhance their cooperative tumor killing.

To complete the translational pipeline, we have developed nanoparticle delivery systems specifically targeting monocytes—the circulating macrophage precursors that naturally home to inflammatory or pathological sites. This strategy enables our NPs' broad application across multiple disease contexts (e.g., cancer, chronic inflammation, fibrosis) while ensuring precise delivery. The integration of our NP delivery system with the drug-inducible polarization platform represents a transformative approach with broad therapeutic potential. Unlike conventional targeted delivery strategies that focus on specific disease sites, our monocyte-directed NP design creates a universally applicable platform for any pathological context where macrophage reprogramming could provide therapeutic benefits. This generalizability mirrors the adaptable nature of our core polarization system, together forming a modular therapeutic framework that can be readily deployed across diverse disease models without requiring fundamental redesign. By leveraging macrophages' unique biological properties—including their phenotypic plasticity, inflammatory sensing capabilities, and tissue-homing potential—our platform represents a comprehensive approach to realizing the full therapeutic potential of engineered macrophage therapies.

4.8 Materials and methods

4.8.1 Mammalian Cell Culture

All cells were maintained in 10 cm treated dishes, 75mL flasks or 175mL flasks at 37 °C and 5% CO_2. Cells were passaged every 3–4 days when they reached 70–80% confluency or ~1million cells/mL. HEK cells and THP1 cells are cultured as described in

Chapter II and III.

Primary monocytes were obtained from whole peripheral blood from healthy donors at the Blood Donor Center at Boston Children's Hospital through a protocol approved by the Boston University Institutional Review Board (IRB). Primary monocytes were isolated using EasySep Human Monocyte Isolation Kit (STEMCELL Technologies 19359) and cultured in RPMI 1640 Medium supplemented with 10% FBS, 1% GlutaMAX, 1% Non-Essential Amino Acids, 1% Sodium Pyruvate (Thermo Scientific 11360070) and 1% Pen-Strep.

4.8.2 Lentiviral Transduction of Primary Monocytes/Macrophages

Lentiviruses were generated with CHEDAR cells in 6 well plates as previously described. VPX VLPs were generated by transfecting CHEDAR cells with 2ng of the pMD2.G VSVG plasmid and 14ng of pSIV-D3psi/delta env/delta Vif/delta Vpr plasmid (Addgene #132928) using TransIT-Lenti Transfection Reagent. Each well of VPX VLPs were concentrated at a 3:1 ratio using Lenti-X Concentrator and resuspended in 100uL Opti-MEM I Reduced Serum Medium.

To transduce primary monocytes, cells were seeded at 1,000,000 cells/well in a 24-well plate in 1mL media. 100uL of synZiFTR LV solution, 50uL of reporter LV solution and 50uL of VPX VLPs solution were added to cells prior to spinfection at 800g for 45mins and overnight incubation. To transduced primary macrophages, 1,000,000/well primary monocytes were seeded in a 6-well plate and differentiated with 100ng/mL Recombinant Human M-CSF (PeproTech 300-25) for 72h. After differentiation into macrophages, cells were treated with 100uL of synZiFTR LV

solution, 50uL of reporter LV solution and 50uL of VPX VLPs solution and incubated for 24h prior to removal of virus. Transduced cells were rested for 3 days and subsequently treated with 1mM GZV or 4OHT then used for downstream induction measurements.

4.8.3 In vitro co-culture killing assay

Primary macrophages were transduced with synZiFTR 2.0, or constitutive CAR or mCherry control with the inducible CD19 CAR expressing plasmid. Cells were rested for 3 days after transduction and treated with 2ug/mL puromycin for 3 days. Survived cells were lifted with TrypLE and replated at 25,000 cells/well in a 48-well plate with the addition of 1mM GZV or DMSO. After 3-day drug induction, 25,000 BFP expressing wild type NALM cells or GFP expressing CD19 KD NALM cells were added to each well and co-cultured with primary macrophages overnight. 20h later, NALM cells in the supernatant were extracted and counted on flow cytometer, using a BFP or GFP gate. Primary macrophages were harvested, and their CAR expression level was measured on flow cytometer. Killing efficiency was calculated as the percentage of cells killed compared to control wells containing NALM6 cells without primary macrophages.

4.8.4 DSPE-PEG(3.4k)-mcp1/scramble peptide conjugation

DSPE-PEG-mcp1 was synthesized with maleimide-thiol reaction. 2mg of mcp1 peptide (YNFTNRKISVQRLASYRRITSSK) or scramble peptide with a cysteine attached on the N terminal was dissolved in 500uL 100mM HEPEs buffer at pH 7-7.5 at room temperature, after degassing the buffer by bubbling through argon gas. 1.98mg TCEP was added to reduce disulfide bonds for 20mins at room temperature. 3.3mg

DSPE-PEG-Maleimide was dissolved in 100uL DMSO and flushed with argon gas. The DSPE-PEG-Maleimide solution was added to the peptide solution dropwise while it is stirring and flushed with argon gas. The reaction was stirred under room temperature for 2h or under 4C overnight. The reaction product was dialyzed overnight using a SnakeSkin Dialysis Tubing (MWCO=10k). The final product was freeze dried and stored in -80C.

4.8.5 Nanoparticle fabrication

PLGA-Lecithin-DSPE-PEG NPs were fabricated using previously established nanoprecipitation method (Chan et al., 2009). In short, PLGA was dissolved in acetonitrile. 7:3 molar ratio of lecithin and DSPE-PEG mixture of 25% (by molar) DSPE-2k PEG and 75% DSPE-3.4k PEG-FITC/peptide was dissolved in 4% EtOH solution at a total of 20% of the PLGA polymer weight and heated to 65C. The PLGA solution was added to the preheated lipid aqueous solution dropwise at 1ml/min using a syringe pump under gentle stirring, followed by 3 minutes of vortexing and 2h continuous stirring. The reaction product was purified with overnight dialysis using SnakeSkin Dialysis Tubing with 100K MWCO (Thermo Scientific). The subsequent product solution was stored under 4C.

4.8.6 Nanoparticle DLS and zeta potential measurements

To assess the size and zeta potential of NPs which inform us of their aggregation with proteins and stability in different FBS concentrations, NP solution was diluted 10x in DI water and their effective diameter profile was measured using dynamic light scattering using a 90Plus DLS Analyzer (Brookhaven Instruments) at a 90˚ detection

angle. Zeta potential measurements were performed on the same samples using the same apparatus

4.8.7 Nanoparticle and THP1 co culture

500ug/mL NPs decorated with different surface peptides were incubate with THP1 monocytes at different temperatures using culture medium containing varying concentrations of FBS. NP solutions were sterilized under UV light for 30mins before addition to the cell culture. Post incubation, cells were washed 3 times in FACS buffer by centrifugation at 300g for 5 mins. Cells were gated on SSC and FSC on flow cytometer and the FITC level was measured for each condition.

4.8.8 Nanoparticle and peritoneal immune cell co culture

The experiment was accomplished in collaboration with Kramnik lab and BUMC Flow Cytometry Core Facility. In short, 5 B6.1H Male DOB 01/26/19 mice were IP injected 0.5ml of Thioglycolate. Mice will be sacrificed on 4^{th} day post stimulation. Peritoneal immune cells were isolated from peritoneal cavity by flushing with 10mL PBS, followed by RBC lysis buffer treatment and multiple washings with 2% FBS-containing PBS. UV sterilized nanoparticles were added to 0.5 million cells per sample to reach a final concentration of 200 or 500ug/mL. Cells and nanoparticles were incubated under 4C for 1h.

Post incubation, cells were collected by centrifugation for 10mins at 1200rpm. Cells were stained with Zombie NIR, followed by Fc block treatment then stained by an antibody cocktail (BUV-CD11b, PE-CD11c, APC-CD45, BV421-F4/80, PE77-Ly6C, PerCP55-Ly6G and BV650-MHCII). All antibodies were obtained from BD Pharmingen.

Beads were stained with each antibody to establish compensation samples. Finally, cells were fixed and resuspended in FACS buffer and analyzed on flow cytometer (Cytek Aurora 5L “Freya”).

CHAPTER FIVE: DISCUSSION AND CONCLUSIONS

In this work, we developed three synergistic components to achieve inducible modulation of macrophage polarization in vivo: (1) engineered STAT protein effectors that enable robust, cytokine-independent activation of M1/M2 polarization; (2) the synZiFTR 2.0 system providing inducible, precise spatiotemporal control over cellular activation; and (3) monocyte-targeting nanoparticles for cell-specific inducer delivery that enhances overall system safety. Notably, we deliberately avoided incorporating cell- or disease-specific elements, preserving the platform's adaptability across diverse disease models. Together, these components form a safe, potent, and modular macrophage therapy system optimized for clinical translation.

The engineered STAT protein effectors were selected for their capacity to globally remodel macrophage activity and sustain responses once translated into functional proteins. While CRISPR-based approaches could potentially upregulate endogenous STAT expression in vivo, they cannot overcome the inherent cytokine dependence of native STAT proteins or their susceptibility to negative regulation by competing polarizing signals. By employing exogenous STAT expression coupled with an inducible control system, we bypass the technical challenges of in vivo gene delivery and potential risks of off-target genome editing, while establishing precise control over therapeutic macrophage activation.

The structural complexity and functional diversity of large therapeutic cargo like STAT proteins necessitated innovative approaches to maximize transactivation potency, leading to the development of synZiFTR 2.0. During its development, we implemented a

novel TAD engineering strategy based on creating kinetic synergy by simultaneously stimulating multiple rate-limiting steps in transcription. This approach led to the discovery of IWS1 TIMs as a potent transcriptional synergizer capable of boosting performance across multiple TADs (p65, NFZ) and induction systems. Mechanistic studies confirmed that TIMs operates through interactions with elongation machinery, complementing p65's or NFZ's transactivation mechanism. We define TIMs domain as a transcriptional enhancer, as it lacks intrinsic transactivation capability and therefore preserves the native regulatory features of any activator it's fused to. This property enables the creation of a novel TAD architecture (2xTIMs-p65) outperforming VPR in potency while maintaining superior control over basal expression. The combination of TIMs' compact size, additive effects, and mechanism-independent enhancement makes it particularly valuable for current human-compatible gene regulation systems.

Beyond advancing TAD engineering principles, the development and implementation of synZiFTR 2.0 in primary macrophages provided valuable insights for designing synthetic genetic tools in these cells. This work represents the first comprehensive evaluation of leading TADs in macrophages and validates multiple novel components—including synthetic zinc fingers, GZV/ERT induction mechanisms, and the synZiFTR platform itself—as valuable modules for constructing complex gene circuits to control macrophage activity and therapeutic functions.

Nanoparticles have emerged as promising delivery vehicles for macrophage reprogramming agents, offering cargo protection, delivery efficiency, and targeting specificity. While over 60 FDA-approved nanocarriers exist on the market, many

approved formulations leverage passive accumulation in tumors via the EPR effect without active targeting moieties. For non-tumor applications, nanoparticle accumulation in spleen and liver remains a challenge, potentially causing off-target effects and liver toxicity—particularly concerning for M1-polarizing agents that could induce local inflammation and tissue damage. Our design innovatively decouples polarization effectors from inducer delivery, ensuring off-target macrophages remain unresponsive to the inducer and thereby adding a critical safety layer to minimize systemic effects.

In conclusion, we developed a modular platform for precise control of macrophage polarization, combining engineered protein effectors, optimized transcriptional regulators, and targeted delivery systems. This work not only establishes a generalizable framework for macrophage therapies with tunable specificity, potency, and safety across diverse diseases, but also provides versatile toolkits that will enable new therapeutic avenues as our understanding of macrophage biology advances.

APPENDIX

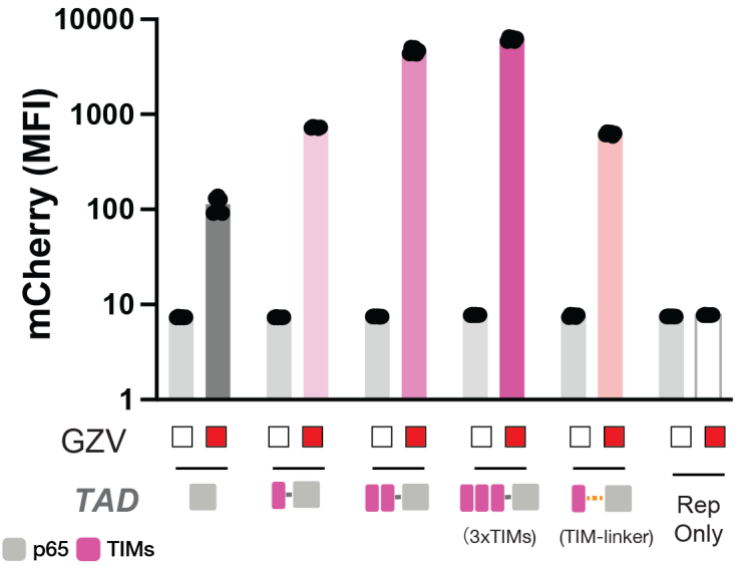

Figure S1. Effects of TIMs copy number on transactivation capability.

3 copies of TIMs further improved transactivation but less significantly compared to adding a second copy. Addition of a linker between TIMs and p65 did not enhance p65 performance

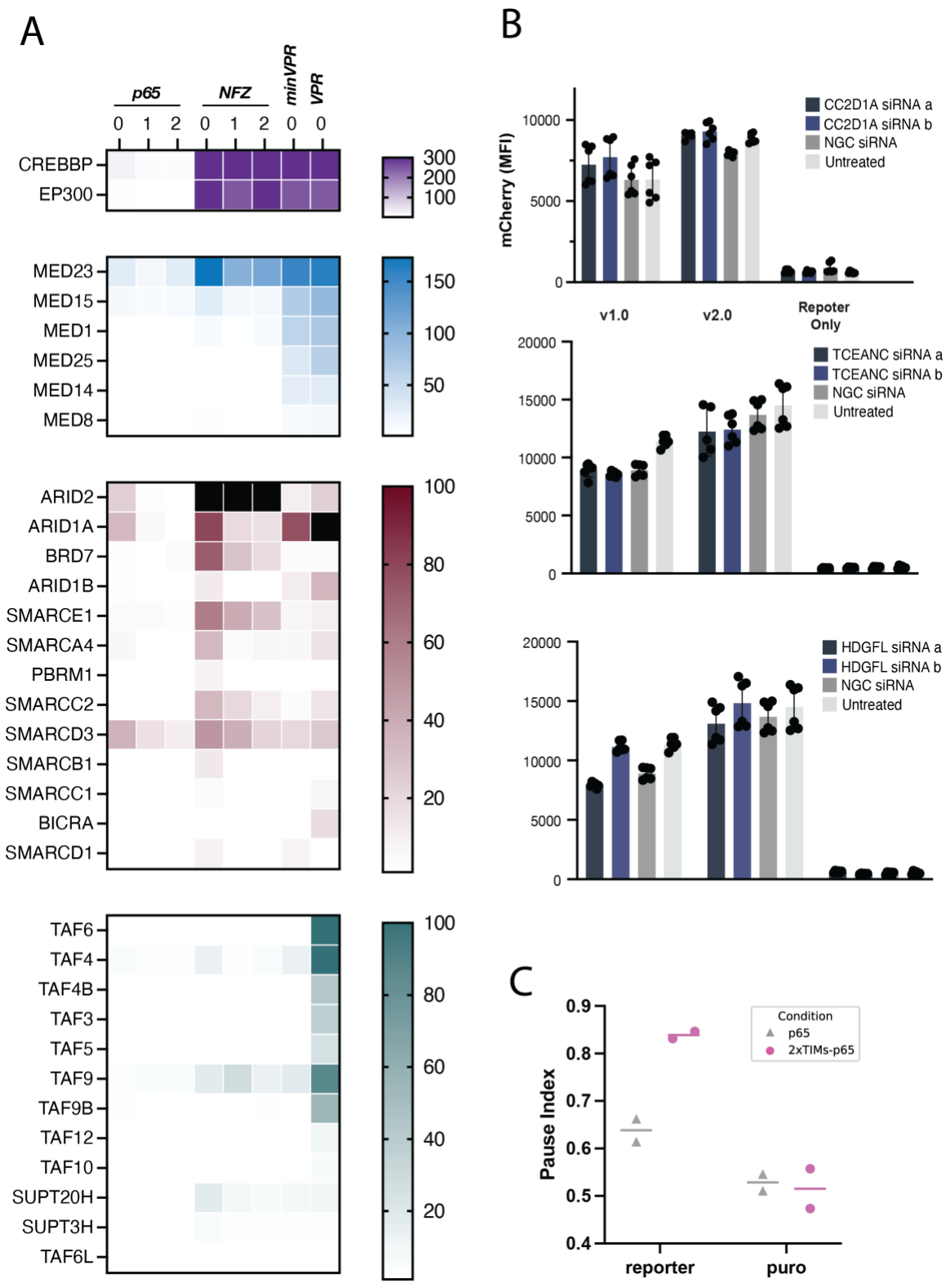
A
p65
NFZ
minVPR
VPR
0 1 2 0 1 2 0 0
CREBBP
EP300
300
200
100
MED23
MED15
MED1
MED25
MED14
MED8
150
100
50
ARID2
ARID1A
BRD7
ARID1B
SMARCE1
SMARCA4
PBRM1
SMARCC2
SMARCD3
SMARCB1
SMARCC1
BICRA
SMARCD1
100
80
60
40
20
TAF6
TAF4
TAF4B
TAF3
TAF5
TAF9
TAF9B
TAF12
TAF10
SUPT20H
SUPT3H
TAF6L
100
80
60
40
20
B
mCherry (MFI)
CC2D1A siRNA a
CC2D1A siRNA b
NGC siRNA
Untreated
v1.0
v2.0
Repoter Only
TCEANC siRNA a
TCEANC siRNA b
HDGFL siRNA a
HDGFL siRNA b
C
Pause Index
Condition
p65
2xTIMs-p65
reporter
puro

Figure S2. Supplementary BioID and PRO Seq results

(A) BioID revealed that non TIMs-dependent interactions are prevalent with non elongation factors, such as transcriptional coactivators and chromosome regulators.

(B)CC2D1A, HDGFL and TCEAN did not functionally contribute to synZiFTR 2.0 activity despite their interactions with the TIMs domain.

(C) Pause index was calculated for each TAD using PRO Seq 3' reads. PI=accumulated reads in [TSS-50BP – TSS+100bp]/ accumulated reads in [TSS+100BP – TSS+250bp]. No significant differences were observed between with and without TIMs.

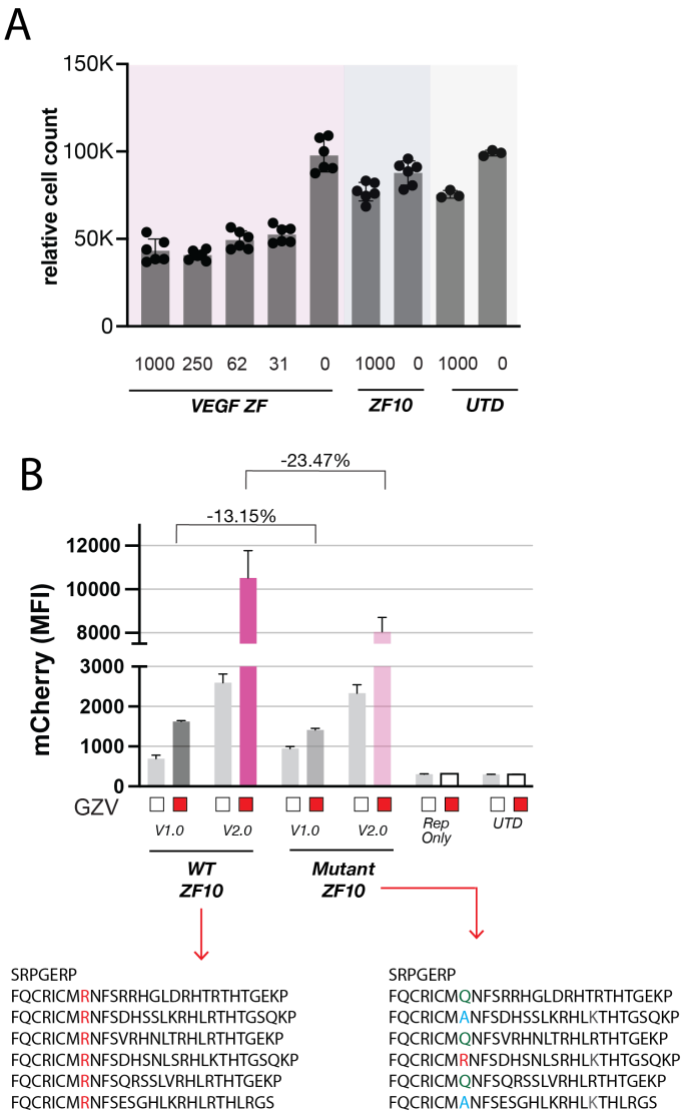

Figure S3. Cell fitness cost and transactivation potency cost with engineered VEGF ZF and ZF10R.

(A) CellTiterGlo assay was used to measure cell viability in inducible VEGF production experiments. Lower cell count was observed across all conditions where cells are secreting VEGF, indicating a metabolic burden and fitness cost of VEGF production. (B)Arginine mutated ZF10 (ZF10R) reduced both on-target and off-target interactions. Reporter output was decreased when using ZF10R in synZiFTRs regardless of TAD architecture.

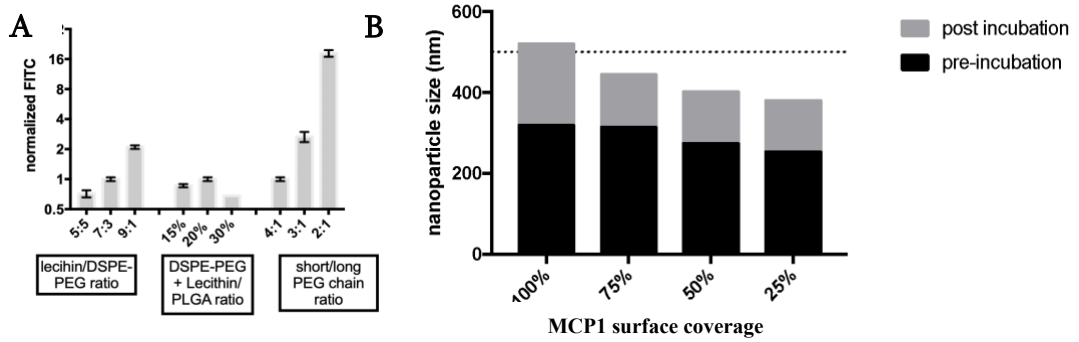

Figure S4. NP formulation optimization for stability and surface coverage.

(A) Different formulations of NPs were tested to maximize the surface coverage of PEG(3.4k) for higher mcp1 coverage (measured by FITC signal). Short/long PEG chain ratio was determined to be the most important parameter and was further studied.

(B) NP stability was tested by measuring the size change on DLS before and after overnight incubation with 10% FBS containing RPMI medium. 100% PEG (3.4k) covered NPs showed most increase in size, resulting in an average diameter >500nm. The other three formulas showed similar level of size change.

BIBLIOGRAPHY

Abdellatif, A.A.H., Alsowinea, A.F., 2021. Approved and marketed nanoparticles for disease targeting and applications in COVID-19. Nanotechnology Reviews 10, 1941–1977. https://doi.org/10.1515/ntrev-2021-0115

Abdou, Y., Pohlmann, P.R., Maziarz, R.T., Murthy, H.S., Yuan, Y., Krishnamurthy, A., Reiss, K., Isaacs, J.M., He, A., Cairo, M.S., Cao, F., Advani, P., Blumenthal, D., Locke, K., Wetzel, J., Klichinsky, M., Condamine, T., Kennedy, E., Sohal, D., 2024. 659 A phase 1, first-in-human study of autologous monocytes engineered to express an anti-HER2 chimeric antigen receptor (CAR) in participants with HER2 overexpressing solid tumors, in: Regular and Young Investigator Award Abstracts. Presented at the SITC 39th Annual Meeting (SITC 2024) Abstracts, BMJ Publishing Group Ltd, pp. A756–A756. https://doi.org/10.1136/jitc-2024-SITC2024.0659

Ahsan, F., Rivas, I.P., Khan, M.A., Torres Suarez, A.I., 2002. Targeting to macrophages: role of physicochemical properties of particulate carriers--liposomes and microspheres--on the phagocytosis by macrophages. Journal of Controlled Release 79, 29–40. https://doi.org/10.1016/s0168-3659(01)00549-1

Alerasool, N., Leng, H., Lin, Z.-Y., Gingras, A.-C., Taipale, M., 2022a. Identification and functional characterization of transcriptional activators in human cells. Molecular Cell 82, 677-695.e7. https://doi.org/10.1016/j.molcel.2021.12.008

Alerasool, N., Leng, H., Lin, Z.-Y., Gingras, A.-C., Taipale, M., 2022b. Identification and functional characterization of transcriptional activators in human cells. Molecular Cell 82, 677-695.e7. https://doi.org/10.1016/j.molcel.2021.12.008

Alexis, F., Pridgen, E., Molnar, L.K., Farokhzad, O.C., 2008. Factors Affecting the Clearance and Biodistribution of Polymeric Nanoparticles. Molecular Pharmaceutics 5(4), 505–515. https://doi.org/10.1021/mp800051m

Austenaa, L.M.I., Barozzi, I., Simonatto, M., Masella, S., Della Chiara, G., Ghisletti, S., Curina, A., de Wit, E., Bouwman, B.A.M., de Pretis, S., Piccolo, V., Termanini, A., Prosperini, E., Pelizzola, M., de Laat, W., Natoli, G., 2015. Transcription of Mammalian *cis*-Regulatory Elements Is Restrained by Actively Enforced Early Termination. Molecular Cell 60, 460–474. https://doi.org/10.1016/j.molcel.2015.09.018

Baxter, E.W., Graham, A.E., Re, N.A., Carr, I.M., Robinson, J.I., Mackie, S.L., Morgan, A.W., 2020. Standardized protocols for differentiation of THP-1 cells to macrophages with distinct M(IFNγ+LPS), M(IL-4) and M(IL-10) phenotypes. Journal of Immunological Methods 478, 112721. https://doi.org/10.1016/j.jim.2019.112721

Bill, R., Wirapati, P., Messemaker, M., Roh, W., Zitti, B., Duval, F., Kiss, M., Park, J.C., Saal, T.M., Hoelzl, J., Tarussio, D., Benedetti, F., Tissot, S., Kandalaft, L., Varrone, M., Ciriello, G., McKee, T.A., Monnier, Y., Mermod, M., Blaum, E.M., Gushterova, I., Gonye, A.L.K., Hacohen, N., Getz, G., Mempel, T.R., Klein, A.M., Weissleder, R., Faquin, W.C., Sadow, P.M., Lin, D., Pai, S.I., Sade-Feldman, M., Pittet, M.J., 2023. CXCL9:SPP1 macrophage polarity identifies a network of cellular programs that control human cancers. Science 381, 515–524. https://doi.org/10.1126/science.ade2292

Bragdon, M.D.J., Patel, N., Chuang, J., Levien, E., Bashor, C.J., Khalil, A.S., 2023. Cooperative assembly confers regulatory specificity and long-term genetic circuit stability. Cell 186, 3810-3825.e18. https://doi.org/10.1016/j.cell.2023.07.012

Brempelis, K.J., Cowan, C.M., Kreuser, S.A., Labadie, K.P., Prieskorn, B.M., Lieberman, N.A.P., Ene, C.I., Moyes, K.W., Chinn, H., DeGolier, K.R., Matsumoto, L.R., Daniel, S.K., Yokoyama, J.K., Davis, A.D., Hoglund, V.J., Smythe, K.S., Balcaitis, S.D., Jensen, M.C., Ellenbogen, R.G., Campbell, J.S., Pierce, R.H., Holland, E.C., Pillarisetty, V.G., Crane, C.A., 2020. Genetically engineered macrophages persist in solid tumors and locally deliver therapeutic proteins to activate immune responses. Journal for Immunotherapy of Cancer 8, e001356. https://doi.org/10.1136/jitc-2020-001356

Brix, D.M., Bundgaard Clemmensen, K.K., Kallunki, T., 2014. When Good Turns Bad: Regulation of Invasion and Metastasis by ErbB2 Receptor Tyrosine Kinase. Cells 3, 53–78. https://doi.org/10.3390/cells3010053

Burkhart, B.A., Hebbar, P.B., Trotter, K.W., Archer, T.K., 2005. Chromatin-dependent E1A Activity Modulates NF-κB RelA-mediated Repression of Glucocorticoid Receptor-dependent Transcription. Journal of Biological Chemistry 280, 6349–6358. https://doi.org/10.1074/jbc.M411147200

Chan, J.M., Zhang, L., Yuet, K.P., Liao, G., Rhee, J.-W., Langer, R., Farokhzad, O.C., 2009. PLGA–lecithin–PEG core–shell nanoparticles for controlled drug delivery. Biomaterials 30, 1627–1634. https://doi.org/10.1016/j.biomaterials.2008.12.013

Chen, Y., Kokic, G., Dienemann, C., Dybkov, O., Urlaub, H., Cramer, P., 2023. Structure of the transcribing RNA polymerase II–Elongin complex. Nature Structural & Molecular Biology 30, 1925–1935. https://doi.org/10.1038/s41594-023-01138-w

Cho, J.H., Okuma, A., Sofjan, K., Lee, S., Collins, J.J., Wong, W.W., 2021. Engineering advanced logic and distributed computing in human CAR immune cells. Nature Communications 12, 792. https://doi.org/10.1038/s41467-021-21078-7

Corraliza, I., 2014. Recruiting specialized macrophages across the borders to restore brain functions. Frontiers in Cellular Neuroscience. 8. https://doi.org/10.3389/fncel.2014.00262

Cortazar, M.A., Sheridan, R.M., Erickson, B., Fong, N., Glover-Cutter, K., Brannan, K., Bentley, D.L., 2019. Control of RNA Pol II Speed by PNUTS-PP1 and Spt5 Dephosphorylation Facilitates Termination by a "Sitting Duck Torpedo" Mechanism. Molecular Cell 76, 896-908.e4. https://doi.org/10.1016/j.molcel.2019.09.031

Cossa, G., Roeschert, I., Prinz, F., Baluapuri, A., Silveira Vidal, R., Schülein-Völk, C., Chang, Y.-C., Ade, C.P., Mastrobuoni, G., Girard, C., Kumar, A., Wortmann, L., Walz, S., Lührmann, R., Kempa, S., Kuster, B., Wolf, E., Mumberg, D., Eilers, M., 2020. Localized Inhibition of Protein Phosphatase 1 by NUAK1 Promotes Spliceosome Activity and Reveals a MYC-Sensitive Feedback Control of Transcription. Molecular Cell 77, 1322-1339.e11. https://doi.org/10.1016/j.molcel.2020.01.008

Cui, K., Ardell, C.L., Podolnikova, N.P., Yakubenko, V.P., 2018. Distinct Migratory Properties of M1, M2, and Resident Macrophages Are Regulated by αDβ2 and αMβ2 Integrin-Mediated Adhesion. Frontiers in Immunology. 9. https://doi.org/10.3389/fimmu.2018.02650

Daniel, C., Salvekar, A., Schindler, U., 2000. A Gain-of-function Mutation in STAT6. Journal of Biological Chemistry 275, 14255–14259. https://doi.org/10.1074/jbc.C000129200

De Henau, O., Rausch, M., Winkler, D., Campesato, L.F., Liu, C., Cymerman, D.H., Budhu, S., Ghosh, A., Pink, M., Tchaicha, J., Douglas, M., Tibbitts, T., Sharma, S., Proctor, J., Kosmider, N., White, K., Stern, H., Soglia, J., Adams, J., Palombella, V.J., McGovern, K., Kutok, J.L., Wolchok, J.D., Merghoub, T., 2016. Overcoming resistance to checkpoint blockade therapy by targeting PI3Kγ in myeloid cells. Nature 539, 443–447. https://doi.org/10.1038/nature20554

DeNardo, D.G., Barreto, J.B., Andreu, P., Vasquez, L., Tawfik, D., Kolhatkar, N., Coussens, L.M., 2009. CD4+ T Cells Regulate Pulmonary Metastasis of Mammary Carcinomas by Enhancing Protumor Properties of Macrophages. Cancer Cell 16, 91–102. https://doi.org/10.1016/j.ccr.2009.06.018

Ewen-Campen, B., Yang-Zhou, D., Fernandes, V.R., González, D.P., Liu, L.-P., Tao, R., Ren, X., Sun, J., Hu, Y., Zirin, J., Mohr, S.E., Ni, J.-Q., Perrimon, N., 2017. Optimized strategy for in vivo Cas9-activation in Drosophila. Proceedings of the National Academy of Sciences of the United States of America 114, 9409–9414. https://doi.org/10.1073/pnas.1707635114

Frontiers | Signal Transducer and Activator of Transcription (STATs) Proteins in Cancer and Inflammation: Functions and Therapeutic Implication [WWW Document], n.d. URL https://www.frontiersin.org/journals/oncology/articles/10.3389/fonc.2019.00048/full (accessed 3.19.25).

Genin, M., Clement, F., Fattaccioli, A., Raes, M., Michiels, C., 2015. M1 and M2 macrophages derived from THP-1 cells differentially modulate the response of cancer cells to etoposide. BMC Cancer 15, 577. https://doi.org/10.1186/s12885-015-1546-9

Getts, D.R., Terry, R.L., Getts, M.T., Deffrasnes, C., Müller, M., van Vreden, C., Ashhurst, T.M., Chami, B., McCarthy, D., Wu, H., Ma, J., Martin, A., Shae, L.D., Witting, P., Kansas, G.S., Kühn, J., Hafezi, W., Campbell, I.L., Reilly, D., Say, J., Brown, L., White, M.Y., Cordwell, S.J., Chadban, S.J., Thorp, E.B., Bao, S., Miller, S.D., King, N.J.C., 2014. Therapeutic Inflammatory Monocyte Modulation Using Immune-Modifying Microparticles. Science Translational Medicine 6, 219ra7. https://doi.org/10.1126/scitranslmed.3007563

Guo, C., Sun, H., Du, Y., Dai, X., Pang, Y., Han, Z., Xiong, X., Li, S., Zhang, J., Zheng, Q., Gui, X., 2025. Specifically blocking αvβ8-mediated TGF-β signaling to reverse immunosuppression by modulating macrophage polarization. Journal of Experimental & Clinical Cancer Research 44, 1. https://doi.org/10.1186/s13046-024-03250-1

Guo, W., Pylayeva, Y., Pepe, A., Yoshioka, T., Muller, W.J., Inghirami, G., Giancotti, F.G., 2006. β4 Integrin Amplifies ErbB2 Signaling to Promote Mammary Tumorigenesis. Cell 126, 489–502. https://doi.org/10.1016/j.cell.2006.05.047

Han, J., Tam, K., Tam, C., Hollis, R.P., Kohn, D.B., 2021. Improved lentiviral vector titers from a multi-gene knockout packaging line. Molecular Therapy Oncolytics 23, 582–592. https://doi.org/10.1016/j.omto.2021.11.012

Hind, L.E., Lurier, E.B., Dembo, M., Spiller, K.L., Hammer, D.A., 2016. Effect of M1–M2 Polarization on the Motility and Traction Stresses of Primary Human Macrophages. Cellular and Molecular Bioengineering 9, 455–465. https://doi.org/10.1007/s12195-016-0435-x

Hoppenbrouwers, T., Bastiaan-Net, S., Garssen, J., Pellegrini, N., Willemsen, L.E.M., Wichers, H.J., 2022. Functional differences between primary monocyte-derived and THP-1 macrophages and their response to LCPUFAs. PharmaNutrition 22, 100322. https://doi.org/10.1016/j.phanu.2022.100322

Ichikawa, D.M., Abdin, O., Alerasool, N., Kogenaru, M., Mueller, A.L., Wen, H., Giganti, D.O., Goldberg, G.W., Adams, S., Spencer, J.M., Razavi, R., Nim, S., Zheng, H., Gionco, C., Clark, F.T., Strokach, A., Hughes, T.R., Lionnet, T., Taipale, M., Kim, P.M., Noyes, M.B., 2023. A universal deep-learning model for zinc finger

design enables transcription factor reprogramming. Nature Biotechnology 41, 1117–1129. https://doi.org/10.1038/s41587-022-01624-4

Jaguin, M., Houlbert, N., Fardel, O., Lecureur, V., 2013. Polarization profiles of human M-CSF-generated macrophages and comparison of M1-markers in classically activated macrophages from GM-CSF and M-CSF origin. Cellular Immunology 281, 51–61. https://doi.org/10.1016/j.cellimm.2013.01.010

Jaiswal, A., Reddy, S.S., Maurya, M., Maurya, P., Barthwal, M.K., 2019. MicroRNA-99a mimics inhibit M1 macrophage phenotype and adipose tissue inflammation by targeting TNFα. Cellular & Molecular Immunology 16, 495–507. https://doi.org/10.1038/s41423-018-0038-7

Jaynes, J.M., Sable, R., Ronzetti, M., Bautista, W., Knotts, Z., Abisoye-Ogunniyan, A., Li, D., Calvo, R., Dashnyam, M., Singh, A., Guerin, T., White, J., Ravichandran, S., Kumar, P., Talsania, K., Chen, V., Ghebremedhin, A., Karanam, B., Bin Salam, A., Amin, R., Odzorig, T., Aiken, T., Nguyen, V., Bian, Y., Zarif, J.C., de Groot, A.E., Mehta, M., Fan, L., Hu, X., Simeonov, A., Pate, N., Abu-Asab, M., Ferrer, M., Southall, N., Ock, C.-Y., Zhao, Y., Lopez, H., Kozlov, S., de Val, N., Yates, C.C., Baljinnyam, B., Marugan, J., Rudloff, U., 2020. Mannose receptor (CD206) activation in tumor-associated macrophages enhances adaptive and innate antitumor immune responses. Science Translational Medicine 12, eaax6337. https://doi.org/10.1126/scitranslmed.aax6337

Kamerkar, S., Leng, C., Burenkova, O., Jang, S.C., McCoy, C., Zhang, K., Dooley, K., Kasera, S., Zi, T., Sisó, S., Dahlberg, W., Sia, C.L., Patel, S., Schmidt, K., Economides, K., Soos, T., Burzyn, D., Sathyanarayanan, S., 2022. Exosome-mediated genetic reprogramming of tumor-associated macrophages by exoASO-STAT6 leads to potent monotherapy antitumor activity. Science Advances 8, eabj7002. https://doi.org/10.1126/sciadv.abj7002

Kapellos, T.S., Taylor, L., Lee, H., Cowley, S.A., James, W.S., Iqbal, A.J., Greaves, D.R., 2016. A novel real time imaging platform to quantify macrophage phagocytosis. Biochemical Pharmacology 116, 107–119. https://doi.org/10.1016/j.bcp.2016.07.011

Kelley, J.R., Dimitrova, E., Maciuszek, M., Nguyen, H.T., Szczurek, A.T., Hughes, A.L., Blackledge, N.P., Kettenbach, A.N., Klose, R.J., 2024. The PNUTS phosphatase complex controls transcription pause release. Molecular Cell 84, 4843-4861.e8. https://doi.org/10.1016/j.molcel.2024.10.045

Khalil, A.S., Lu, T.K., Bashor, C.J., Ramirez, C.L., Pyenson, N.C., Joung, J.K., Collins, J.J., 2012. A Synthetic Biology Framework for Programming Eukaryotic Transcription Functions. Cell 150, 647–658. https://doi.org/10.1016/j.cell.2012.05.045

Kim, B., Nesvizhskii, A.I., Rani, P.G., Hahn, S., Aebersold, R., Ranish, J.A., 2007. The transcription elongation factor TFIIS is a component of RNA polymerase II preinitiation complexes. Proceedings of the National Academy of Sciences of the United States of America 104, 16068–16073. https://doi.org/10.1073/pnas.0704573104

Kim, J., Kim, M., Yong, S.-B., Han, H., Kang, S., Lahiji, S.F., Kim, S., Hong, J., Seo, Y., Kim, Y.-H., 2023. Engineering TGF-β inhibitor-encapsulated macrophage-inspired multi-functional nanoparticles for combination cancer immunotherapy. Biomaterials Research 27, 136. https://doi.org/10.1186/s40824-023-00470-y

Klichinsky, M., Ruella, M., Shestova, O., Lu, X.M., Best, A., Zeeman, M., Schmierer, M., Gabrusiewicz, K., Anderson, N.R., Petty, N.E., Cummins, K.D., Shen, F., Shan, X., Veliz, K., Blouch, K., Yashiro-Ohtani, Y., Kenderian, S.S., Kim, M.Y., O'Connor, R.S., Wallace, S.R., Kozlowski, M.S., Marchione, D.M., Shestov, M., Garcia, B.A., June, C.H., Gill, S., 2020. Human chimeric antigen receptor macrophages for cancer immunotherapy. Nature Biotechnology 38, 947–953. https://doi.org/10.1038/s41587-020-0462-y

Lam, J.H., Ng, H.H.M., Lim, C.J., Sim, X.N., Malavasi, F., Li, H., Loh, J.J.H., Sabai, K., Kim, J.-K., Ong, C.C.H., Loh, T., Leow, W.Q., Choo, S.P., Toh, H.C., Lee, S.Y., Chan, C.Y., Chew, V., Lim, T.S., Yeong, J., Lim, T.K.H., 2019. Expression of CD38 on Macrophages Predicts Improved Prognosis in Hepatocellular Carcinoma. Frontiers in Immunology 10, 2093. https://doi.org/10.3389/fimmu.2019.02093

Landsverk, H.B., Sandquist, L.E., Bay, L.T.E., Steurer, B., Campsteijn, C., Landsverk, O.J.B., Marteijn, J.A., Petermann, E., Trinkle-Mulcahy, L., Syljuåsen, R.G., 2020. WDR82/PNUTS-PP1 Prevents Transcription-Replication Conflicts by Promoting RNA Polymerase II Degradation on Chromatin. Cell Reports 33, 108469. https://doi.org/10.1016/j.celrep.2020.108469

Lecoq, L., Raiola, L., Chabot, P.R., Cyr, N., Arseneault, G., Legault, P., Omichinski, J.G., 2017. Structural characterization of interactions between transactivation domain 1 of the p65 subunit of NF-κB and transcription regulatory factors. Nucleic Acids Research 45, 5564–5576. https://doi.org/10.1093/nar/gkx146

Lee, J.-H., You, J., Dobrota, E., Skalnik, D.G., 2010. Identification and Characterization of a Novel Human PP1 Phosphatase Complex*. Journal of Biological Chemistry 285, 24466–24476. https://doi.org/10.1074/jbc.M110.109801

LeRoy, G., Oksuz, O., Descostes, N., Aoi, Y., Ganai, R.A., Kara, H.O., Yu, J.-R., Lee, C.-H., Stafford, J., Shilatifard, A., Reinberg, D., 2019. LEDGF and HDGF2 relieve the nucleosome-induced barrier to transcription in differentiated cells. Science Advances 5, eaay3068. https://doi.org/10.1126/sciadv.aay3068

Liu, Z., Wu, A., Wu, Z., Wang, T., Pan, Y., Li, B., Zhang, X., Yu, M., 2022. TOX4 facilitates promoter-proximal pausing and C-terminal domain dephosphorylation of RNA polymerase II in human cells. Communications Biology 5, 300. https://doi.org/10.1038/s42003-022-03214-1

Ma, C., He, D., Tian, P., Wang, Y., He, Y., Wu, Q., Jia, Z., Zhang, X., Zhang, P., Ying, H., Jin, Z.-B., Hu, G., 2022. miR-182 targeting reprograms tumor-associated macrophages and limits breast cancer progression. Proceedings of the National Academy of Sciences of the United States of America 119, e2114006119. https://doi.org/10.1073/pnas.2114006119

Ma, P.-F., Gao, C.-C., Yi, J., Zhao, J.-L., Liang, S.-Q., Zhao, Y., Ye, Y.-C., Bai, J., Zheng, Q.-J., Dou, K.-F., Han, H., Qin, H.-Y., 2017. Cytotherapy with M1-polarized macrophages ameliorates liver fibrosis by modulating immune microenvironment in mice. Journal of Hepatology 67, 770–779. https://doi.org/10.1016/j.jhep.2017.05.022

Ma, S., Sun, B., Duan, S., Han, J., Barr, T., Zhang, J., Bissonnette, M.B., Kortylewski, M., He, C., Chen, J., Caligiuri, M.A., Yu, J., 2023. YTHDF2 orchestrates tumor-associated macrophage reprogramming and controls antitumor immunity through CD8+ T cells. Nature Immunology 24, 255–266. https://doi.org/10.1038/s41590-022-01398-6

Madhvi, A., Mishra, H., Leisching, G., Mahlobo, P., Baker, B., 2019. Comparison of human monocyte derived macrophages and THP1-like macrophages as *in vitro* models for *M. tuberculosis* infection. Comparative Immunology, Microbiology and Infectious Diseases 67, 101355. https://doi.org/10.1016/j.cimid.2019.101355

Maeder, M.L., Thibodeau-Beganny, S., Osiak, A., Wright, D.A., Anthony, R.M., Eichtinger, M., Jiang, T., Foley, J.E., Winfrey, R.J., Townsend, J.A., Unger-Wallace, E., Sander, J.D., Müller-Lerch, F., Fu, F., Pearlberg, J., Göbel, C., Dassie, J.P., Pruett-Miller, S.M., Porteus, M.H., Sgroi, D.C., Iafrate, A.J., Dobbs, D., McCray, P.B., Cathomen, T., Voytas, D.F., Joung, J.K., 2008. Rapid "open-source" engineering of customized zinc-finger nucleases for highly efficient gene modification. Mol ecular Cell 31, 294–301. https://doi.org/10.1016/j.molcel.2008.06.016

Mahata, B., Cabrera, A., Brenner, D.A., Guerra-Resendez, R.S., Li, J., Goell, J., Wang, K., Guo, Y., Escobar, M., Parthasarathy, A.K., Szadowski, H., Bedford, G., Reed, D.R., Kim, S., Hilton, I.B., 2023. Compact engineered human mechanosensitive transactivation modules enable potent and versatile synthetic transcriptional control. Nature Methods 20, 1716–1728. https://doi.org/10.1038/s41592-023-02036-1

Martinez-Corral, R., Park, M., Biette, K.M., Friedrich, D., Scholes, C., Khalil, A.S., Gunawardena, J., DePace, A.H., 2023. Transcriptional kinetic synergy: A complex landscape revealed by integrating modeling and synthetic biology. Cell Systems 14(4), 324–339.e7. https://doi.org/10.1016/j.cels.2023.02.003

Mertens, C., Zhong, M., Krishnaraj, R., Zou, W., Chen, X., Darnell, J.E., 2006. Dephosphorylation of phosphotyrosine on STAT1 dimers requires extensive spatial reorientation of the monomers facilitated by the N-terminal domain. Genes & Development 20, 3372–3381. https://doi.org/10.1101/gad.1485406

Mimoso, C.A., Goldman, S.R., 2023. PRO-seq: Precise mapping of engaged RNA Pol II at single nucleotide resolution. Current Protocols 3, e961. https://doi.org/10.1002/cpz1.961

Mohd Yasin, Z.N., Mohd Idrus, F.N., Hoe, C.H., Yvonne-Tee, G.B., 2022. Macrophage polarization in THP-1 cell line and primary monocytes: A systematic review. Differentiation 128, 67–82. https://doi.org/10.1016/j.diff.2022.10.001

Mukherjee, S.P., Behar, M., Birnbaum, H.A., Hoffmann, A., Wright, P.E., Ghosh, G., 2013. Analysis of the RelA:CBP/p300 Interaction Reveals Its Involvement in NF-κB-Driven Transcription. PLoS Biology 11, e1001647. https://doi.org/10.1371/journal.pbio.1001647

Mukund, A.X., Tycko, J., Allen, S.J., Robinson, S.A., Andrews, C., Sinha, J., Ludwig, C.H., Spees, K., Bassik, M.C., Bintu, L., 2023. High-throughput functional characterization of combinations of transcriptional activators and repressors. Cell Systems 14, 746-763.e5. https://doi.org/10.1016/j.cels.2023.07.001

Nascimento, C.R., Rodrigues Fernandes, N.A., Gonzalez Maldonado, L.A., Rossa Junior, C., 2022. Comparison of monocytic cell lines U937 and THP-1 as macrophage models for in vitro studies. Biochemistry and Biophysics Reports 32, 101383. https://doi.org/10.1016/j.bbrep.2022.101383

Partikel, K., Korte, R., Stein, N.C., Mulac, D., Herrmann, F.C., Humpf, H.-U., Langer, K., 2019. Effect of nanoparticle size and PEGylation on the protein corona of PLGA nanoparticles. European Journal of Pharmaceutics and Biopharmaceutics 141, 70–80. https://doi.org/10.1016/j.ejpb.2019.05.006

Phillips, R.J., Lutz, M., Premack, B., 2005. Differential signaling mechanisms regulate expression of CC chemokine receptor-2 during monocyte maturation. Journal of Inflammation (London) 2, 14. https://doi.org/10.1186/1476-9255-2-14

Piette, B.L., Alerasool, N., Lin, Z.-Y., Lacoste, J., Lam, M.H.Y., Qian, W.W., Tran, S., Larsen, B., Campos, E., Peng, J., Gingras, A.-C., Taipale, M., 2021. Comprehensive interactome profiling of the human Hsp70 network highlights functional differentiation of J domains. Molecular Cell 81, 2549-2565.e8. https://doi.org/10.1016/j.molcel.2021.04.012

Pyonteck, S.M., Akkari, L., Schuhmacher, A.J., Bowman, R.L., Sevenich, L., Quail, D.F., Olson, O.C., Quick, M.L., Huse, J.T., Teijeiro, V., Setty, M., Leslie, C.S., Oei,

Y., Pedraza, A., Zhang, J., Brennan, C.W., Sutton, J.C., Holland, E.C., Daniel, D., Joyce, J.A., 2013. CSF-1R inhibition alters macrophage polarization and blocks glioma progression. Nature Medicine 19, 1264–1272. https://doi.org/10.1038/nm.3337

Raimondo, T.M., Mooney, D.J., 2018. Functional muscle recovery with nanoparticle-directed M2 macrophage polarization in mice. Proceedings of the National Academy of Sciences of the United States of America 115, 10648–10653. https://doi.org/10.1073/pnas.1806908115

Rannikko, J.H., Hollmén, M., 2024. Clinical landscape of macrophage-reprogramming cancer immunotherapies. British Journal of Cancer 131, 627–640. https://doi.org/10.1038/s41416-024-02715-6

Reiss, K.A., Angelos, M.G., Dees, E.C., Yuan, Y., Ueno, N.T., Pohlmann, P.R., Johnson, M.L., Chao, J., Shestova, O., Serody, J.S., Schmierer, M., Kremp, M., Ball, M., Qureshi, R., Schott, B.H., Sonawane, P., DeLong, S.C., Christiano, M., Swaby, R.F., Abramson, S., Locke, K., Barton, D., Kennedy, E., Gill, S., Cushing, D., Klichinsky, M., Condamine, T., Abdou, Y., 2025. CAR-macrophage therapy for HER2-overexpressing advanced solid tumors: a phase 1 trial. Nature Medicine 31, 1171–1182. https://doi.org/10.1038/s41591-025-03495-z

Riebeling, T., Staab, J., Herrmann-Lingen, C., Meyer, T., 2014. DNA binding reduces the dissociation rate of STAT1 dimers and impairs the interdimeric exchange of protomers. BMC Biochemistry 15, 28. https://doi.org/10.1186/s12858-014-0028-z

Ries, C.H., Cannarile, M.A., Hoves, S., Benz, J., Wartha, K., Runza, V., Rey-Giraud, F., Pradel, L.P., Feuerhake, F., Klaman, I., Jones, T., Jucknischke, U., Scheiblich, S., Kaluza, K., Gorr, I.H., Walz, A., Abiraj, K., Cassier, P.A., Sica, A., Gomez-Roca, C., de Visser, K.E., Italiano, A., Le Tourneau, C., Delord, J.-P., Levitsky, H., Blay, J.-Y., Rüttinger, D., 2014. Targeting Tumor-Associated Macrophages with Anti-CSF-1R Antibody Reveals a Strategy for Cancer Therapy. Cancer Cell 25, 846–859. https://doi.org/10.1016/j.ccr.2014.05.016

Ritz, S., Schöttler, S., Kotman, N., Baier, G., Musyanovych, A., Kuharev, J., Landfester, K., Schild, H., Jahn, O., Tenzer, S., Mailänder, V., 2015. Protein Corona of Nanoparticles: Distinct Proteins Regulate the Cellular Uptake. Biomacromolecules 16, 1311–1321. https://doi.org/10.1021/acs.biomac.5b00108

Rivard, A., Silver, M., Chen, D., Kearney, M., Magner, M., Annex, B., Peters, K., Isner, J.M., 1999. Rescue of Diabetes-Related Impairment of Angiogenesis by Intramuscular Gene Therapy with Adeno-VEGF. The American Journal of Pathology 154, 355–363. https://doi.org/10.1016/S0002-9440(10)65282-0

Rodell, C.B., Arlauckas, S.P., Cuccarese, M.F., Garris, C.S., Li, R., Ahmed, M.S., Kohler, R.H., Pittet, M.J., Weissleder, R., 2018. TLR7/8-agonist-loaded nanoparticles promote the polarization of tumour-associated macrophages to enhance cancer immunotherapy. Nature Biomedical Engineering 2, 578–588. https://doi.org/10.1038/s41551-018-0236-8

Sadzak, I., Schiff, M., Gattermeier, I., Glinitzer, R., Sauer, I., Saalmüller, A., Yang, E., Schaljo, B., Kovarik, P., 2008. Recruitment of Stat1 to chromatin is required for interferon-induced serine phosphorylation of Stat1 transactivation domain. Proceedings of the National Academy of Sciences of the United States of America 105, 8944–8949. https://doi.org/10.1073/pnas.0801794105

Saha, T., Fojtů, M., Nagar, A.V., Thurakkal, L., Srinivasan, B.B., Mukherjee, M., Sibiyon, A., Aggarwal, H., Samuel, A., Dash, C., Jang, H.L., Sengupta, S., 2024. Antibody nanoparticle conjugate–based targeted immunotherapy for non–small cell lung cancer. Science Advances 10, eadi2046. https://doi.org/10.1126/sciadv.adi2046

Salmaso, S., Caliceti, P., 2013. Stealth Properties to Improve Therapeutic Efficacy of Drug Nanocarriers. Journal of Drug Delivery 2013, e374252. https://doi.org/10.1155/2013/374252

Satoh, J., Tabunoki, H., 2013. A Comprehensive Profile of ChIP-Seq-Based STAT1 Target Genes Suggests the Complexity of STAT1-Mediated Gene Regulatory Mechanisms. Gene Regulation and Systems Biology 7, 41–56. https://doi.org/10.4137/GRSB.S11433

Shi, Y., Giammartino, D.C.D., Taylor, D., Sarkeshik, A., Rice, W.J., Yates, J.R., Frank, J., Manley, J.L., 2009. Molecular Architecture of the Human Pre-mRNA 3′ Processing Complex. Molecular Cell 33, 365–376. https://doi.org/10.1016/j.molcel.2008.12.028

Shields, C.W., Evans, M.A., Wang, L.L.-W., Baugh, N., Iyer, S., Wu, D., Zhao, Z., Pusuluri, A., Ukidve, A., Pan, D.C., Mitragotri, S., 2020. Cellular backpacks for macrophage immunotherapy. Science Advances 6, eaaz6579. https://doi.org/10.1126/sciadv.aaz6579

Sironi, J.J., Ouchi, T., 2004. STAT1-induced Apoptosis Is Mediated by Caspases 2, 3, and 7. Journal of Biological Chemistry 279, 4066–4074. https://doi.org/10.1074/jbc.M307774200

Tycko, J., DelRosso, N., Hess, G.T., Aradhana, Banerjee, A., Mukund, A., Van, M.V., Ego, B.K., Yao, D., Spees, K., Suzuki, P., Marinov, G.K., Kundaje, A., Bassik, M.C., Bintu, L., 2020. High-Throughput Discovery and Characterization of Human Transcriptional Effectors. Cell 183, 2020-2035.e16. https://doi.org/10.1016/j.cell.2020.11.024

Wang, C., Li, Y., Wang, L., Han, Y., Gao, X., Li, T., Liu, M., Dai, L., Du, R., 2024. SPP1 represents a therapeutic target that promotes the progression of oesophageal squamous cell carcinoma by driving M2 macrophage infiltration. British Journal of Cancer 130, 1770–1782. https://doi.org/10.1038/s41416-024-02683-x

Wang, L., Hu, Y.-Y., Zhao, J.-L., Huang, F., Liang, S.-Q., Dong, L., Chen, Y., Yu, H.-C., Bai, J., Yang, J.-M., Fan, J.-Y., Feng, L., Li, S.-Z., Han, H., Qin, H.-Y., 2020. Targeted delivery of miR-99b reprograms tumor-associated macrophage phenotype leading to tumor regression. Journal for Immunotherapy of Cancer 8, e000517. https://doi.org/10.1136/jitc-2019-000517

Wang, S., Zhang, Y., Zhong, Y., Xue, Y., Liu, Z., Wang, C., Kang, D.D., Li, H., Hou, X., Tian, M., Cao, D., Wang, L., Guo, K., Deng, B., McComb, D.W., Merad, M., Brown, B.D., Dong, Y., 2024. Accelerating diabetic wound healing by ROS-scavenging lipid nanoparticle–mRNA formulation. Proceedings of the National Academy of Sciences of the United States of America 121, e2322935121. https://doi.org/10.1073/pnas.2322935121

Wu, X., Singh, R., Hsu, D.K., Zhou, Y., Yu, S., Han, D., Shi, Z., Huynh, M., Campbell, J.J., Hwang, S.T., 2020. A Small Molecule CCR2 Antagonist Depletes Tumor Macrophages and Synergizes with Anti–PD-1 in a Murine Model of Cutaneous T-Cell Lymphoma (CTCL). Journal of Investigative Dermatology 140, 1390-1400.e4. https://doi.org/10.1016/j.jid.2019.11.018

Wu, Y., Park, J., Xu, E., Kim, D., Lee, J., Oh, Y.-K., 2025. MicroRNA-induced reprogramming of tumor-associated macrophages for modulation of tumor immune microenvironment. Journal of Controlled Release 381, 113593. https://doi.org/10.1016/j.jconrel.2025.113593

Yamagata, T., Raveau, M., Kobayashi, K., Miyamoto, H., Tatsukawa, T., Ogiwara, I., Itohara, S., Hensch, T.K., Yamakawa, K., 2020. CRISPR/dCas9-based *Scn1a* gene activation in inhibitory neurons ameliorates epileptic and behavioral phenotypes of Dravet syndrome model mice. Neurobiology of Disease 141, 104954. https://doi.org/10.1016/j.nbd.2020.104954

Yang, H., Song, L., Sun, B., Chu, D., Yang, L., Li, M., Li, H., Dai, Y., Yu, Z., Guo, J., 2021. Modulation of macrophages by a paeoniflorin-loaded hyaluronic acid-based hydrogel promotes diabetic wound healing. Materials Today. Bio 12, 100139. https://doi.org/10.1016/j.mtbio.2021.100139

Yang, K., Xu, C., Zhang, Y., He, S., Li, D., 2017. Sestrin2 Suppresses Classically Activated Macrophages-Mediated Inflammatory Response in Myocardial Infarction through Inhibition of mTORC1 Signaling. Frontiers in Immunology. 8. https://doi.org/10.3389/fimmu.2017.00728

Yin, Y., Huang, X., Lynn, K.D., Thorpe, P.E., 2013. Phosphatidylserine-Targeting Antibody Induces M1 Macrophage Polarization and Promotes Myeloid-Derived Suppressor Cell Differentiation. Cancer Immunology Research 1, 256–268. https://doi.org/10.1158/2326-6066.CIR-13-0073

Yuan, A., Hsiao, Y.-J., Chen, H.-Y., Chen, H.-W., Ho, C.-C., Chen, Y.-Y., Liu, Y.-C., Hong, T.-H., Yu, S.-L., Chen, J.J.W., Yang, P.-C., 2015. Opposite Effects of M1 and M2 Macrophage Subtypes on Lung Cancer Progression. Scientific Reports 5, 14273. https://doi.org/10.1038/srep14273

Yuan, Y., Fan, D., Shen, S., Ma, X., 2022. An M2 macrophage-polarized anti-inflammatory hydrogel combined with mild heat stimulation for regulating chronic inflammation and impaired angiogenesis of diabetic wounds. Chemical Engineering Journal 433, 133859. https://doi.org/10.1016/j.cej.2021.133859

Zeisberger, S.M., Odermatt, B., Marty, C., Zehnder-Fjällman, A.H.M., Ballmer-Hofer, K., Schwendener, R.A., 2006. Clodronate-liposome-mediated depletion of tumour-associated macrophages: a new and highly effective antiangiogenic therapy approach. British Journal of Cancer 95, 272–281. https://doi.org/10.1038/sj.bjc.6603240

Zhang, F., Ayaub, E.A., Wang, B., Puchulu-Campanella, E., Li, Y., Hettiarachchi, S.U., Lindeman, S.D., Luo, Q., Rout, S., Srinivasarao, M., Cox, A., Tsoyi, K., Nickerson-Nutter, C., Rosas, I.O., Low, P.S., 2020. Reprogramming of profibrotic macrophages for treatment of bleomycin-induced pulmonary fibrosis. EMBO Molecular Medicine 12, e12034. https://doi.org/10.15252/emmm.202012034

Zhang, F., Parayath, N.N., Ene, C.I., Stephan, S.B., Koehne, A.L., Coon, M.E., Holland, E.C., Stephan, M.T., 2019. Genetic programming of macrophages to perform anti-tumor functions using targeted mRNA nanocarriers. Nature Communications 10, 3974. https://doi.org/10.1038/s41467-019-11911-5

Zhang, S., Yu, B., Sheng, C., Yao, C., Liu, Y., Wang, J., Zeng, Q., Mao, Y., Bei, J., Zhu, B., Chen, S., 2024. SHISA3 Reprograms Tumor-Associated Macrophages Toward an Antitumoral Phenotype and Enhances Cancer Immunotherapy. Advanced Science 11, 2403019. https://doi.org/10.1002/advs.202403019

Zhang, Xue, Liu, M., Qiao, L., Zhang, Xin-yu, Liu, X., Dong, M., Dai, H., Ni, M., Luan, X., Guan, J., Lu, H., 2018. Ginsenoside Rb1 enhances atherosclerotic plaque stability by skewing macrophages to the M2 phenotype. Journal of Cellular and Molecular Medicine 22, 409–416. https://doi.org/10.1111/jcmm.13329

Zhao, G., Xue, L., Geisler, H.C., Xu, J., Li, X., Mitchell, M.J., Vaughan, A.E., 2024. Precision treatment of viral pneumonia through macrophage-targeted lipid nanoparticle delivery. Proceedings of the National Academy of Sciences of the

United States of America 121, e2314747121. https://doi.org/10.1073/pnas.2314747121

Zhao, M., Cheng, X., Shao, P., Dong, Y., Wu, Y., Xiao, L., Cui, Z., Sun, X., Gao, C., Chen, J., Huang, Z., Zhang, J., 2024. Bacterial protoplast-derived nanovesicles carrying CRISPR-Cas9 tools re-educate tumor-associated macrophages for enhanced cancer immunotherapy. Nature Communications 15, 950. https://doi.org/10.1038/s41467-024-44941-9

Zhao, Y., Yin, W., Yang, Z., Sun, J., Chang, J., Huang, L., Xue, L., Zhang, X., Zhi, H., Chen, S., Chen, N., Li, Y., 2024. Nanotechnology-enabled M2 macrophage polarization and ferroptosis inhibition for targeted inflammatory bowel disease treatment. Journal of Controlled Release 367, 339–353. https://doi.org/10.1016/j.jconrel.2024.01.051

Zhou, X., Huang, D., Wang, R., Wu, M., Zhu, L., Peng, W., Tu, H., Deng, X., Zhu, H., Zhang, Z., Wang, X., Cao, X., n.d. Targeted therapy of rheumatoid arthritis via macrophage repolarization. Drug Delivery 28, 2447–2459. https://doi.org/10.1080/10717544.2021.2000679

Zhou, Y., Que, K.-T., Tang, H.-M., Zhang, P., Fu, Q.-M., Liu, Z.-J., 2020. Anti-CD206 antibody-conjugated Fe_3O_4-based PLGA nanoparticles selectively promote tumor-associated macrophages to polarize to the pro-inflammatory subtype. Oncology Letters 20, 298. https://doi.org/10.3892/ol.2020.12161

Zhu, J., Yu, J., Hu, A., Liu, J.-Q., Pan, X., Xin, G., Carson, W.E., Li, Z., Yang, Y., Bai, X.-F., 2023. IL-27 gene therapy induces Stat3-mediated expansion of CD11b+Gr1+ myeloid cells and promotes accumulation of M1 macrophages in tumor microenvironment. Journal of Immunology 211, 895–902. https://doi.org/10.4049/jimmunol.2300176

CURRICULUM VITAE

Hanrong (Belle) Ye

• Email: yehr@bu.edu

EDUCATION

Boston University, Boston, MA
Doctor of Philosophy in Biomedical Engineering — Sep 2017–Present
GPA: 3.76

Vanderbilt University, Nashville, TN
Bachelor of Engineering — Sep 2013-May 2017
Double Major: Biomedical Engineering; Chemical and Biomolecular Engineering
Honors: Magna Cum Laude, GPA: 3.86/4.00

RESEARCH EXPERIENCE

Department of Biomedical Engineering, Boston University
Graduate Researcher — Sep 2017–Jan 2020, Apr 2021–Present
Advisors: Dr. Ahmad (Mo) Khalil; Dr. Joyce Wong

- Designed, optimized, and produced lentiviral vectors for highly efficient gene delivery in primary cells.
- Leveraged synthetic biology and gene editing to develop macrophage-based immunotherapies for oncology and infectious diseases by modulating macrophage phenotypes using lentiviral-transduced synthetic transcriptional regulators.
- Discovered and optimized a novel synthetic transcriptional activator architecture that boosted transactivation potency over 10-fold, enabling high therapeutic outputs in primary CAR T cells and macrophages, including tumor cell killing, pro-inflammatory cytokine release and cell proliferation.
- Initiated and led an interdisciplinary project bridging biomaterials and synthetic biology, fostering collaboration between research labs by coordinating experimental plans and task delegation among four graduate students and one undergraduate mentee.
- Established and strengthened scientific collaborations with national and international research labs, leading to a patent application, one peer-reviewed publication, and a manuscript under preparation.

Advanced Therapeutics Lab, Vanderbilt University
Undergraduate Research Assistant — Mar 2015–May 2017
Advisor: Craig Duvall

- Fabricated drug-loaded microparticles and developed in vitro assays to assess their reactive oxygen species (ROS)-scavenging efficiency.
- Assessed pathological conditions in animal tissue samples by monitoring bone deformities and ROS biomarkers using X-ray and imaging tools.

HuaZhong Pharmaceuticals LTD, Qingdao, China
Lab Analyst — Summer 2016

- Conducted quality control by extracting, analyzing, and quantifying active substances in raw materials and drug products.

LEADERSHIP AND VOLUNTEER EXPERIENCE

Office of Technology Development, Boston University
Analyst — Jan 2021–Present

- Developed high-level one-pager summaries for diverse biomedical technologies, including medical devices and therapeutic gene circuits, to drive commercialization efforts.
- Evaluated technical innovations, potential patent conflicts, and commercialization challenges for BU biomedical inventions through comprehensive literature and patent searches.
- Conducted market research to estimate market size and share, identify licensing opportunities, assess the competition landscape, and explore alternative market entry strategies.

Nucleate, Boston
Lead of Culture and Networking — Sep 2021–Sep 2022

- Planned and coordinated networking and social events for MBA and PhD students, industry mentors, and the leadership team to foster communication and team building.
- Organized and hosted a Regulatory Workshop to provide education on regulatory pathways and strategies for successful biotech entrepreneurship.
- Identified, recruited, and engaged with industry leaders in regulatory affairs and strategically paired experts with teams based on expertise alignment to establish tailored one-on-one mentorships.

PUBLICATIONS

- Hanrong Ye*, Kok Ann Gan*, Thea Ornstein, et al., *manuscript in preparation*
- Josh Tycko*, Mike V. Van*, Aradhana, Nicole DelRosso, Hanrong Ye, David Yao, Raeline Valbuena, Alun Vaughan-Jackson, Xiaoshu Xu, Connor Ludwig, Kaitlyn Spees, Katherine Liu, Mingxin Gu, Venya Khare, Adi Xiyal Mukund, Peter H. Suzuki, Sophia Arana, Catherine Zhang, Peter P. Du, Thea S. Ornstein, Gaelen T. Hess, Roarke A. Kamber, Lei S. Qi, Ahmad S. Khalil, Lacramioara Bintu, Michael C. Bassik. "Development of compact transcriptional effectors using high-throughput measurements in diverse contexts," *Nature Biotechnology*, 2024
- Kristin P. O'Grady, Taylor E. Kavanaugh, Hongsik Cho, Hanrong Ye, Mukesh K. Gupta, Megan C. Madonna, Jinjoo Lee, Christine M. O'Brien, Melissa C. Skala, Karen A. Hasty, and Craig L. Duvall. "Drug-Free ROS Sponge Polymeric Microspheres Reduce Tissue Damage from Ischemic and Mechanical Injury," *ACS Biomaterials Science & Engineering*, 2018, 4 (4), 1251-1264

FELLOWSHIPS

- **BUnano Cross-Disciplinary Fellowship**, Boston University — Aug 2019–May 2020

PATENTS

- Khalil, Gan, Ye, Ornstein, "Regulated Synthetic Gene Activation Systems," US Application No. 18/756,596, PCT Application No. PCT/US2024/035774, filed June 27, 2024. Patent Pending

CONFERENCES

- **2024 International Mammalian Synthetic Biology Workshop (mSBW)** — Aug 2024
  Selected Abstract Talk: "SynZiFTR 2.0: Development of novel transcriptional activation domain architectures for clinically optimized gene circuit engineering"
- **2024 Cell Therapies and Immunotherapy Conference** — Oct 2024
  Oral Presentation: "Synziftr 2.0: Expanding the Clinical Potential of Synthetic Gene Circuits for Advanced Cell Therapies with Novel Transcriptional Activation Domain (TAD) Architectures"

SKILLS

Laboratory Skills:

- **Cell Culture**: Suspension and adherent cell line maintenance, primary cell isolation from blood samples, primary T cell activation and maintenance, primary macrophage differentiation and maintenance, 2D cell co-culture, 3D spheroid models.
- **Cellular Techniques**: Immunostaining, ELISA, cytokine assays, DNA/RNA isolation, Western Blot, RNAi knockdown, CRISPR knockout, sample preparation for Precision Run-On Sequencing (PRO-seq), transcriptome analysis, tumor cell killing.
- **Cell Engineering**: Transfection, lentiviral vector design, lentivirus production, lentiviral transduction.
- **Molecular Biology**: PCR, qPCR, cloning, plasmid design, circuit design, bacterial transformation.
- **Equipment**: Multi-color flow cytometer/FACS, confocal microscopy, X-ray microtomography, plate reader.

Computational Skills:

- MATLAB, Python, Microsoft Office Suite, LabVIEW, LT-SPICE, Wolfram Mathematica, Aspen Plus, FlowJo, Arduino.

Languages:

- Fluent in Mandarin